

New Simocetidae (Cetacea, Odontoceti) from the Pysht Formation in Washington State, U.S.A. (#80454)

1

First submission

Guidance from your Editor

Please submit by **22 Jan 2023** for the benefit of the authors (and your token reward) .



Structure and Criteria

Please read the 'Structure and Criteria' page for general guidance.



Custom checks

Make sure you include the custom checks shown below, in your review.



Author notes

Have you read the author notes on the [guidance page](#)?



Raw data check

Review the raw data.



Image check

Check that figures and images have not been inappropriately manipulated.

Privacy reminder: If uploading an annotated PDF, remove identifiable information to remain anonymous.

Files

Download and review all files from the [materials page](#).

20 Figure file(s)

6 Table file(s)

1 Raw data file(s)

! Custom checks

New species checks



Have you checked our [new species policies](#)?



Do you agree that it is a new species?



Is it correctly described e.g. meets ICZN standard?




Structure and Criteria

Structure your review

The review form is divided into 5 sections. Please consider these when composing your review:

1. BASIC REPORTING
2. EXPERIMENTAL DESIGN
3. VALIDITY OF THE FINDINGS
4. General comments
5. Confidential notes to the editor






 You can also annotate this PDF and upload it as part of your review

When ready [submit online](#).





Editorial Criteria

Use these criteria points to structure your review. The full detailed editorial criteria is on your [guidance page](#).




BASIC REPORTING

-  Clear, unambiguous, professional English language used throughout.
-  Intro & background to show context. Literature well referenced & relevant.
-  Structure conforms to [Peerj standards](#), discipline norm, or improved for clarity.
-  Figures are relevant, high quality, well labelled & described.
-  Raw data supplied (see [Peerj policy](#)).

EXPERIMENTAL DESIGN

-  Original primary research within [Scope of the journal](#).
-  Research question well defined, relevant & meaningful. It is stated how the research fills an identified knowledge gap.
-  Rigorous investigation performed to a high technical & ethical standard.
-  Methods described with sufficient detail & information to replicate.

VALIDITY OF THE FINDINGS

-  Impact and novelty not assessed. *Meaningful* replication encouraged where rationale & benefit to literature is clearly stated.
-  All underlying data have been provided; they are robust, statistically sound, & controlled.
-  Conclusions are well stated, linked to original research question & limited to supporting results.



The best reviewers use these techniques

Tip

Example

Support criticisms with evidence from the text or from other sources

Smith et al (J of Methodology, 2005, V3, pp 123) have shown that the analysis you use in Lines 241-250 is not the most appropriate for this situation. Please explain why you used this method.

Give specific suggestions on how to improve the manuscript

Your introduction needs more detail. I suggest that you improve the description at lines 57- 86 to provide more justification for your study (specifically, you should expand upon the knowledge gap being filled).

Comment on language and grammar issues

The English language should be improved to ensure that an international audience can clearly understand your text. Some examples where the language could be improved include lines 23, 77, 121, 128 - the current phrasing makes comprehension difficult. I suggest you have a colleague who is proficient in English and familiar with the subject matter review your manuscript, or contact a professional editing service.

Organize by importance of the issues, and number your points

1. Your most important issue
2. The next most important item
3. ...
4. The least important points

Please provide constructive criticism, and avoid personal opinions

I thank you for providing the raw data, however your supplemental files need more descriptive metadata identifiers to be useful to future readers. Although your results are compelling, the data analysis should be improved in the following ways: AA, BB, CC

Comment on strengths (as well as weaknesses) of the manuscript

I commend the authors for their extensive data set, compiled over many years of detailed fieldwork. In addition, the manuscript is clearly written in professional, unambiguous language. If there is a weakness, it is in the statistical analysis (as I have noted above) which should be improved upon before Acceptance.

New Simocetidae (Cetacea, Odontoceti) from the Pysht Formation in Washington State, U.S.A.

Jorge Velez-Juarbe ^{Corresp. 1}

¹ Department of Mammalogy, Natural History Museum of Los Angeles County, Los Angeles, California, USA

Corresponding Author: Jorge Velez-Juarbe
Email address: jvelezjuar@nhm.org

Odontocetes first appeared by the early Oligocene and their early evolutionary history can provide clues as to how some of their unique adaptations, such as echolocation, evolved. Here, three new specimens from the middle Oligocene Pysht Formation are described further increasing our understanding of richness and diversity of early odontocetes, particularly for the North Pacific region. Phylogenetic analysis shows that the new specimens are part of a more inclusive, redefined Simocetidae, which now includes *Simocetus rayi*, *Olympicetus* sp. 1, *Olympicetus avitus*, *O. thalassodon* sp. nov., and a large unnamed taxon, all part of an endemic, North Pacific clade. Of these, *Olympicetus thalassodon* sp. nov. represents one of the best known simocetids, offering new information on the cranial and dental morphology of early odontocetes. Additionally, the inclusion of CCNHM 1000, here considered to represent a neonate of *Olympicetus* sp., as part of the Simocetidae, suggests that this group represents a clade of non-echolocating odontocetes, further implying that some morphological features that have been correlated with the capacity to echolocate appeared before the acquisition of ultrasonic hearing. The dentition of simocetids is interpreted as being plesiomorphic, with a tooth count more akin to that of basilosaurids and early toothed mysticetes, while other features of the skull and hyoid suggests various forms of prey acquisition, including raptorial or combined feeding and in *Olympicetus* spp., and suction feeding in *Simocetus*. Finally, body size estimates show that small to moderately large taxa are present in Simocetidae, with a largest taxon represented by LACM 124104 with an estimated body length of 3 meters, which places it as the largest known simocetid, and amongst the largest Oligocene odontocetes. The new specimens described here add to a growing list of Oligocene marine tetrapods from the North Pacific, further promoting faunistic comparisons across other contemporaneous and younger assemblages, that will allow for an improved understanding of the evolution of marine faunas in the region.

1 **New Simocetidae (Cetacea, Odontoceti) from the** 2 **Pysht Formation in Washington State, U.S.A.**

3

4

5 Jorge Vélez-Juarbe

6

7 Department of Mammalogy, Natural History Museum of Los Angeles County, Los Angeles, CA
8 90007, U.S.A.

9

10

11 Corresponding Author:

12 Jorge Vélez-Juarbe

13 Email address: jvelezjuar@nhm.org

14

15 **Abstract**

16 Odontocetes first appeared by the early Oligocene and their early evolutionary history can
17 provide clues as to how some of their unique adaptations, such as echolocation, evolved. Here,
18 three new specimens from the middle Oligocene Pysht Formation are described further
19 increasing our understanding of richness and diversity of early odontocetes, particularly for the
20 North Pacific region. Phylogenetic analysis shows that the new specimens are part of a more
21 inclusive, redefined Simocetidae, which now includes *Simocetus rayi*, *Olympicetus* sp. 1,
22 *Olympicetus avitus*, *O. thalassodon* sp. nov., and a large unnamed taxon, all part of an endemic,
23 North Pacific clade. Of these, *Olympicetus thalassodon* sp. nov. represents one of the best known
24 simocetids, offering new information on the cranial and dental morphology of early odontocetes.
25 Additionally, the inclusion of CCNHM 1000, here considered to represent a neonate of
26 *Olympicetus* sp., as part of the Simocetidae, suggests that this group represents a clade of non-
27 echolocating odontocetes, further implying that some morphological features that have been
28 correlated with the capacity to echolocate appeared before the acquisition of ultrasonic hearing.
29 The dentition of simocetids is interpreted as being plesiomorphic, with a tooth count more akin to
30 that of basilosaurids and early toothed mysticetes, while other features of the skull and hyoid
31 suggests various forms of prey acquisition, including raptorial or combined feeding and in
32 *Olympicetus* spp., and suction feeding in *Simocetus*. Finally, body size estimates show that small
33 to moderately large taxa are present in Simocetidae, with a largest taxon represented by LACM
34 124104 with an estimated body length of 3 meters, which places it as the largest known
35 simocetid, and amongst the largest Oligocene odontocetes. The new specimens described here
36 add to a growing list of Oligocene marine tetrapods from the North Pacific, further promoting
37 faunistic comparisons across other contemporaneous and younger assemblages, that will allow
38 for an improved understanding of the evolution of marine faunas in the region.

39

40 Introduction

41 The Eastern North Pacific Region is recognized as one of the best sources for early
42 marine mammals belonging to various groups, particularly desmostylians, pinnipeds, and early
43 mysticetes ~~mysticetes~~ (Emlong, 1966; Russell, 1968; Domning et al., 1986; Berta, 1991; Ray et
44 al., 1994; Barnes et al., 1995; Beatty, 2006; Beatty and Cockburn, 2015; Marx et al., 2015,
45 2016b; Peredo and Uhen, 2016; Peredo and Pyenson, 2018; Peredo et al., 2018; Poust and
46 Boessenecker, 2018; Shipps et al., 2019; Solis-Añorve et al., 2019; Hernández-Cisneros, 2018,
47 2022; Hernández-Cisneros and Nava-Sánchez, 2022). However, while odontocetes have also
48 been found in these **units**, and have been remarked in the literature in non-taxonomic context
49 (e.g. Whitmore and Sanders, 1977; Goedert et al., 1995; Barnes, 1998; Barnes et al., 2001; **Kiel**
50 **et al.**, 2013; Hernández Cisneros et al., 2017), only a handful are described (Fordyce, 2002;
51 Boersma and Pyenson, 2016; Vélez-Juarbe, 2017). These include *Simocetus rayi* Fordyce, 2002,
52 from the early Oligocene Alsea Formation, in Oregon, U.S.A., the platanistoid *Arktocara*
53 *yakataga* Boersma and Pyenson, 2016, from the **middle Oligocene** Poul Creek Fm., in Alaska,
54 U.S.A., and the more recently described, *Olympicetus avitus* Vélez-Juarbe, 2017, from the
55 middle Oligocene Oligocene Pysht Fm., in Washington State. The presence of stem (i.e.
56 *Simocetus*, *Olympicetus*) and crown (*Arktocara*) odontocetes in similar-aged rocks point to a
57 complex **early history for odontocetes**, hence the description of new material will advance our
58 current understanding of odontocete evolution.

59 In this work three additional specimens of stem odontocetes collected from the **mid-**
60 **Oligocene** Pysht Formation of Washington are described. The morphology of these new
61 specimens show similarities with *Simocetus* and *Olympicetus*, and provide further **insight** into
62 the diversity of early odontocetes in the North Pacific. The Pysht Fm. has a rich fossil record of
63 marine tetrapods, including plesiosaurs (Olson, 1980; Dyke et al., 2011; Mayr and Goedert,
64 2016), desmostylians (Domning et al., 1986), aetiocetids (Barnes et al., 1995; Shipps et al.,
65 2019), stem mysticetes (Peredo and Uhen, 2016), and many others still remaining to be described
66 (Whitmore and Sanders, 1977; Hunt and Barnes, 1994; Barnes et al., 2001; Marx et al., 2016b).
67 The fossils described in this work demonstrate that stem odontocetes were ~~much~~
68 **the North Pacific Region** and hint at the presence of clade of stem odontocetes that were
69 geographically confined to this region **that parallels** aetiocetid mysticetes (Hernández Cisneros
70 and Vélez-Juarbe, 2021).

71 **Abbreviations**—c., character state as described and numbered by Sanders and Geisler (2015)
72 and subsequent works, e.g. (c.15[0]) refers to state 0 of character 15; **LACM**, Vertebrate
73 Paleontology Collection, Natural History Museum of Los Angeles County, Los Angeles, CA,
74 U.S.A.; **KMNH VP**, Kitakyushu Museum of Natural History, Kitakyushu City, Japan; **USNM**,
75 Department of Paleobiology, National Museum of Natural History, Smithsonian Institution,
76 Washington, D.C., U.S.A.

77 Materials & Methods

78 Phylogenetic analysis

79 The phylogenetic analysis was performed using the morphological matrix of Albright et al.
80 (2018) as modified recently by Boessenecker et al. (2020), with the addition of two new
81 characters. The first one (c.335) refers to the presence of a transverse cleft on the apex of the
82 zygomatic process of the squamosal (first noted by Racicot et al., 2019), while the other new
83 character (c.336) relates to the morphology of the thyrohyoid/thyrohyal, for a total of 336
84 characters (see Supplemental File 1). Besides LACM 124104, LACM 124105 and LACM
85 158720, one additional odontocete from the Pysht Fm. was added, CCNHM 1000, based on the
86 description from Racicot et al. (2019:S1). All otherwise undescribed specimens in earlier
87 versions of this matrix were removed from this analysis as their character states cannot be
88 independently corroborated, resulting in a total of three outgroup and 106 ingroup taxa. The
89 matrix was analyzed using PAUP* (v. 4.0a169; Swofford, 2003), all characters were treated as
90 unordered and with equal weights. A heuristic search of 10000 replicates was performed using
91 the tree bisection-reconnection (TBR) algorithm and using a backbone constraint based on the
92 phylogenetic tree from McGowen et al. (2020); bootstrap values were obtained by performing
93 10000 replicates.

94

95 Taxonomy

96 The electronic version of this article in portable document format will represent a published work
97 according to the International Commission on Zoological Nomenclature (ICZN), and hence the
98 new names contained in the electronic version are effectively published under that Code from the
99 electronic edition alone. This published work and the nomenclatural acts it contains have been
100 registered in ZooBank, the online registration system for the ICZN. The ZooBank LSIDs (Life
101 Science Identifiers) can be resolved and the associated information viewed through any standard
102 web browser by appending the LSID to the prefix <http://zoobank.org/>. The LSID for this
103 publication is LSIDurn:lsid:zoobank.org:pub:D190F6B6-FB67-4F2B-AC24-145DF06D3FD3
104 The online version of this work is archived and available from the following digital repositories:
105 PeerJ, PubMed Central, and CLOCKSS.

106

107 Systematic Paleontology

108 CETACEA Brisson, 1762

109 ODONTOCETI Flower, 1867

110 SIMOCETIDAE Fordyce, 2002

111 **Type**—*Simocetus rayi* Fordyce, 2002.

112 **Included Species**—*Simocetus rayi*; *Olympicetus avitus* Velez-Juarbe, 2017; *Olympicetus*
113 *thalassodon* sp. nov.; *Olympicetus* sp. 1; Simocetidae gen. et sp. A.

114 **Range**—early-late Oligocene (Rupelian–early Chattian) of the eastern North Pacific.

115 **Emended Diagnosis**—Stem odontocetes displaying a mosaic of plesiomorphic and derived
116 characters that sets them apart from other basal odontocetes, particularly the Xenorophidae,
117 Patriocetidae and Agorophidae. Characterized by the following combination of characters:
118 rostrum fairly wide (c.7[1]; shared with *Ashleycetetus planicapitis* Sanders and Geisler, 2015,

119 *Agorophius pygmaeus* [Müller, 1849], and *Ankylorhiza tiedemani* [Allen, 1887]);
120 palatine/maxilla suture anteriorly bowed (21[0]; shared with *Patriocetus kazakhstanicus*
121 Dubrovo and Sanders, 2000); seven to eight teeth completely enclosed by the maxilla (c.25[1]);
122 lacrimal restricted to below the supraorbital process of frontal (c.52[0]; shared with *A.*
123 *planicapitis*, *P. kazakhstanicus* and *An. tiedemani*); relatively small ventral (orbital) exposure of
124 the lacrimal (c.56[0]; shared with *A. planicapitis*, *Archaeodelphis patrius* Allen, 1921, and *P.*
125 *kazakhstanicus*); postorbital process of frontal relatively long and oriented posterolaterally and
126 ventrally (c.62[0]; shared with *A. planicapitis*, *Mirocetus riabinini* and *P. kazakhstanicus*); lack
127 of a rostral basin (c.66[0]), differing from most xenorophids which have a well-defined basin;
128 presence of a long posterolateral sulcus extending from the premaxillary foramen (c.73[2];
129 shared with *A. planicapitis*); maxilla only partially covering supraorbital processes (c.77[1];
130 shared with *A. planicapitis* and *Ar. patrius*); posteriormost edge of nasals in line with the anterior
131 half of the supraorbital processes (c.123[1]); frontals slightly lower than nasals (c.125[0]; shared
132 with *Cotylocara macei* Geisler et al., 2014); supraoccipital at about the same level as the nasals
133 (c.129[1]), differing from xenorophids where the supraoccipital is higher; intertemporal region
134 with an ovoid cross section (c.137[1]; shared with *A. planicapitis*, *Echovenator sandersi*
135 Churchill et al., 2016, and *C. macei*); floor of squamosal fossa thickens posteriorly (c.149[1]);
136 distal end of postglenoid process is anteroposteriorly wide (c.152[2]); anterior end of
137 supraoccipital is semicircular (c.153[1]; shared with *P. kazakhstanicus*); occipital shield with
138 distinct **sagittal crest** (c.156[1]; shared with *Albertocetus meffordorum* Uhen, 2008, *P.*
139 *kazakhstanicus*, *Ag. pygmaeus*, and *An. tiedemani*); a nearly transverse pterygoid-palatine suture
140 (c.163[1]; shared with *Ar. patrius*); long and subconical hamular process of the pterygoid
141 (c.173[1]); hamular processes unkeeled (c.174[0]); hamular processes extending to a point in line
142 with the middle of the zygomatic processes (c.175[3]); cranial hiatus constricted by medial
143 projection of the parietal (c.184[2]); absent to poorly defined rectus capitus anticus muscle fossa
144 (c.193[0]), differing from the well-defined fossa of xenorophids; posteroventral end of
145 basioccipital crest forming a posteriorly oriented flange (c.194[2]); anterior process of periotic
146 short (c.204[2]; shared with *C. macei*); anterior process of periotic with well-defined fossa for
147 contact with tympanic (c.210[3]); lateral tuberosity of periotic forming a bulbous prominence
148 lateral to malleolar fossa (c.212[1]); tegment tympani at the base of the anterior process
149 unexcavated (c.232[0]), differing from the excavated surface in xenorophids; articular surface of
150 the posterior process of periotic is smooth (c.242[0]) and concave (c.243[0]); posterolateral
151 sulcus of premaxilla deeply entrenched (c.310[1]).

152

153 SIMOCETIDAE GEN. ET SP. A

154 (Figs. 1-5; Tables 1-2)

155 **Material**—LACM 124104, posterior part of ~~skull~~ skull, missing most parts anterior to the
156 frontal/parietal suture and the left squamosal; including one molariform tooth and partial atlas,
157 axis and third cervical vertebrae. Collected by J. L. Goedert and G. H. Goedert March 21, 1984.

158 **Locality and Horizon**—LACM Loc. 5123, Murdock Creek, Clallam Co., Washington, U.S.A.
159 (48° 09' 25"N, 123° 52' 10"W; = locality JLG-76). At this locality specimens are found as
160 concretions along a beach terrace about 40 m north of the mouth of Murdock Creek. Besides
161 LACM 124104, additional specimens known from this locality include the desmostylian
162 *Behemotops proteus* (LACM 124106; Ray et al., 1994), additional material of the simocetid
163 *Olympicetus* spp. (LACM 124105 and LACM 158720; described below), aff. *Olympicetus* sp.
164 (Racicot et al., 2019), and the aetiocetid *Borealodon osedax* (Shipps et al., 2019).

165 **Formation and Age**—Pysht Formation, between 30.5–26.5 Ma (Oligocene: late Rupelian-early
166 Chattian; Prothero et al., 2001; Vélez-Juarbe, 2017).

167 **Range**—Oligocene of Washington, U.S.A.

168

169 **Description**

170 The partial skull, LACM 124104, is missing most parts anterior to the fronto-parietal suture, the
171 left squamosal, and some parts of the palatines and earbones (Figs. 1-4). The preserved portion
172 of the skull has a pachyostotic appearance, in comparison with the other described simocetids.
173 The estimated bizygomatic width, 322 mm (c.333[2]), suggests a body length of around 3 m
174 (based on equation “I” from Pyenson and Sponberg, 2011), which is larger than any of the other
175 described simocetids.

176 **Vomer**—Most of the palatal surface of the vomer is missing as is much of the rostrum.
177 Posteriorly, it seems to have been exposed along an elongated, diamond-shaped, window
178 between the palatines and pterygoids as in other simocetids (Fig. 2C-D; Fordyce, 2002; Vélez-
179 Juarbe, 2017; see below). From this point, the vomerine keel extends posterodorsally, separating
180 the choanae along the midline and extending to about 20 mm from the posterior edge of the bone
181 (Fig. 2C-D). The horizontal plate extends posteriorly to a point in line with the anterior end of
182 the basioccipital crests, thus covering the suture between the basisphenoid and basioccipital
183 (c.191[0]; Fig. 2C-D). The choanal surface of the horizontal plate forms a ventrally concave
184 choanal roof, with its lateral edges slightly flared and forming a nearly continuous surface with
185 the internal lamina of the pterygoid.

186 **Palatine**—Only the posteriormost parts of the palatines are preserved, these are separated along
187 the midline by the vomer, resembling the condition of other simocetids (Fig. 2C-D; Fordyce,
188 2002; see below). In anterior view, the palatines formed the ventral and lateral surface of the
189 internal nares, while the vomer formed the medial and dorsal surfaces. Ventrolaterally, the
190 palatines form a vertical to semilunar contact with the pterygoids, best observed in ventral,
191 ventrolateral and lateral views (c.163[1]; Figs. 2C-D, 3-4), resembling the contact in *Simocetus*
192 *rayi* and *Olympicetus* spp. (Fordyce, 2002; Vélez-Juarbe, 2017). An elongated groove along the
193 ventrolateral end of the left palatine seems to have been part of the palatine foramen/canal.

194 **Frontal**—Only the posteriormost portion of the frontals are preserved, but are eroded (Fig. 1).
195 Dorsally, the interfrontal suture seems to have been completely fused, and posteriorly formed a
196 broad V-shaped contact with the parietals, which continues as a vertical contact along the
197 temporal surface (Fig. 3).

198 **Parietal**—As in other simocetids, the parietals are broadly exposed dorsally, and the interparietal
199 is either absent or fused early in **ontogeny** (c.135[0], 136[1]; Fig. 1). The parietals do not extend
200 anterolaterally, resembling *Simocetus rayi*, and differing from *Olympicetus* where the parietals
201 extend into the base of the supraorbital processes. The parietal exposure in the intertemporal
202 region is anteroposteriorly short and broad in dorsal view, **with an ovoid cross section** (c.137[1]).
203 Posterodorsally, the parietal-supraoccipital contact is **broad** and anteriorly convex, while along
204 the temporal surface, **it** forms a vertical contact with the frontals (c.134[0]; Fig. 1), and seems to
205 have formed part of the posterior edge of the optic infundibulum; abaft to this point the parietals
206 become laterally convex towards the contact with the squamosals (Figs. 3-4). Anteroventrally, on
207 the temporal surface, the parietal descends to contact the orbitosphenoid, a portion of the dorsal
208 lamina of the pterygoid, the alisphenoid, and the squamosal, with which it forms part of the
209 subtemporal crest (Fig. 4). Its contact with the squamosal on the temporal surface becomes an
210 interdigitated, dorsally arched suture posterior to this point. In ventral view the parietals contact
211 the squamosal medially, partially constricting the cranial hiatus (c.184[2]; Figs. 2C-D, 4).

212 **Supraoccipital**—The anterior half of the supraoccipital is not preserved, but based **on its contact**
213 with the parietal, its anterior edge formed a gentle semicircular arch that reached anteriorly to a
214 level in line with the anterior half of the squamosal fossa (c.140[0], 153[1]; Fig. 1), resembling
215 the condition observed in *Olympicetus* spp. The preserved portion of the supraoccipital forms a
216 gently concave surface that seems to have lacked **the sagittal crest** (c.156[?0], 311[0]; Figs. 1,
217 2A-B) observed in other simocetids. The nuchal crest **are** oriented dorsolaterally (c.154[1],
218 c.155[0]), and seem to have been gently sinuous, descending posterolaterally to meet the
219 supramastoid crest (Figs. 1, 2A-B, 3).

220 **Exoccipital**—The occipital condyles are semilunar in outline, with well-defined edges, and
221 bounded dorsally by shallow, transversely oval supracondylar fossae (c.157[1]; Fig. 2A-B) as in
222 *Simocetus rayi* and *Olympicetus avitus*. The foramen magnum has an oval outline, being slightly
223 wider than high. The paroccipital processes are transversely broad and **oriented** posteroventrally,
224 **approximating** the posterior edge of the condyles (c.198[1]; Fig. 2). The ventral edge of the
225 paroccipital processes **are** anteroposteriorly broad, becoming thinner medially towards the broad
226 jugular notch (c.197[0]). The hypoglossal foramen is rounded (~4 mm in diameter), located
227 ventrolateral to the **occipital condyles** and well separated from the jugular notch (c.196[0]; Fig.
228 2).

229 **Basioccipital**—The basioccipital crests are short, transversely thin, oriented ventrolaterally, and
230 diverging posteroventrally at an angle between 58-60° (c.192[0], 195[2]; Fig. 2). **The crest**
231 contacts the **posterior lamina** of the pterygoid along a posteroventrally oriented suture. The
232 ventral surface between the crest **is** flat, with no distinct Rectus capitis anticus fossa (c.193[0]).
233 Anteriorly the contact with the basisphenoid is obscured by the vomer (Fig. 2C-D).

234 **Squamosal**—The **squamous portion** is flat to gently convex, contacting the parietals along a
235 dorsally arched suture that **extends along a sinuous path** to form the posteromedial edge of the
236 subtemporal crest (Figs. 1, 3). Only the right zygomatic process is preserved, although
237 incompletely, missing its anterolateral corner. The process is long, oriented anteriorly, robust and

238 somewhat cylindrical when viewed dorsally, constricting the squamosal fossa (c.143[0], 189[3];
239 Figs. 1, 2C-D, 3-4). The squamosal fossa is relatively deep, with a moderately sigmoidal outline
240 and gently sloping anteriorly (c.147[2], 148[1], 149[1]; Fig. 1). When viewed laterally, the dorsal
241 edge of the zygomatic process is flat to gently convex (c.144[0]), while its ventral edge was
242 concave (c.151[0]; Fig. 3-4). The supramastoid crest is more prominent proximally, continuing
243 posteromedially to join the nuchal crest (c.150[0]). The sternomastoid muscle fossa on the
244 posterior edge of the zygomatic process is a large, shallow oval depression, broadly visible in
245 posterior or lateral view (c.145[1]; Figs. 2A-B, 3). The squamosal exposure lateral to the
246 paroccipital processes is moderate in posterior view (c.146[1]; Fig. 2A-B). Ventrally, the
247 postglenoid process is incompletely preserved, but seems to have been broad as in other
248 simocetids. Posterior to the base of the postglenoid process, the external auditory meatus seems
249 to have been broad (c.190[?0]; the posttympanic process is not preserved). The glenoid fossa is
250 shallowly concave with nearly indistinct borders. Medial to the glenoid fossa is a shallow, oval
251 tympanosquamosal recess (c.179[2]; Fig. 2C-D). The falciform process is anteroposteriorly long
252 (c.177[0]; Figs. 2C-D, 3-4). The periotic fossa is partially obscured by a fragment of periotic; the
253 anterior part of the fossa contains a small foramen spinosum close to the medial suture with the
254 parietal (c.187[1]; Fig. 2C-D), resembling the condition observed in *Olympicetus avitus*.
255 Anteromedially, the squamosal contacts the alisphenoid along an anterolaterally oriented suture that
256 follows the anterodorsal edge of the groove for the mandibular branch of the trigeminal nerve
257 (c.181[1]); the groove wraps around the posterior end of the pterygoid sinus fossa, opening
258 anteriorly (c.182[1]; Figs. 2C-D, 4).

259 **Pterygoid**—The pterygoids are incompletely preserved, missing the hamular processes (Fig. 2C-
260 D). As in other simocetids, the palatal surface seems to have been separated along the midline by
261 a diamond-shaped palatal exposure of the vomer (Fig. 2C-D). Anteriorly, the contact between the
262 pterygoids and palatine is nearly vertical in lateral view. The pterygoid sinus fossa is
263 anteroposteriorly long (99 mm) and dorsoventrally deep (at least 63 mm on the left side),
264 transversely narrower anteriorly (25 mm) and becoming broader posteriorly (46 mm) (Fig. 2C-D,
265 4). The anterior edge of the pterygoid sinus fossa is at the level of the pterygo-palatine suture,
266 extending posteriorly to the anterior edge of the foramen ovale (c.164[2]; Fig. 2C-D). The dorsal
267 lamina contacts the orbitosphenoid anterodorsally, the frontal and the alisphenoid
268 posterodorsally, along an irregularly sinuous contact, and forms the roof of the pterygoid sinus
269 (c.166[0]; Fig. 4). The lateral lamina seems to have descended ventromedially, but its full extent
270 is unknown (c.165[?0]; Figs. 2C-D, 3-4). The medial lamina is incompletely preserved, but
271 medially contacts the lateral flanges of the horizontal plate of the vomer to form the lateral wall
272 of the choana, while laterally they form the medial wall of the sinus fossa (Figs. 2C-D, 3-4).

273 **Alisphenoid**—Only a small portion of the alisphenoid can be observed on the temporal wall,
274 where its exposure is small, wedged in between the squamosal, frontal and lateral lamina of the
275 pterygoid (c.142[1]; Figs. 3-4). Ventrally, its suture with the squamosal runs along the anterior
276 border of the sulcus for the mandibular branch of the trigeminal nerve; its more anteromedal
277 portions are covered by sediment.

278 **Orbitosphenoid/Optic Infundibulum**—The orbitosphenoid is exposed on the temporal wall
279 where it is in contact with the parietal dorsally and palatine and pterygoid ventrally. Medially,
280 the bones are eroded and the distinct features of the optic infundibulum cannot be properly
281 interpreted.

282 **Mandible**—The mandible is missing for the most part, with the exception of the left coronoid
283 process (Fig. 1). The process has a subtriangular outline, as preserved being about as long as
284 high, with the dorsal edge slightly recurved medially. The general outline resembles the coronoid
285 process of *Olympicetus avitus* (Velez-Juarbe, 2017:fig. 7A–B).

286 **Dentition**—Only a double-rooted molariform is preserved in association with the specimen (Fig.
287 5A-C). The mesial root is mostly missing, but seems to have been buccolingually broader than
288 the distal root, which is more cylindrical and slightly recurved buccally. The crown (length = 10
289 mm; height = 7 mm; width = 8 mm) is worn, and is longer than tall, and buccolingually broader
290 on its anterior half, somewhat resembling tooth ‘mo3’ of *Olympicetus avitus* (see Velez-Juarbe,
291 2017:fig.7O,Bb), however, differing by lacking a well-defined buccal ridge with denticles. The
292 crown has three denticles, with the apical one being slightly larger than the two on the distal
293 carina, while there are no denticles on the blunter, mesial carina (Fig. 5A-C). There are no buccal
294 cingula, and only a nearly inconspicuous cingula is present on the distolingual corner of the base
295 of the crown.

296 **Cervical Vertebrae**—Only the first three cervical vertebrae are preserved and are unfused
297 (c.279[0], 280[?0] ; Fig. 5D-I). The dorsal arch of the atlas is missing, as are the distal end of the
298 transverse processes. The anterior articular facets have a semilunar outline, and are shallowly
299 concave, with relatively poorly defined ventrolateral and medial edges. The posterior facets for
300 articulation with the axis have a suboval outline, with gently convex articular surfaces and sharp,
301 well-defined edges. The posterior facets gently merge ventromedially with the articular surface
302 for the odontoid (Fig. 5E). The ventral arch has a more prominent hypapophysis than that
303 observed in *Olympicetus* spp. (Fig. 5E). The base of the transverse processes flare
304 posterolaterally.

305 The axis is missing most of the apex and left half of the dorsal arch and the left transverse
306 process (Fig. 5F-G). The pedicle is anteroposteriorly broad, and flat transversely, the
307 postzygapophysis is oriented posterolateroventrally, forming a flat, smooth surface (Fig. 5G).
308 The anterior articular surface is broad, with a suboval outline, and raised edges, the surface is
309 shallowly concave, merging ventromedially with the ventral surface of the odontoid (Fig. 5F).
310 The odontoid is short, broad and blunt, with a mid-dorsal ridge that extends along the dorsal
311 surface of the centrum, reaching the distal end (Fig. 5F). Posteriorly, the centrum has a cardiform
312 outline and the epiphysis is fused, and its surface is concave, and has a mid-ventral cleft that
313 slightly bifurcates its posteroventral end. The ventral surface of the centrum has a mid-ventral
314 keel that becomes broader and more prominent towards the posterior end of the centrum. The
315 transverse process is anteroposteriorly flat, and oriented mainly laterally, there are no transverse
316 foramina (Fig. 5F-G).

317 The third cervical preserves only a portion of the right neural arch; the pedicle is
318 anteroposteriorly flat and transversely broad, both anterior and posterior; epiphyses are fused
319 (Fig.5H-I). The prezygapophysis consists of a rounded, flat surface that is oriented
320 anterodorsomedially, complementing its counterpart in the axis. The transverse foramen is large,
321 being slightly broader than tall (16 mm x 11 mm). The transverse process is mainly oriented
322 laterally; its posterior surface forms a low keel that extends from the base to the apex, and its
323 anteroventral edge is flared (Fig. 5I). The centrum is rounded, anteroposteriorly short, with
324 shallowly concave proximal and distal articular surfaces. Low midline keels are present along the
325 ventral and dorsal surfaces of the centrum. A pair of small (~4 mm) nutrient foramina are present
326 on each side of the middorsal keel.

327 **Remarks**—LACM 124104 represents the largest known simocetid, with an estimated
328 bizygomatic width of 322 mm, in comparison with that of *Simocetus rayi* (238 mm), which
329 (using equation “i” from from Pyenson and Sponberg, 2011) results in estimated body lengths of
330 about 3 m and 2.3 m, respectively, both which are larger than those estimated for *Olympicetus*
331 spp. (see below). This large simocetid shows a unique combination of characters, some which
332 are shared with *Olympicetus* spp. such as the more retracted position of the supraoccipital
333 (c.140[0]), the dorsolateral orientation of the lambdoidal crest (c.154[1]), a shallow
334 tympanosquamosal recess (c.179[1,2]), an alisphenoid/squamosal suture that courses along the
335 groove for the mandibular branch of the trigeminal nerve (c.181[1]). At the same time, some of
336 the preserved characters seem to be unique to this taxon amongst simocetids, such as a deep
337 squamosal fossa (c.147[2]) and the path of the groove for the mandibular branch of the
338 trigeminal nerve which wraps around the posterior end of the pterygoid sinus fossa (c.182[1]).
339 This specimen does preserve a remarkable amount of details of the size and morphology of the
340 pterygoid sinus fossa, which together with other simocetids, suggest that they had a well
341 developed, large fossae, particularly when compared to those of other early odontocetes, such as
342 *Archaeodelphis patrius*, which seems to have a much shorter fossa (pers. obs. LACM 149261,
343 cast of type). LACM 124104 resembles, and may be congeneric, with an odontocete skull from
344 the early Oligocene Lincoln Creek Formation of Washington State, briefly described by Barnes
345 et al. (2001), in many characters of its morphology, including its large size (bizygomatic width =
346 265 mm) and the pachyostotic appearance of some of the cranial bones, and will be addressed in
347 more detail in a follow-up study.

348

349 *OLYMPICETUS* Velez-Juarbe, 2017

350 **Type**—*Olympicetus avitus* Velez-Juarbe, 2017.

351 **Included Species**—*Olympicetus avitus*; *Olympicetus thalassodon* sp. nov., *Olympicetus* sp. 1.

352 **Range**—Oligocene (late Rupelian–early Chattian; 33.7–26.5 Ma;) of Washington, U.S.A.

353 **Emended Diagnosis**—Small odontocetes, with bizygomatic width ranging from 145–220 mm

354 (c.333[0,1]), with symmetric skulls and heterodont dentition, resembling *Simocetus rayi*

355 Fordyce, 2002. Differs from *Simocetus*, other simocetids, and other stem odontocetes by the

356 following combination of characters: having a concave posterior end of the palatal surface of the

357 rostrum (c.19[0]; shared with Xenorophidae); posterior buccal teeth closely spaced (c.26[0];
358 shared with *Ashleycetetus planicapitis*, *Patriocetus kazakhstanicus*, *Agorophius pygmaeus* and
359 *Ankylorhiza tiedemani*), differing from the widely-spaced teeth of *S. rayi*; buccal teeth with ecto-
360 and entocingula (c.32[1], 33[0]; shared with *Xenorophus sloani* Kellogg, 1923, *Echovenator*
361 *sandersi*, *Cotylocara macei* and *P. kazakhstanicus*), and unlike *S. rayi* where these features are
362 absent; lacrimal and jugal separated (c.54[0]; shared with CCNHM 1000, Xenorophidae, *P.*
363 *kazakhstanicus*, *Ag. pygmaeus* and *An. tiedemani*); presence of a short maxillary infraorbital
364 plate (c.60[1]; shared with CCNHM 1000 and *Archaeodelphis patrius*); infratemporal crest of
365 the frontal forming a well-defined ridge along the posterior edge of the sulcus for the optic nerve
366 (c.63[0]; shared with Xenorophidae); posteriormost end of the nasal process of the premaxilla in
367 line with the anterior half of the supraorbital process of the frontal (c.75[2]), differing from the
368 longer process of *S. rayi*; absence of a posterior dorsal infraorbital foramen (= maxillary
369 foramen; c.76[0]), differing from *S. rayi* which has two foramina on each side located medial to
370 the orbit; posteriormost end of the ascending process of the maxilla in line with the posterior half
371 of the supraorbital process of the frontal (c.78[2]; shared with *Ashleycetetus planicapitis* and
372 *Archaeodelphis patrius*); lack of a premaxillary cleft (c.110[0]; present in *S. rayi*); anteriormost
373 point of the supraoccipital in line with the floor of the squamosal fossa (c.140[0]), differing from
374 the more anterior position in *S. rayi*; having a relatively shallow squamosal fossa (c.147[1];
375 shared with *Ar. patrius* and *P. kazakhstanicus*), thus differing from the deeper fossae of
376 *Simocetus rayi* and Simocetidae gen. et sp. A; involucrem of the tympanic bulla lacking a
377 transverse groove (c.272[1]; shared with *C. macei*); dorsal process of atlas larger than ventral
378 process (c.278[2]); presence of three mesial and four distal denticles on **main molars** (c.328[1],
379 329[2]); presence of a transverse cleft on the apex of the zygomatic process of the squamosal
380 (c.335[1]); arched palate, and, saddle-like profile of the skull roof (when viewed laterally).

381

382 *OLYMPICETUS THALASSODON*, sp. nov.

383 (Figs. 6-13; Tables 1-5)

384 **Holotype**—LACM 158720, partial skull with articulated mandibles, including 18 teeth,
385 **tympanic bullae**, cervical vertebrae 1–6, and hyoids; missing distal end of rostrum/mandible.
386 Collected by J. L. Goedert and G. H. Goedert, July 30, 1983.

387 **Type Locality and Horizon**—LACM Loc. 5123, Murdock Creek, Clallam Co., Washington,
388 U.S.A. (48° 09' 25"N, 123° 52' 10"W). See above for additional details.

389 **Formation and Age**—Pysht Formation, between 30.5–26.5 Ma (Oligocene: late Rupelian-early
390 Chattian; Prothero et al., 2001; Velez-Juarbe, 2017).

391 **Range**—Oligocene of Washington, U.S.A.

392 **Differential Diagnosis**—Species of relatively small bodied odontocete with bizygomatic width
393 of about 220 mm (c. 333[1]), differing from other simocetids by the following combination of
394 characters: posterior wall of the antorbital notch formed by the lacrimal (c.16[1]; shared with
395 *Simocetus rayi* and Xenorophidae); mandible with a relatively straight profile in lateral view
396 (c.39[0]), differing from the more strongly arched mandible of *S. rayi*; mandibular condyle

397 positioned at about the same level as the alveolar row (c.46[1]); dorsal edge of orbit relatively
398 low (c.48[2]; shared with *Olympicetus avitus*, *Ashleycetetus planicapitis* and *Xenorophus* spp.);
399 dorsolateral edge of ventral infraorbital foramen formed by lacrimal (c.58[2]; shared with
400 *Archaeodelphis patrius*, *Albertocetus meffordorum* and *Inermorostrum xenops* Boessenecker et
401 al., 2017), differing from *Olympicetus* sp. 1 where it is formed by the maxilla, and *O. avitus*
402 where it is formed by the maxilla and lacrimal; posterior edge of zygomatic process forming
403 nearly a right angle with the dorsal edge of the process (c.145[0]); lack of a well-defined dorsal
404 condyloid fossa (c.157[0]; otherwise present on other simocetids); posterior process of the
405 periotic exposed on the outside of the skull (c.250[0]); tympanic bulla proportionately narrow
406 and long (c.252[0]; shared with *Echovenator sandersi* and *Cotylocara macei*), differing from the
407 shorter, wider bulla of *Olympicetus avitus* and *Olympicetus* sp. 1; moderately large bizygomatic
408 width (c.333[2]; shared with *S. rayi*), differing from the smaller size of *O. avitus* and
409 *Olympicetus* sp. 1, or the relatively larger Simocetidae gen. et sp. A; parietals not forming part of
410 the supraorbital processes, differing from *O. avitus* where they extend into the posteromedial part
411 of the process, nasals contacting the maxillae along their posterolateral corners; longer
412 paroccipital and postglenoid processes; teeth with more conical cusps, contrasting with the more
413 lanceolate ones of *O. avitus*; and, thyrohyals tubular and not fused to basihyal (c.336[0]).
414 **Etymology**—Combination of *thalasso-* from the Greek word ‘thalassa’ meaning ‘sea’ and *-odon*
415 from the Greek word ‘odon’ meaning ‘tooth’, in reference to the marine habitat of the species
416 and its particular tooth morphology.

417

418 **Description**

419 Description is based on the holotype (LACM 158720), which consists of a nearly complete skull
420 of an adult individual with articulated mandibles and preserving 18 teeth, cervical vertebrae and
421 hyoid elements (Figs. 6-13). Some of the preserved mandibular and maxillary teeth are in situ,
422 allowing for determination of associated, loose teeth. The estimated body length is ~2.15 m,
423 based on equation “i” for stem Odontoceti in Pyenson and Sponberg (2011). The terminology
424 used herein follows Mead and Fordyce (2009).

425 **Premaxilla**—The part of the premaxillae anterior to the premaxillary foramen is not preserved.
426 Each premaxillae preserve a single, small (diam. = 3 mm) foramen located far anterior to the
427 antorbital notch (c.70[1], 71[0], 72[0]; Fig. 6). The ascending process adjacent to the external
428 nares is divided by a long posterolateral sulcus (c.73[2]) and a short, incipient, posteromedial
429 sulcus (c.319[1]), both which extend from the premaxillary foramen, forming the lateral and
430 anteromedial limits of the premaxillary sac fossa (Fig. 6). The premaxillary sac fossae are flat to
431 shallowly concave, transversely narrow and anteroposteriorly long (c.69[0]; 320[0], 324[1]),
432 resembling the condition observed in *O. avitus*. The premaxilla forms the lateral edges of the
433 external nares and mesorostral canal (c.74[0]). Posterior to the premaxillary sac fossae, the
434 ascending process extends posteriorly as a transversely thin flange, reaching a level just beyond
435 the preorbital process of the frontal (c.75[2]), leaving a narrow gap where the premaxilla contacts
436 the nasal. In contrast, in *O. avitus* the ascending process extends farther posteriorly, to a point

437 closer to the middle of the supraorbital processes, separating the nasals from the maxillae (Velez-
438 Juarbe, 2017).

439 **Maxilla**—As preserved, the palatal surface is anteroposteriorly concave and transversely convex
440 to flat (c.17[0]). Anteriorly the vomer is exposed ventrally through an elongated window
441 between the maxillae as in *Simocetus rayi*; similarly, a pair of major palatine foramina are
442 located on each side at the proximal end of this opening (c.18[0]; Fig. 7C-D). Posteriorly, the
443 maxilla contacts the palatines along an anteriorly-bowed contact (c.20[0], 21[0]). The alveolar
444 row diverge posteriorly (c.23[0]); it is incompletely preserved anteriorly, but based on the
445 preserved dentition and visible alveoli, there were at least seven closely-spaced maxillary teeth,
446 with the most posterior six representing double-rooted P1-4, M1-2, with the most anterior of the
447 preserved alveoli representing an anteroventrally-oriented single rooted ?canine (c.24[4], 26[0];
448 Fig. 8). Posteriorly, the maxillary tooth row extends beyond the antorbital notch, forming a short
449 **infraorbital plate** (c.60[1]; Fig. 9). The ventral infraorbital foramen has an oval outline (15mm
450 wide by 9mm high) and is bounded laterally and dorsally by the lacrimal and ventrally and
451 medially by the maxilla (c.58[2], 59[0]; Fig. 9).

452 Proximally, the rostrum is wide, relative to the width across the orbits (c.7[1]) and the lateral
453 edges of the maxillae are bowed out, giving the antorbital notch a ‘V’-shaped outline (c.12[1];
454 Fig. 6). The surface of the maxillae anterior and anteromedial to the orbits is flat to shallowly
455 convex (c.66[0]), lacking the rostral basin observed in some xenorophids (e.g. *Cotylocara macei*;
456 Geisler et al., 2014). As in *O. avitus*, this surface has clusters of three to four anterior dorsal
457 infraorbital foramina with diameters ranging between 4-6 mm with the posteriormost foramen
458 located dorsomedial to the antorbital notches (c.65[3]). However, in contrast to *O. avitus* the
459 maxillae does not extend anterolaterally to form the posterior wall of the antorbital notch
460 (c.16[1]; Figs. 6, 8), thus more closely resembling the condition observed in *Simocetus rayi*.
461 Posteromedial to the antorbital notches, the maxillae extends over the supraorbital processes,
462 covering a little more than the anterior half of the processes and laterally to within 12 mm of the
463 edge of the orbit, while medially they contact the ascending process of the premaxillae and the
464 nasals, forming a gently sloping dorsolaterally-facing surface (c. 49[0], 77[1], 78[], 79[0], 80[0],
465 130[0], 308[1]; Figs. 6, 8).

466 **Vomer**—Dorsally the vomer forms the ventral and lateral surfaces of the **mesorostral fossa**,
467 which seems to have been dorsally open, at least for the length of the rostrum that is preserved,
468 and has a V- to U-shaped cross section, having a more acute ventral edge anteriorly (c. 5[0]; Fig.
469 6). Anteriorly, along the palatal surface of the rostrum, the **vomer is exposed through a narrow**
470 **elongate window mostly between the maxillae and the premaxillae distally**, resembling the
471 condition in *S. rayi* and possibly, *Olympicetus avitus* (Fig. 7C-D; Fordyce, 2002; Velez-Juarbe,
472 2017). The vomer is exposed again towards the posterior end of the palate along a diamond-
473 shaped window between the palatines and the pterygoids, resembling *S. rayi* (Fig. 7C-D;
474 Fordyce, 2002); similarly, the vomer seems to have been exposed posteriorly in *O. avitus*,
475 although the window may have been comparably smaller. The choanae are **not prepared** thus
476 making it impossible to determine the posterodorsal extension of the vomer (c. 191[?]).

477 **Palatine**—As in *Simocetus* and *Olympicetus avitus* the anterior edge of the horizontal plate of
478 the palatines extend to about 10 mm anterior to the level of the antorbital notches, forming the
479 shallowly concave proximal surface of the palate (Fig. 7C-D). The posterior edge of the palatines
480 are separated in the midline by the vomer even more than in *Simocetus* (Fig. 7C-D; Fordyce,
481 2002). Posterolaterally there is an elevated palatal crest that originates at the contact with the
482 pterygoid hamuli and extends anterodorsally on the orbital lamina, approximating, but not
483 reaching, the infundibulum for the sphenopalatine and infraorbital foramina, it instead become a
484 shallow groove that reaches the sphenopalatine foramen as in *O. avitus* (Figs. 7C-D, 8). The
485 orbital lamina of the palatine contacts the frontal dorsally to form the posteroventral edge of the
486 sphenopalatine foramen, and the maxilla anteriorly, and forms the ventral edge of the
487 infundibulum for the sphenopalatine and infraorbital foramina (Figs. 8-9). In posterolateral view,
488 the infundibulum has an oval outline, measuring 28 x 15 mm, while the rounded sphenopalatine
489 foramen has a diameter of about 8 mm. Ventrally and laterally, the palatines have a nearly
490 transverse contact with the pterygoids (c. 163[1]; Figs. 7C-D, 8), resembling the condition
491 observed in *O. avitus*, *Simocetus rayi* and *Archaeodelphis patrius*.

492 **Nasal**—The nasals are poorly preserved and seem to have formed the highest point of the vertex
493 (c. 114[?0], 124[0], 125[0], 312[0]; Figs. 6, 8) as in *Olympicetus avitus* and *Simocetus*.
494 Anteriorly, the nasals reach to about 24 mm beyond the antorbital notches, while posteriorly they
495 are in line with the preorbital process of the frontals (c. 81[3], 123[1]; Fig. 6). The nasals are
496 anteroposteriorly elongated, facing dorsally, forming a low transversely convex arch, are
497 dorsoventrally thin (<3 mm) and are separated posteriorly by the narial process of the frontal (c.
498 116[0], 118[0], 120[1], 121[2], 122[1], 312[0], 321[0]). The nasals seem to contact the ascending
499 process of the premaxillae for most of their lengths with only their posterolateral corners
500 contacting the maxilla, differing from *Olympicetus avitus* where the premaxilla extend beyond
501 the posterior edge of the nasals (Velez-Juarbe, 2017).

502 **Frontal**—Dorsally along the midline, the frontals are wedged between the maxillae and
503 posterior edge of the nasals forming a large semi-rectangular surface (c. 126[1]; Fig. 6). Aft to
504 this point, the frontals are shallowly depressed towards their contact with the parietals, forming a
505 saddle-like outline of the skull roof in lateral view, resembling the condition observed in *O.*
506 *avitus* (Fig. 8). The interfrontal suture is completely fused; dorsally the frontals form a broad, V-
507 shaped contact with the parietals, while its contact along the temporal surface is nearly vertical.
508 The supraorbital processes gently slope ventrolaterally from the midline (c. 47[0]), and only their
509 anterior half is covered by the ascending process of the maxillae (Fig. 6, 8). The preorbital
510 processes are rounded and only partially covered by the maxilla and are thus exposed dorsally;
511 anteriorly they contact the maxilla and the lacrimals anteroventrally. The postorbital processes
512 are blunt, longer and oriented posterolaterally and ventrally to a level nearly in line with the
513 lacrimals when viewed laterally (c. 62[0]; Fig. 8). The orientation of the postorbital processes
514 give the orbit a slight anterolateral orientation in dorsal view, while in lateral view, the orbits are
515 highly arched and positioned high relative to the rostral maxillary edge as in *O. avitus* (c. 48[2];
516 Figs. 6, 8). The posterior edge of the supraorbital process is defined by a relatively sharp

517 orbitotemporal crest that becomes blunter towards its contact with the orbital processes of the
518 parietals.

519 Ventrally, in the orbital region, the frontals contact lacrimals anterolaterally to form the anterior
520 edge of the orbits (Figs. 8-9). More medially the frontals contact the maxillae and palatines,
521 forming the posterodorsal border of the infundibulum for the sphenopalatine and infraorbital
522 foramina (Figs. 8-9). Medially, the optic foramen has an oval outline (~10 x 5 mm) and is
523 oriented anterolaterally; the posterior edge of the optic foramen and infundibulum is defined by a
524 low infratemporal crest (c. 63[0]; Fig. 9). As in *Simocetus rayi* and *O. avitus* a small (~3 mm
525 diameter) ethmoid foramen (sensu Fordyce, 2002) is located anterolateral to the optic foramen,
526 while a series of additional, smaller foramina (1-2 mm) are located more laterally.

527 **Lacrimal + Jugal**—Only a small, cylindrical portion of the proximal end of the jugal is
528 preserved, it is set in a close-fitting socket formed by the lacrimal anterodorsally, and the maxilla
529 anteriorly and ventrally (c. 54[0], 55[0]; Figs. 8-9). As preserved, the jugal is visible only in
530 lateral or ventral views, as dorsally it is covered by the lacrimal, and resembles the condition
531 observed in cf. *Olympicetus* sp. of Racicot et al. (2019). The lacrimals are enlarged and shaped
532 like a thick rod that covers the anterior surface of the preorbital processes of the frontals (c.
533 51[1], 52[0], 53[1]; Figs. 6, 8-9). The lacrimals are broadly visible in dorsal view as they are not
534 covered by the maxilla as in *Olympicetus avitus*, thus resembling the condition observed in
535 *Simocetus rayi*; ventrally their exposure is anteroposteriorly short relative to the length of the
536 supraorbital process of the frontal (c. 56[0]), but are elongated mediolaterally, forming the
537 dorsolateral and dorsal edges of the ventral infraorbital foramen (c. 58[2]), differing from *O.*
538 *avitus* where it is formed by the maxilla and lacrimal.

539 **Parietal**—The parietals are broadly exposed in dorsal view, with no clear indication of the
540 presence of an interparietal (c. 135[0], 136[1]; Fig. 6), although it is visible in some
541 ontogenetically young specimens that can be referred to *Olympicetus* (Racicot et al., 2019; see
542 discussion). Anteriorly in dorsal view, the parietals meet the frontals along a broad V-shaped
543 suture, with its anterolateral corners extending for a short distance along the base of the
544 postorbital processes of the frontals, although not as far as in *Olympicetus avitus*. Posterior to the
545 frontal-parietal suture there is a low incipient crest that gives the intertemporal region an ovoid
546 cross section (c. 137[1]), similar to the condition in *O. avitus* and *Simocetus rayi*. As in *O. avitus*,
547 the parietals contact the supraoccipital along an anteriorly convex suture when viewed dorsally.
548 The temporal surface of the parietal is flat to shallowly concave anteriorly, with a near vertical
549 suture with the frontal (c. 134[0]; Fig. 9) as it descends to form the posterior wall of the optic
550 infundibulum; the temporal surface of the parietal then becomes more inflated posteriorly and
551 posteroventrally where it contacts the squamosal and alisphenoid (Figs. 6, 8). The anteroventral
552 edge of the parietals form a semilunar notch that likely contacted part of the alisphenoid and the
553 dorsal lamina of the pterygoid, then continuing posteriorly to form part of the subtemporal crest.

554 **Supraoccipital**—The anterior edge of the supraoccipital form a semicircular arch when viewed
555 posteriorly and dorsally, extending as far anteriorly to nearly the anterior edge of the squamosal
556 fossa (c.140[0], 153[1]) as in *Olympicetus avitus* and *Simocetus rayi* (Figs. 6-7A-B). The

557 posterior surface is incompletely preserved, but seems to have had a low **sagittal crest** (c.156[?1],
558 311[?0]). The nuchal crest **are** oriented dorsolaterally (c.154[1]), curving posteriorly and
559 ventrally to meet the supramastoid crest of the squamosals (Figs. 6, 7A-B, 8).

560 **Exoccipital**—The occipital condyles have a semilunar outline and are **transversely and**
561 **dorsoventrally convex**, with sharp dorsal and lateral edges. Although the bone is poorly
562 preserved, there is no indication for the presence of well-defined dorsal condyloid fossae
563 (c.157[0]), differing from *Olympicetus avitus* (Fig. 7A-B). The surface lateral to the condyles is
564 shallowly convex transversely and the paroccipital processes **are** broad, oriented posteroventrally
565 to a point nearly, but not reaching the posterior edge of the condyles (c.198[2]; Fig. 6).

566 **Basioccipital**—The basioccipital is partially covered by part of the atlas posteriorly and hyoids
567 posteroventrally (Fig. 7). The basioccipital crest **are** oriented ventrolaterally, diverging
568 posteriorly at about an angle **of** between 60-70°, and **seem to** have been transversely narrow
569 (c.192[0]; 195[2]), with their posteroventralmost end forming a small flange as in *Simocetus*
570 *rayi* (c.194[2]; Fig 7C-D). No well-developed Rectus capitus anticus fossa is discernible on the
571 ventral surface (c.193[0]).

572 **Squamosal**—The zygomatic processes are partially eroded, more so on the left side, however, **its**
573 **general morphology** is conserved. The processes are oriented anteriorly (c.143[0]) and seems to
574 have been relatively long (c.189[?3]). In lateral view the dorsal edge of the zygomatic process is
575 greatly convex dorsally (c.144[0]), while ventrally **they are** strongly concave (c.151[0]) (Fig. 8).
576 The apex of the zygomatic process has a transverse cleft (best preserved on the right side;
577 c.335[1]; Fig. 8), which is present in the type of *Olympicetus avitus* as well as in **CCNHM 1000**,
578 and may as well be a unique feature of the genus (Racicot et al., 2019). Posteriorly the
579 sternomastoid fossa is nearly absent (c.145[0]), contrasting with the deeper fossa observed in *O.*
580 *avitus* and *Olympicetus* sp. A (see below). In dorsal view, the zygomatic processes **are**
581 mediolaterally broad, forming a transversely narrow and relatively shallow squamosal fossa as in
582 *O. avitus* (c.147[1]; Fig. 6). The floor of the squamosal fossa is slightly sigmoidal, **sloping gently**
583 towards its anterior end (c.148[1], 149[0]), and is bounded laterally and posteriorly by a fairly
584 continuous supramastoid crest (c.150[0]), which extends medially to join the nuchal crest (Fig.
585 6). Medially, the **squamous portion** is flat, with an interdigitated suture with the parietals that
586 slope **anteroventrally** at about 45° towards the anterior edge of the squamosal fossa and
587 subtemporal crest and **contacting** the alisphenoid. Posteroventrally, the postglenoid process is
588 long, more so than in *Simocetus rayi* and *O. avitus*, and anteroposteriorly broad, with near
589 parallel anterior and posterior borders that end in a squared-off ventral end (c.152[2]; Figs. 7C-
590 D, 8). Aft the postglenoid process, the external auditory meatus is deep and anteroposteriorly
591 broad (c.190[0]), bounded anteriorly by a low anterior meatal crest, that, as in *O. avitus*, seems to
592 have formed the posterior edge of a fossa for the reception of the sigmoid process of the
593 squamosal. The posttympanic process does not extend as far ventrally as the postglenoid process;
594 its ventral surface is **well** sutured to the posterior process of the tympanic bulla (Figs. 7C-D, 8).
595 In ventral view, the glenoid fossa is poorly defined, although medially there is a very shallow,
596 nearly indistinguishable tympanosquamosal recess (c.179[?1,2]), as in *O. avitus* and *S. rayi*.

597 Anteromedially the falciform process anteroposteriorly broad with a nearly square outline (about
598 15 mm by 15 mm; c.177[0]), contacting most of the anterior process of the periotic (fig. 10C). In
599 posterior view, the squamosal has a relatively small exposure lateral to the exoccipitals (c.
600 146[1]; Fig. 7A-B).

601 **Pterygoid**—In ventral view, the pterygoids form robust, cylindrical hamular processes that are
602 not excavated by the pterygoid sinus (c.173[1], 174[0]) and are separated anteriorly along the
603 midline by a diamond-shaped exposure of the vomer, resembling the condition observed in
604 *Simocetus rayi* (Fig. 7; Fordyce, 2002:fig. 4). The hamuli are long, extending posteriorly as far as
605 the level of the middle of the zygomatic processes (c.175[3]). Although not preserved, the lateral
606 lamina likely formed the anterior and lateral surfaces of the pterygoid sinus fossa. The dorsal
607 lamina extends dorsally, reaching the frontal, and, judging from the preserved sutures,
608 posteriorly, to join the parietal and alisphenoid, forming the roof of the sinus fossa as in
609 *Olympicetus avitus* (c.166[0]; Fig. 8-9). As in *Simocetus rayi*, the ventralmost point of the
610 pterygoid sinus fossa is at the base of the hamuli just anterior to the eustachian notch, suggesting
611 that the nasal passages were underlaid by the sinus fossa (Fig. 7C-D). The medial lamina forms
612 the deep eustachian notch, and bulges laterally at this point; posteriorly, it extends to contact the
613 basioccipital crests. The pterygoid sinus fossa is dorsoventrally broad (~45 mm high), and
614 somewhat compressed mediolaterally (~23 mm wide), extending forwards to the level of the
615 posterior edge of the supraorbital process of the frontal (c. 164[2]; Figs. 7C-D, 8-9).

616 **Alisphenoid**—Only small portions of the alisphenoids can be observed on both sides. In lateral
617 view, only a small portion of the alisphenoid is exposed on the temporal fossa, where it forms the
618 posteromedial part of the subtemporal crest (c.142[1], 166[0]) as in other *Olympicetus* (Velez-
619 Juarbe, 2017; see below).

620 **Orbitosphenoid/Optic Infundibulum**—The orbitosphenoid is fused with surrounding bones,
621 unlike the ontogenetically younger specimen of *Olympicetus avitus*. Within the optic
622 infundibulum, the foramen rotundum and orbital fissure seem to have a similar diameter, both
623 being transversely broader (~10 mm) than high (~6 mm) (Fig. 9), with the first located in a
624 slightly more posteromedial position, resembling the condition in *O. avitus* (Fig. 9). However, no
625 distinct groove for the ophthalmic artery is preserved in *Olympicetus thalassodon*, differing from
626 *Simocetus rayi*, *O. avitus* and *Olympicetus* sp. A (Fordyce, 2002:fig.13; Figs. X-X). The foramen
627 rotundum is not prepared, but is inferred that, as in *O. avitus*, it opens ventrolateral to the orbital
628 fissure, with the path for the maxillary nerve (V2) being bound ventrally by the pterygoid and
629 palatine (Fig. 9).

630 **Periotic**—Only a small portion is visible on the right side. The anterior process contacts the
631 falciform process anteriorly for about half its length. Posterior to this contact, a portion of the
632 anterior process is visible, as is the epitympanic hiatus, which is bounded posteriorly by a
633 prominent ventrolateral tuberosity (Fig. 10C).

634 **Tympanic Bulla**—Both bullae are still articulated with the cranium and mainly visible in ventral
635 view (Fig. 10). The tympanic bullae are transversely narrow and elongated (c.252[0]), differing
636 from the proportionately broader bullae of *Olympicetus avitus* and *O. sp. A* (see below). In

637 ventral view, the lateral surface is more convex and the ~~more~~ straight medial side, ~~anteriorly~~ it is
638 gently convex, with not indications of the presence of a spine (c.251[0]). The posterior surface of
639 the bullae is bilobed, being divided by a broad interprominential notch (c.267[1]) that is divided
640 by a transverse ridge (c.268[0]), differing from the bulla of *Olympicetus avitus*, but resembling
641 that of *Olympicetus* sp. A. Both posterior prominences are level with each other (c.270[0]), the
642 ventromedial keel forms a smooth curve posteriorly (c.253[0]), while more anteriorly it is poorly
643 defined as this surface is nearly flat (c.274[2], 275[?0]). The outer posterior prominence forms a
644 continuous curve along its length, connecting with the conical process.

645 A vertical, broad lateral furrow can be observed in lateral view (c.257[0], 258[0]), while more
646 dorsally the sigmoid process curves posteriorly at the base, and is nearly vertical and
647 perpendicular to the long axis of the bulla (c.259[0], 260[0]; Fig. 10B-C). Although not entirely
648 visible, the dorsal edge of the sigmoid process likely contacted the sigmoid fossa of the
649 squamosal (c.261[?0]). The posterior process is partially visible at its contact with the
650 posttympanic process and is visible in lateral view (c.250[0]; Figs. 7C-D, 8, 10A-B), and seems
651 to have had more or less the same thickness throughout its length (c.266[0]).

652 **Mandible**—Left and right mandibular rami are nearly in articulation with the skull and are only
653 missing coronoid processes and their distal ends, including the symphyseal region (Figs. 7C-D,
654 8). As preserved, the mandibles are nearly straight, gently arching dorsally at about mid length
655 (c.39[0], 43[1]; Figs. 7C-D, 8), differing from the highly arched mandible of *Simocetus rayi*
656 (Fordyce, 2002). Proximally, the bone seems to be thin, likely forming an enlarged mandibular
657 fossa (c.44[1]). Posterodorsally on the right side, the lateral edge of the condyle can be observed,
658 suggesting that its dorsal surface sits at a level at, or below the alveolar row (c.46[1]; Fig. 8).
659 Anteriorly, the right ramus preserved five double-rooted teeth in-situ, which are interpreted as
660 representing p3-4 and m1-3, while the left ramus preserves three, that are interpreted as m1-2
661 and p4 (Figs. 8-9, 11-12). Multiple mental foramina are longitudinally arranged along the rami
662 below the alveolar row; most are oval, ranging in size from 2 to 4 mm in height and up to 10 mm
663 long, with the more posterior ones connected by a fissure as in *Olimpicetus avitus* (Fig. 8; Velez-
664 Juarbe, 2017:fig.7A).

665 **Dentition**—Taking a conservative approach to the tooth count, it is interpreted as non-polydont
666 as in *Simocetus rayi* (Fordyce, 2002), although incipient polydonty cannot be entirely ruled out,
667 as it seems to be present on other stem odontocetes from the eastern North Pacific (e.g. LACM
668 140702; Barnes et al., 2001). Between the teeth and alveoli, the preserved upper and lower
669 dentition is interpreted to represent C, P1-4, M1-2 and p3-4, m1-3 (Figs. 8-9, 11-12). The teeth
670 are proportionately large, heterodont, multicusped, transversely flattened and nearly as high as
671 long (c.31[1], 314[0]), resembling the condition observed in postcanine teeth of *Olympicetus*
672 *avitus*, *Olympicetus* sp. A and *Simocetus rayi* (Figs. 8-9, 11-12). As in *Olympicetus avitus* and
673 *Simocetus rayi*, the postcanine teeth of *O. thalassodon* have a more concave buccal surface,
674 while being more convex lingually, with the apex of the crowns slightly recurved lingually; the
675 base of the crowns are ornamented with vertical striae extending apically from ecto- and
676 entocingula, particularly on the posteriormost upper teeth (c.27[1], 32[1], 33[0]; Figs. 11-12).

677 The crowns consist of a main apical denticle, and smaller accessory denticles along the mesial
678 and distal edges, both apical and accessory denticles are more triangular than the more lanceolate
679 ones observed in *O. avitus* (c.34[0]; 35[0]; Figs. 11-12; Velez-Juarbe, 2017). In double-rooted
680 teeth, the roots become fused proximally, with broad grooves on both, buccal and lingual sides
681 that extend to the base of the crowns, giving them an 8-shaped cross section as in *Simocetus rayi*
682 (Fordyce, 2002). In P4 and M1 the anterior root is cylindrical, tapering distally, while the
683 posterior roots are buccolingually broader and oblong in cross section, while in M2 this
684 condition is reversed, with the anterior root being transversely broader; the roots of the lower
685 teeth seem to be subequal in size, both being cylindrical and tapering distally.

686 The anteriormost end of the right maxilla has a single alveolus (diameter = 6mm) that curves
687 posterodorsally and is interpreted as that of a canine, which is separated by a short interalveolar
688 septum from two adjoining alveoli (each with a diameter ~7mm) for a double-rooted P1 (Figs. 8,
689 11B). The second (P2) and third (P3) upper premolars are missing on the left side and
690 incompletely preserved on the right; they are slightly higher than long, consisting of a main
691 denticle with at least two accessory denticles on the mesial and distal edges, resembling teeth
692 ‘ap1’ and ‘ap2’ of *O. avitus* (Velez-Juarbe, 2017:fig.7D-E, Q-R). Three closely associated teeth
693 that became disarticulated from the maxilla, but still joined by matrix, and three other loose
694 teeth, represent left and right P4, M1-2; these are more equilateral, being as long as wide, with
695 stronger lingual and labial cingula and ornamentation along the base of the crowns; P4 and M1
696 consist of a main apical denticle, with four distal and three mesial accessory denticles that
697 diminish in size towards the base (c.328[1], 329[2]; Figs. 11E-H, 12A-B, 12E-F), their overall
698 morphology resembles that of teeth ‘mo1’ and ‘mo2’ of *Olympicetus avitus* (Velez-Juarbe,
699 2017;fig.7M-N, Z-Aa). The second molar (M2) is the smallest of the series and the crown is
700 longer than tall, it consists of a main apical denticle, four distal and two mesial accessory
701 denticles, the apices of all denticles are slightly slanted distally (Figs. 11D, 11I, 12C-D). As in
702 *Simocetus rayi* and *Xenorophus sloanii*, the mesial and distal keels on the upper posterior
703 postcanines trend towards the buccal side of the teeth so that in occlusal view, the apical and
704 accessory denticles are arranged in an arch (Fordyce, 2002; Uhen, 2008). These characteristics
705 allow for the reassignment of some of the teeth of *Olympicetus avitus*, with teeth ‘mo1’ and
706 ‘mo2’ representing right and left M2, respectively, while ‘ap1’ and ‘ap2’ represent left upper
707 premolars (Velez-Juarbe, 2017:fig.7). An isolated single-rooted tooth is interpreted as a canine or
708 incisor (Fig. 12H-I). The crown is conical, with vertical striation along its lingual surface and a
709 buccal cingulum; anterior and posterior carinae seem to be present, with larger denticles along
710 the distal edge. Another isolated tooth adjacent to the posterior end of the left maxilla, seems to
711 represent a more anterior upper postcanine tooth (Fig. 12J). Overall, it resembles M2, but it's
712 mesial carina is partially damaged, so it is unclear if any accessory denticles were present, while
713 the distal carina contains three denticles that diminish in size basally; however, the denticles are
714 not recurved distally, and is larger than M2, but smaller than M1.

715 The preserved lower dentition includes p3-4, m1-3, and p4, m1-2 on the right and left mandibles,
716 respectively (Figs. 8, 11A-C, 12C). As with the upper premolars, p3-4, m1-3 have a triangular

717 outline, with mesial and distal carinae aligned vertically, not trending lingually as the upper
718 molars. Furthermore, in p3-4 and m1-2 the mesial carinae has two accessory denticles that are
719 much smaller than the apical denticle, while along the distal carinae there are three to four
720 accessory denticles, with the apical ones being nearly as big as the apical denticle, and then
721 diminish in size towards the base of the crown (Fig. 8, 11A-C, 12C). There is nearly no
722 ornamentation along the buccal side of the lower premolars and molars, with only a few
723 inconspicuous vertical striae, but no prominent cingulum, while lingually striae are more
724 prevalent, and a cingulum is present (Figs. 11A-C, 12G). As in the upper toothrow, m3 is the
725 smallest in the series, seemingly lacking accessory denticles on the mesial carina, and having
726 three subequal ones along the distal carina. As with the preceding teeth, ornamentation is nearly
727 absent on the buccal side (Fig. 11A). The lower postcanine dentition of *Olympicetus thalassodon*
728 then seems to be characterized by having less conspicuous ornamentation on the buccal side, and
729 more vertically aligned carinae, based on these characteristics, it is proposed that teeth ‘pp1’,
730 ‘pp2’ and ‘pp5’, ‘pp7’ of *Olympicetus avitus* (see Velez-Juarbe, 2017:fig.7F-G, J, L, S-T, W, Y)
731 represent lower anterior molars or premolars from the left and right side respectively.

732 **Hyoid**—Most of the hyoid elements are preserved in LACM 158720, including the basihyal,
733 stylohyals and thyrohyals (Fig. 13A-C). The basihyal has a rectangular, blocky outline, with both
734 ends expanded, forming broad, quadrangular rugose surfaces for the articulation of the paired
735 elements (stylo- and thyrohyals). The mid portion is subtriangular cross section; the dorsal
736 surface is shallowly concave transversely; the partial, left thyrohyal obscures the posteroventral
737 surface of the bone. The partial left and the complete right thyrohyals and stylohyals are
738 preserved (Fig. 13A-C). The thyrohyals are not fused to the basihyal and are fairly straight, with
739 a transversely oval cross section at mid-length; overall they are shorter, but more robust than the
740 stylohyals, and not flattened, wing-like as in derived mysticetes and odontocetes (c.336[0]; Fig.
741 13). The proximal articular surface has a rectangular outline, and the surface is rugose and
742 shallowly convex; distally, the shaft is twisted, so that the distal articular surface is nearly
743 perpendicular to the long axis of the proximal surface. The distal articular surface has a more
744 oval outline that is rugose and shallowly convex. The stylohyals are long and slender, and, on the
745 right side, nearly in articulation with the paroccipital process (Fig. 13A-B). Along the long axis
746 they are bowed laterally, with the shaft having a more flattened, oval cross section along its
747 length, with both, proximal and distal ends expanded, being overall, nearly identical to the
748 stylohyoid of *Olympicetus avitus* (Velez-Juarbe, 2017). The proximal end is transversely
749 expanded with a nearly flat, rugose articular surface; distally, the shaft becomes twisted, so that
750 the distal end is offset at about 45° from the proximal articular surface. The lack of fusion
751 between the thyrohyal and basihyal, and the cylindrical shape of the thyrohyal resembles the
752 condition observed in basilosaurids (e.g. *Durodon atrox* [Andrews, 1906], *Cyhiacetus*
753 *peruvianus* Martínez-Cáceres and de Muizon, 2011; Uhen, 2004; Martínez-Cáceres et al., 2017);
754 some stem mysticetes (e.g. *Mammalodon colliveri* Pritchard, 1939, *Fucaia buelli* Marx et al.,
755 2015, *Mystacodon selenensis* Lambert et al., 2017; Fitzgerald, 2010; Muizon et al., 2019); while
756 in more derived odontocetes (e.g., *Brygmophyseter shigensis* (Hirota and Barnes, 1995), *Kogia*

757 *breviceps* (Blainville, 1838), *Albireo whistleri* Barnes, 1984, *Kentriodon nakajimai* Kimura and
758 Hasegawa, 2019, *Tursiops truncatus* (Montagu, 1821); Fig. 13D-G) these bones are partially or
759 completely fused and the thyrohyals tend to be more flattened and plate- or wing-like
760 (Reidenberg and Laitman, 1994; Hirota and Barnes, 1995; Barnes, 2008; Johnston and Berta,
761 2011; Kimura and Hasegawa, 2019).

762 **Cervical Vertebrae**—The atlas, axis and C3-7 are partially preserved, and unfused (c.279[0],
763 280[0]; Fig. 14; Table 2). The dorsal arch of the atlas has a low, blunt middorsal ridge that
764 extends nearly the whole length of the arch. The vertebral foramen is broken, although it seems
765 to have occupied the same position as that of *Olympicetus avitus* (Velez-Juarbe, 2017). The
766 anterior articular facets are obscured as the atlas is still attached to the skull, while the posterior
767 facets have a reniform outline, and form a dorsoventrally elongate, smooth, flat surface that
768 extends dorsal to the articulation for the odontoid (Fig. 14A). On the ventral arch, the
769 hypapophysis that would have articulated with the odontoid is short as in *O. avitus* and unlike the
770 longer, more robust process of Simocetidae gen. et sp. A, and *Echovenator sandersi* (Churchill et
771 al., 2016). The transverse processes are gently oriented posterolaterally, and are divided into a
772 larger, more robust dorsal process and a smaller, knob-like ventral process that are divided by a
773 broad, rounded notch (c.278[2]; Fig. 14A). The neural canal has an oval outline.
774 The axis is missing the dorsal arch, the odontoid is short and blunt. The anterior articular surface
775 has a subtriangular outline forming a flat to shallowly concave surface that extends
776 anteroventrally, being continuous with the ventral surface of the odontoid (Fig. 14B). The
777 transverse processes are oriented posterolaterally, with a triangular outline when viewed
778 anteriorly, their ventral surface is anteroposteriorly broad, forming a flat surface that faces
779 ventrally and slightly posteriorly, with a sharp anterior edge (Fig. 14B-D). Dorsomedially, the
780 posterior surface of the transverse processes form a relatively deep, concave surface. Cervicals 3-
781 6 are missing their dorsal arches and transverse processes for the most part, while only a small
782 portion of C7 is preserved. The centra are anteroposteriorly flat and slightly wider than high, the
783 epiphyses are unfused (Fig. 14C-D). The transverse process of C3 is partially preserved and its
784 morphology is similar to that of the axis.

785

786 *OLYMPICETUS* sp. 1

787 (Figs. 15-19; Tables 1, 3, 6)

788 **Material**—LACM 124105, partial skull, including two partial teeth, left tympanic bulla and
789 right periotic; missing distal end of rostrum, zygomatic arches, parts of the neurocranium and
790 mandible. Collected by J. L. Goedert December 17, 1983.

791 **Locality and Horizon**—LACM Loc. 5123, Murdock Creek, Clallam Co., Washington, U.S.A.
792 (48° 09' 25"N, 123° 52' 10"W). See above for additional information from this locality.

793 **Formation and Age**—Pysht Formation, between 30.5–26.5 Ma (Oligocene: late Rupelian-early
794 Chattian; Prothero et al., 2001; Velez-Juarbe, 2017).

795 **Range**—Oligocene of Washington, U.S.A.

796

797 Description

798 The description is based solely on LACM 124105 and will focus on morphological characters
799 that differentiates from *Olympicetus avitus* and *O. thalassodon*. As with the type of *Olympicetus*
800 *avitus*, LACM 124105 seems to represent a subadult individual, showing some partially open
801 sutures. Multiple areas of the skulls show evidence of erosion (e.g. rostrum, skull roof), likely as
802 a result of wave action as specimens from this locality are usually recovered as concretions along
803 the beach.

804 **Premaxillae**—Only part of the left ascending process of the premaxilla is preserved (Fig 15).
805 The ascending process borders the external nares as it ascends towards the vertex (c.74[0]),
806 however, its incomplete preservation posterior to the nasals does not permit identification of its
807 posteriormost extent. A relatively deep sulcus extends along its anterior border which is
808 consistent with the placement and morphology of the posterior extent of the posterolateral sulcus
809 in *Olympicetus avitus* (c.73[2]; Fig. 15; Velez-Juarbe, 2017).

810 **Maxilla**—Only part of the rostral portion of the maxilla is preserved (Figs. 15-17). Ventrally, the
811 palatal surface is incompletely preserved along the midline and along the alveolar rows,
812 however, the parts that are preserved indicate that it was transversely convex, with the alveolar
813 rows slightly more elevated. Posteriorly, the contact between the maxillae and palatines is bowed
814 anteriorly (c.20[?0], 21[1]; Fig. 16) as in other *Olympicetus*. The alveolar row, although
815 incompletely preserved, diverged posteriorly, and had at least three pairs of closely-spaced,
816 double-rooted postcanine teeth (c.23[0], 26[0]). Based on the preserved posterior border of the
817 alveolar row, it seems that at least a short maxillary infraorbital plate was present (c.60[1]). In
818 posteroventral view, the ventral infraorbital foramen has an oval outline (~12 mm wide by 9 mm
819 high); its dorsolateral edge is formed by the maxilla, dorsomedially by the frontal, and ventrally
820 and ventromedially by the maxilla (c.58[0], [59[0]).

821 In dorsal view, the rostrum seems to have been fairly wide (c.7[1]; Fig. 15). At the base of the
822 rostrum, the maxillary surface faces dorsolaterally, and is shallowly convex to flat as it ascends
823 over the supraorbital processes of the frontal; thus as in other species of *Olympicetus*, it lacks a
824 rostral basin (c.66[0]; Fig. 15). At the base of the rostrum, there are at least three anterior dorsal
825 infraorbital foramina ranging in diameter between 2-5 mm, with a fourth, more posterior
826 foramen, dorsomedial to the antorbital notch (c.65[3]; Figs. 16, 17). The maxillae are eroded at
827 the level of the antorbital notch, so it is uncertain if these formed part of the posterior wall of the
828 notch as in *Olympicetus avitus*. The ascending process of the maxillae partially covers the
829 supraorbital processes of the frontal, extending posteriorly beyond the anterior half of the
830 processes, and posteromedially, coming into contact with the frontals and forming a gently
831 sloping surface towards the edge of the orbits, but not reaching its borders (c.49[0], 77[1], 78[2],
832 79[0], 80[0], 130[0], 308[1]; Fig. 15).

833 **Vomer**—The vomer is mostly missing anterior to the antorbital notches and eroded
834 anteroventrally, nevertheless, it is evident that it formed the lateral and ventral surfaces of the
835 mesorostral fossa. Ventrally, the vomer likely was exposed through a diamond-shaped window
836 towards the posterior end of the palate as in other simocetids (Fig. 16). Dorsal and posterodorsal

837 to this point the vomer forms the nasal septum, forming the medial walls of the choanae. From
838 the posterior palatal exposure, the vomer gently slopes posterodorsally, to form a triangular,
839 horizontal plate extending over the **still open**, basisphenoid-presphenoid **contact**, but not reaching
840 as far posterior as the fused basisphenoid/basioccipital contact (c.191[0]; Fig. 16). The horizontal
841 plate of the vomer has a **triangular** outline, contacting the dorsal laminae of the pterygoids along
842 its anterolateral end (Figs. 16-17).

843 **Palatine**—Only some very small fragments of the right palatine are preserved. The contact
844 between the palatines and maxilla **seems to have been bowed anteriorly** (c.20[?0], 21[1]; Figs.
845 16-17). Posterodorsally, a fragment of the orbital lamina of the palatine reaches the frontal,
846 forming part of the infundibulum for the sphenopalatine and infraorbital **foramen**, as well as the
847 posterior border of a round (~5 mm diameter) sphenopalatine foramen (Fig. 17). The
848 infundibulum has an oval outline, being broader than high (20 mm x 10 mm), and is bounded
849 dorsally by the frontal and lacrimal, and the maxilla ventrally and ventrolaterally (Fig. 17).

850 **Nasal**—Although incompletely preserved, the nasals seem to have been the highest point of the
851 vertex, were longer than wide and dorsoventrally thin, as in other simocetids (c.114[0], 116[0],
852 118[?0], 124[0], 125[0], 312[0]; Fig. 15). Along their posterior border, they are separated by the
853 narrow, narial process of the frontal (Fig. 15). The anterior edge of the nasals is incompletely
854 preserved, but extended far forward of the anterior edge of the supraorbital processes, **while**
855 **posteriorly they reach a level in line with midpoint of the supraorbital processes** (c.81[3], 123[1];
856 Fig. 15).

857 **Frontal**—As in other *Olympicetus*, there is a wedge-shaped exposure of the frontal along the
858 midline, surrounded by the maxilla laterally and nasals anteriorly, although poor preservation of
859 the surrounding bones does not allow precise determination of **size** relative to the nasals (Fig.
860 15). Along the midline, the bone is poorly preserved, although it does seem like the frontal are
861 lower than the nasals, preserving the saddle-like profile (in lateral view) seen in other species of
862 *Olympicetus*. Posteriorly, the frontal-parietal suture seems to have been broadly V-shaped
863 dorsally, and sinusoidal in the temporal region, with no intervention of the parietals into the
864 supraorbital processes. Laterally, the supraorbital processes slope very gently ventrolaterally
865 (c.47[?0]). **Dorsally, the maxillae only cover the supraorbital processes to a point beyond their**
866 **mid-point, but do not extend laterally over the orbit (c.78[2]), leaving the preorbital and**
867 **postorbital processes broadly exposed dorsally** (Fig. 15). Anteroventrally, the preorbital
868 processes **contact** the lacrimal. The postorbital processes are incompletely preserved, but seem to
869 have been relatively short, robust, and oriented posteroventrolaterally (Fig. 15). **In lateral view**
870 **the dorsal edge of the orbit is highly arched, but positioned at a lower position (c.48[1]), relative**
871 to the lateral edge of the rostrum, than is observed in *Olympicetus avitus* or *O. thalassodon*. A
872 low, sharp temporal crest extends anterolaterally from near the frontal/parietal suture and into the
873 posterodorsal and dorsal surface of the supraorbital process (c.132[2]; Fig. 15), differing from
874 the condition in other *Olympicetus*.

875 Ventrally, the frontal **contact** the lacrimal anteroventrally, and the maxilla and/or palatine more
876 medially, resulting in the frontal forming part of the posterodorsal edge of the infundibulum for

877 the ventral infraorbital and sphenopalatine foramina (Figs. 16-17). The optic foramen is partially
878 covered by sediment, its general orientation seems to be anterolateral, with its posterior border
879 being defined by a low, but sharp infratemporal crest (c.63[0]). Similar to other simocetids, a
880 small (~3 mm diameter) ethmoid foramen is anterolateral to the optic foramen, and is
881 accompanied by four to five smaller (1-2 mm) foramina located along the dorsolateral roof of the
882 orbit (Figs. 16-17).

883 **Lacrimal + Jugal**—Only a small portion of the jugal is preserved, but it is evident that it was
884 not fused with the lacrimal (c.54[0], 55[0]; Fig. 17). The portion of the jugal that is preserved is
885 stout and cylindrical, tapering medially, and wedged between the lacrimal and maxilla, which
886 excludes it from forming part of the ventral infraorbital foramen (Fig. 17). The lacrimals are
887 large, and rod-like, but with a relatively small ventral exposure (c.51[1], 56[0]). It contacts the
888 preorbital process of the frontal anteroventrally, tapering medially, and seems to have been
889 exposed anteriorly, forming part of the posterior wall of the antorbital notch, but not extending
890 dorsally onto the supraorbital process (c.52[0]; Fig. 15, 17).

891 **Parietal**—the parietals are exposed dorsally, but badly eroded (c.135[0], 136[?]; Fig. 15). The
892 parietals contact the frontal along a broad, V-shaped suture, but differ from other species of
893 *Olympicetus* in that they do not extend into the base of the supraorbital processes. In cross
894 section through the intertemporal region, the parietals seem to have an ovoid outline (c.137[?1]),
895 resembling the condition in other *Olympicetus*. Along the temporal surface the parietal has a
896 sinuous suture with the frontals anteriorly, and the temporal surface becomes more inflated
897 posteriorly towards its contact with the squamosal and alisphenoid (Fig. 17). Ventrally, the
898 parietal has an internal projection that contacts the squamosal medial to the periotic fossa,
899 constricting the cranial hiatus as in other simocetids (c.184[2]; Fig. 16).

900 **Supraoccipital**—The supraoccipital is only partially preserved, with the exception of its
901 dorsolateral borders. The lambdoidal crests are sharp, directed dorsolaterally and only slightly
902 overhanging the temporal fossa (c.154[1]; Fig. 15), curving posteroventrally to join the
903 supramastoid crest of the squamosal.

904 **Exoccipital**—Generally poorly preserved. Dorsal to the remaining parts of the right occipital
905 condyle, there is what seems to be a shallow dorsal condyloid fossa (c.157[?1]). The surface
906 lateral to the condyles is flat to shallowly convex.

907 **Basioccipital**—As preserved, the basioccipital crests seem to have been relatively thick
908 transversely (c.192[?1]) and oriented posterolaterally, at about an angle of 45 degrees (c.195[3];
909 Fig. 16). The rest of the ventral surface is incompletely preserved.

910 **Squamosal**—The zygomatic processes are incompletely preserved. Posteromedially, the
911 sternomastoid fossa forms a distinct emargination that is overhung dorsally by the supramastoid
912 crest much more than in *Olympicetus avitus* (c.145[1]; Fig. 15). The supramastoid crest seems to
913 have been continuous with the lambdoidal crest (c.150[0]). The squamous portion contacts the
914 parietal along an anteroventrally sloping interdigitated suture, meeting the alisphenoid to form
915 part of the subtemporal crest. Ventrally, the squamosal is heavily eroded, and only a small

916 portion of the periotic fossa is preserved, where it contacts the medial extension of the parietal
917 (Fig. 16).

918 **Pterygoid**—Most of the pterygoid is missing on both sides of the skull. A portion of the dorsal
919 lamina extends posterodorsally towards the parietal and contributes to the posteroventral edge of
920 the optic infundibulum as in *Olympicetus avitus* (Fig. 17). As preserved, the pterygoid sinus
921 fossa is anteroposteriorly longer than wide, and is located entirely anterior to the **foramen ovale**
922 (c.164[2], 169[0]; Figs. 16-17).

923 **Alisphenoid**—As in *Olympicetus avitus*, the alisphenoid forms the posterodorsal surface of the
924 pterygoid sinus fossa (Figs. 16-17). The medial and posterior ends of the bone are incompletely
925 preserved or eroded on both sides, making it difficult to determine the position of the alisphenoid
926 squamosal suture or the path of the mandibular nerve (V3). On the temporal wall, the exposure
927 of the alisphenoid is limited to a small sliver, as it is mostly overlapped by the parietal and the
928 squamosal (c.142[1]; Fig. 17).

929 **Basisphenoid**—Posteriorly the basisphenoid is fused with the basioccipital, while anteriorly its
930 **contact** to the presphenoid (sphenoidal synchondrosis) is still open, resembling the growth stage
931 of the type of *Olympicetus avitus* (Velez-Juarbe, 2017). The ventral surface is flat, and covered
932 by the horizontal plate of the vomer (Fig. 16).

933 **Optic Infundibulum**—The optic infundibulum is a slightly sinusoidal opening bounded by the
934 frontal anteriorly and dorsally, parietal posteriorly, pterygoid ventrally and anteroventrally (Fig.
935 17). The optic foramen, orbital fissure and foramen rotundum are still partly covered by
936 sediment. The frontal forms most of the borders of the optic foramen anterodorsally, while
937 posteroventrally the foramen rotundum was bounded laterally by the parietals and floored by the
938 pterygoid. The anteroventral edge of the parietals that forms part of the infundibulum, has a
939 narrow groove that trends anterodorsally, and would have carried the ophthalmic artery,
940 resembling the condition in *Simocetus rayi* and *Olympicetus avitus* (Fig. 17; Fordyce, 2002;
941 Velez-Juarbe, 2017). While along the ventral edge of the infundibulum, the pterygoid has a
942 distinct, but shallow groove, that would have presumably carried the maxillary nerve (V2),
943 extending along its dorsolateral surface and diverging slightly over its lateral surface anteriorly
944 (Fig. 17).

945 **Malleus**—The left **malleus** is still **articulated** with the corresponding tympanic (Fig. 18). The
946 head has a semicircular outline, with paired facets for articulation with the incus, that are
947 oriented at about 90 degrees to each other; the more anterior facet is about **as** twice as large as
948 the posterior one as in *Olympicetus avitus* (Fig. 18; Velez-Juarbe, 2017). The **tubercle** is
949 relatively large, nearly as long as the head (c.199[0]; Fig. 18). The **manubrium** is prominent and
950 slightly recurved posteroventrally (Fig. 18). The anterior process is fused laterally to the
951 tympanic, dorsally forming a continuous surface with the malleolar ridge, while its ventral edge is
952 shelf-like, **together** forming a deep, narrow sulcus for the chorda tympani (Fig. 18A, C, E).

953 **Tympanic Bulla**—Only the left tympanic bulla is preserved (Fig. 18), but missing its posterior
954 process, overall it closely resembles in size and morphology that of *Olympicetus avitus* (Velez-
955 Juarbe, 2017). In dorsal or ventral view, the bulla has a heart-shaped outline, being relatively

956 short and wide (c.252[1]), unlike the larger and transversely narrower bulla of *Olympicetus*
957 *thalassodon* (Figs. 10, 18). The lateral surface is broadly convex, while ~~medially it~~ is straight; the
958 posterior prominences gives the bulla a bilobed outline posteriorly while anteriorly, the lateral
959 surface converges medially more steeply than the medial surface along a smooth curve, ~~there is~~
960 no indication of the presence of an anterior spine (c.251[0]). Posteriorly, a broad
961 interprominential notch extends from the level below the elliptical foramen, **continuing along the**
962 **ventral surface of the bulla** for only about a third of its length (c.267[0]). The interprominential
963 notch is divided by a transverse ridge (c.268[0]; Fig. 18D), resembling the condition observed in
964 *Olympicetus thalassodon*, ~~differing~~ from that of *O. avitus*, which does not have an
965 interprominential ridge. The inner and outer prominences extend posteriorly to nearly the same
966 level (c.270[0]). The ventromedial keel is poorly defined, forming a smooth curve around the
967 posterior part of the involucrum, its posteromedial surface just slightly bulging farther medially
968 than the rest of the involucrum (c.253[0], 274[2], 275[0], 276[0]). The elliptical foramen seems
969 to have been narrow, and nearly vertical (c.262[0]).

970 In lateral view, the ventral edge of the bulla is nearly flat (c.269[0]), differing from the more
971 broadly concave ventral margin observed in some xenorophids, like *Albertocetus meffordorum*
972 (Uhen, 2008). The ventrolateral keel forms a blunt ridge that descends ventrolaterally from the
973 conical **pyramidal** process. The lateral furrow is nearly vertical, forming a relatively broad sulcus
974 (c.257[0], 258[0]; Fig. 18B). Dorsally, the sigmoid process is vertical and perpendicular to the
975 long axis of the bulla (c.259[0]), with its posterior edge curving anteriorly along a smooth curve
976 (c.260[0]). The malleolar ridge extends obliquely from the anteromedial base of the sigmoid
977 process towards the dorsalmost extension of the lateral furrow. A narrow, dorsally open sulcus
978 for the chorda tympani extends anteriorly for a length of 17 mm along the dorsomedial edge of
979 the outer lip, originating at the junction between the anterior process of the malleus and the
980 malleolar ridge (Fig. 18A, C, E). The anterodorsal crest descends steeply towards the anterior edge
981 of the bulla.

982 In medial view the dorsal and ventral edges of the involucrum gradually converge towards the
983 anterior end of the bulla (c.271[0]; Fig. 18A). The involucrum has numerous, faint vertical ridges
984 (c.272[1]), differing from the deeper grooves observed in xenorophids, like *Albertocetus*
985 *meffordorum* (Uhen, 2008).

986 **Periotic**—Only the right periotic is preserved (Fig. 19A-H) and is overall very similar to that of
987 **CCNHM 1000** described by Racicot et al. (2019). The anterior process is oriented anteriorly and
988 short relative to the length of the cochlea, with its anteroventral and anterodorsal ends being
989 bluntly pointed, ~~that~~ together gives it a nearly **squared-off outline** (c.201[0], 202[0], 204[2]; Fig.
990 19C-D). In medial view, the apex of the anterior process is slightly deflected ventrally, **forming a**
991 **slightly convex to flat surface** (c.203[1], 205[0]; Fig. 19C-D). In lateral view, at the base of the
992 anterior process there is a shallow, C-shaped sulcus that begins near the **anterodorsal** edge,
993 curves posteroventrally towards the lateral tuberosity, then ~~curving~~ ~~anterodorsally~~, ~~that~~ is
994 interpreted as a combined anteroexternal+parabullary sulcus (sensu Tanaka and Fordyce, 2014;
995 Fig. 19G-H). This condition resembles that of other early odontocetes such as *Waipatia*

996 *maerewhenua* Fordyce, 1994, *Papahu taitapu* Aguirre-Fernández and Fordyce, 2014, and
997 *Notocetus vanbenedeni* Moreno, 1892, but differs from others like *Otekaieka marplei* (Dickson,
998 1964) where these sulci are separate, and from the much deeper sulcus in *P. taitapu* (Tanaka and
999 Fordyce, 2014; Viglino et al., 2022). In cross-section, the anterior process is ovoid, being taller
1000 (~14 mm) than wide (~9 mm) (c.209[1]). The anteroventral surface of the anterior process has as
1001 well-defined anterior bullar facet (c.210[3]; Fig. 19E-F). Posterior to the anterior bullar facet, the
1002 fovea epitubaria forms a smooth curve that is interrupted by a prominent lateral (ventrolateral)
1003 tuberosity (c.212[1]). The lateral process has a triangular outline in ventral view, but does not
1004 extend as far laterally as in other stem odontocetes such as *Cotylocara macei* (Geisler et al.,
1005 2014), being instead barely visible in dorsal view. A similarly, broadly arched epitympanic
1006 hiatus lies posterior to the lateral tuberosity and anterior to the base of the posterior process
1007 (c.213[1]). Posteromedial to the epitympanic hiatus, is a small (diameter: ~2 mm) rounded fossa
1008 incudis, while anterior to it and medial to the lateral tuberosity is a broad (diameter: ~6 mm),
1009 circular malleolar fossa (c.214[1], 215[0]; Fig. 19E-F). The lateral surface of the periotic is
1010 generally smooth with the exception of the posterior process, whose lateral surface is rugose
1011 (c.217[2]; Fig. 19G-H). Medially, the anterior process is separated from the cochlea by a well-
1012 defined groove (anterior incisure, *sensu* Mead and Fordyce, 2009) that extends anterodorsally,
1013 and marks the origin for the tensor tympani muscle (c.218[1]).
1014 In dorsal view, a low crest delimits the dorsolateral surface of the periotic, it extends from the
1015 low pyramidal process towards the anterodorsal spine of the anterior process (Fig. 19A-B).
1016 Medial to this crest is an elongated depression, the suprimeatal fossa, which is about 13.5 mm
1017 long by 7 mm wide, and around 1.5 mm deep (Fig. 19A-B). The fundus of the internal acoustic
1018 meatus is funnel-shaped, with an oval outline, delimited by a low ridge (c.235[0]; 236[0]). The
1019 area cribosa media and the spiral cribriform tract are separated by a very low ridge, these two are
1020 in turn separated from the superior vestibular area (previously called the foramen singulare;
1021 Ichishima et al., 2021) by a low transverse crest that lies about 3 mm below the upraised rim of
1022 the internal acoustic meatus, while its separation from the dorsal opening of the facial canal by a
1023 ridge that is slightly lower (~4 mm from the edge of the rim) (c.237[2]; Fig. 19A-B). The
1024 proximal opening of the facial canal has an oval outline and located anterolateral to the spiral
1025 cribriform tract (c.238[0], 239[1]); anterodorsally it is bridged, forming a “second” foramen,
1026 which is smaller and rounded (Fig. 19A-D), resembling the condition observed in other early
1027 odontocetes, such as *Waipatia maerewhenua*, and similarly, it is interpreted as the foramen for
1028 the greater petrosal nerve (Fordyce, 1994). The endolymphatic duct (vestibular aqueduct) is slit-
1029 like (~4 mm long by 1 mm wide), and located posterolateral to the internal acoustic meatus, just
1030 below the more vertical posterior surface of the pyramidal process, and separated from the
1031 fenestra rotunda by a very wide distance (c.230[3]; Fig. 19A-D). In contrast, the perilymphatic
1032 duct (cochlear aqueduct) is rounded (diameter = 3mm) and located posteromedial to the internal
1033 acoustic meatus and medial to the endolymphatic duct, and broadly separated from the fenestra
1034 rotunda (c.228[1], 229[2]). A small, curved depression posteroventral to the endolymphatic duct
1035 is interpreted as a shallow stylomastoid fossa (c.225[1]). The dorsomedial surface of the cochlear

1036 portion has a shallow depression that accentuates the raised medial rim of the internal acoustic
1037 meatus. In medial view, the cochlea is relatively flat (maximum height ~11 mm), its
1038 ventromedial surface is anteroposteriorly convex and a low, faint ridge extends along its
1039 ventrolateral end (c.221[0]; Fig. 19C-F). In ventral view, the cochlear portion has a
1040 subrectangular outline (c.219[1], 220[1], 222[1]). Posteriorly, the fenestra rotunda is located
1041 towards the lower half of the posterior surface, and it is wider than high (4 x 2 mm), with a
1042 kidney-shaped outline (c.223[0]). Posterolateral to the fenestra rotunda, the caudal tympanic
1043 process projects farther posteriorly than the rest of the posterior surface of the cochlea, although
1044 it is not as prominent as that of other simocetids (i.e. CCNHM 1000; Racicot et al., 2019), and its
1045 ventral and posterior borders intersect along a curved edge (c.226[1]; Fig. 19C-F). Ventrally, the
1046 foramen ovale is longer than wide (4 x 3 mm), and located towards the posterior half of the
1047 cochlea. The ventral opening of the facial canal (~2 mm in diameter) is lateral to the foramen
1048 ovale, and are separated by a sharp crest. The facial canal opens posteroventrally, and continues
1049 as a groove that merges with the stapedia muscle fossa at the base of the posterior process; the
1050 fossa is deep and rounded, with its posterodorsal edge nearly in line with the fenestra rotunda
1051 (c.224[0]).

1052 The posterior process is short and robust, with its long axis is oriented posterolaterally (c.246[1],
1053 247[1], 249[0]; Fig. 19A-B, E-F). Proximally, the lateral surface of the posterior process is
1054 rough, with an irregular, near vertical ridge interpreted here as a poorly-developed articular rim
1055 (c.240[1]), resembling the condition in other simocetids (i.e. CCNHM 1000) and early
1056 odontocetes like *Notocetus vanbenedeni*, and differing from the more prominent articular rim
1057 observed in platanistids (Muizon, 1987; Racicot et al., 2019; Viglino et al., 2022; Fig. 19A-B).
1058 the dorsal edge of the posterior process forms a straight line (c.248[0]). The posterior bullar facet
1059 has a kite-shaped outline, its surface is smooth and shallowly concave transversely (c.242[0],
1060 243[0]); the edges of the facet are sharp, with the exception of the posteromedial edge which is
1061 rounder (c.244[0]).

1062 **Dentition**—Only two, incompletely preserved teeth are associated with LACM 124105 (Fig.
1063 19I-L). Both are postcanine teeth, with striated enamel and ecto- and entocingula and denticles
1064 (c.27[1], 32[1] 33[0], 35[?1]). As in other simocetids, the buccal surface of the crowns are more
1065 concave. The roots are long and conical, becoming fused proximally. Tooth PCa (Fig. 19I, K)
1066 measures 12 mm long by 6 mm wide, while tooth PCb (Fig. 19J, L) measures 9 mm high and 6
1067 mm wide.

1068 **Remarks**—LACM 124105 shows multiple diagnostic features with the other named species of
1069 *Olympicetus*, such as having a broadly open temporal fossa, unfused lacrimal/jugal (c.54[0]),
1070 lacking a maxillary foramen (c.76[0]), and maxilla covering only about the anterior half of the
1071 supraorbital process (c.77[1]). However, it does differ by having a more sharply defined
1072 infratemporal crest, orbit at a lower position relative to the edge of the rostrum (c.48[1]),
1073 dorsolateral edge of ventral infraorbital foramen formed by the maxilla (c.58[0]), and more
1074 notably, the lateral end of the temporal crest extends along the posterodorsal surface of the
1075 supraorbital process of the frontal (c.132[2]; Fig. 15). These differences are considered to be

1076 species-related, and not the result of ontogenetic change as this specimen shows a similar growth
1077 stage as the type of *Olympicetus avitus* (LACM 149156; Vélez-Juarbe, 2017). Nevertheless,
1078 because of its incomplete preservation, it is preferably left in open nomenclature until better
1079 material belonging to this taxon is identified.

1080

1081 Discussion

1082 While particular attention has been paid to Oligocene mysticetes from the North Pacific over the
1083 last few decades (e.g. Barnes et al., 1995; Okazaki, 2012; Marx et al., 2015; Peredo et al., 2018;
1084 Solis-Añorve et al., 2019; Hernández-Cisneros, 2022; Hernández-Cisneros and Nava-Sánchez,
1085 2022), the same cannot be said with regards to the odontocetes. Oligocene odontocetes from
1086 around the North Pacific are not entirely missing from the scientific literature and have been
1087 mentioned multiple times, often identified informally as “non-squalodontid odontocetes”,
1088 “agorophiid” or “*Agorophius*-like” (see Whitmore and Sanders, 1977; Goedert et al., 1995;
1089 Barnes, 1998; Barnes et al., 2001; Fordyce, 2002; Hernández Cisneros et al., 2017). However,
1090 given their importance, most of these have yet to be properly described and our understanding of
1091 species richness and relationships between Oligocene odontocetes from the North Pacific is not
1092 fully understood.

1093 The first of these taxa to be described was *Simocetus rayi* from the early Oligocene Alsea Fm. of
1094 Oregon which was placed in its own family, Simocetidae (Fordyce, 2002). Since then, only two
1095 other North Pacific Oligocene odontocetes had been named, specifically, the platanistoid
1096 *Arktocara yakataga* from the Oligocene Poul Creek Fm. in Alaska, which is likely one of the
1097 earliest crown odontocetes, and the stem odontocete *Olympicetus avitus* from the Pysht Fm. in
1098 Washington (Boersma and Pyenson, 2016; Vélez-Juarbe, 2017). More recently, Racicot et al.
1099 (2019) described a neonatal skull (CCNHM 1000) from the Pysht Fm. in Washington, that
1100 closely resembles *Olympicetus avitus*, but did not group with *Simocetus rayi* nor with *O. avitus*,
1101 and instead all three taxa occupied different positions outside of crown odontocetes (Racicot et
1102 al., 2019).

1103 Herein, the description of three additional specimens from the mid-Oligocene Pysht Formation in
1104 Washington have potentially clarified the relationship between stem odontocetes from the North
1105 Pacific. The phylogenetic analysis including these new specimens, resulted in 36 most
1106 parsimonious trees 3649 steps long, with retention index (RI) = 0.520 and consistency index (CI)
1107 = 0.182. Other statistical values are shown in the strict consensus tree (Fig. 20). Based on these
1108 results, Simocetidae now seem to form a monophyletic group that includes *S. rayi*, CCNHM
1109 1000, *Olympicetus* spp. and a large unnamed simocetid (Fig. 20). Furthermore, the phylogenetic
1110 analysis recovered CCNHM 1000 as part of the Simocetidae, differing from the analysis of
1111 Racicot et al. (2019) where it was recovered at the base of a clade including all odontocetes, with
1112 the exception of Xenorophidae. As discussed by Racicot et al. (2019) CCNHM 1000 does
1113 resemble *Olympicetus avitus*, more specifically, based on the new specimens described here, it
1114 shares with *Olympicetus* spp. having closely-spaced posterior buccal teeth (c.26[0]), buccal teeth
1115 with ecto- and entocingula (c.32[1], 33[0]), presence of a small maxillary infraorbital plate

1116 (c.60[1]), and the presence of a transverse cleft on the apex of the zygomatic process (c.335[1]),
1117 amongst others. However, CCNHM 1000, does show some dental characteristics that sets it apart
1118 from *O. avitus* as discussed by Racicot et al. (2019), and others that differentiates it from other
1119 specimens of *Olympicetus*, such as having a relatively lower position of the orbit (c.48[1]; shared
1120 with *S. rayi* and *Olympicetus* sp.), 63[1], presence of an interparietal (c.136[0]), a more anterior
1121 position of the apex of the supraoccipital (c.140[1]), and a very low lambdoidal crest (c.154[2]).
1122 Some of these characters, such as the position of the apex of the supraoccipital and the
1123 morphology of the lambdoidal crest are also observed in the neonate skull referred to *O. avitus*,
1124 suggesting that these characters change ontogenetically, with neonatal individuals displaying
1125 more plesiomorphic conditions. Along these same lines, the presence of a distinct interparietal in
1126 CCNHM 1000 is considered as another plesiomorphic character, that when combined with the
1127 other characters mentioned previously, it is suggestive that this may account for the more basal
1128 position of CCNHM 1000 in the phylogenetic analysis (Fig. 20). Besides this, it seems clear that
1129 CCNHM 1000 should be regarded as a neonate of *Olympicetus* sp.
1130 The inclusion of CCNHM 1000 has some interesting implications for Simocetidae. Racicot et al.
1131 (2019) described the inner ear morphology of CCNHM 1000 showing that it does not have the
1132 capability of ultrasonic hearing, which is suggestive that other taxa within this clade are also
1133 non-echolocating odontocetes and may be a characteristic unique to this family. Future studies
1134 on the inner ear morphology of the periotics of other simocetids, such as *Simocetus rayi*,
1135 *Olympicetus* sp. 1 (LACM 124105), will likely provide more information to this regard.
1136

1137 **Stem Odontocetes from the North Pacific**

1138 The early odontocete clade Simocetidae now includes six OTUs: *Simocetus rayi*, *Olympicetus*
1139 *avitus*, *Olympicetus* sp. (LACM 124105), *O. thalassodon* (LACM 158720), an unnamed large
1140 simocetid (LACM 124104) and CCNHM 1000 (Fig. 20). All specimens, with the exception of *S.*
1141 *rayi*, are from the Pysht Fm., with four of them: LACM 124104, LACM 124105, LACM 158720
1142 and CCNHM 1000, coming from the same general area (LACM Loc. 5123). The results of the
1143 phylogenetic analysis resemble those of an earlier, preliminary study that also recovered a
1144 monophyletic Simocetidae composed of most of the OTU's used here as well as a few others
1145 undescribed specimens from the eastern North Pacific, but that also recovered *Ashleycetetus*
1146 *planicapitis*, from the early Oligocene of South Carolina, as part of that clade (Velez-Juarbe,
1147 2015). In contrast, the results of the present work suggest that Simocetidae represents an endemic
1148 radiation of North Pacific stem odontocetes, that parallels that of the Aetiocetidae in the same
1149 region (Hernández Cisneros and Velez-Juarbe, 2021), and the Xenorophidae (here considered to
1150 include Ashleycetidae and Mirocetidae; Fig. 20) in the North Atlantic and Para-Tethys (Marx et
1151 al., 2016a). The occurrence of crown (i.e. *Arktocara yakataga*) as well as stem (Simocetidae)
1152 odontocetes in the Oligocene of the North Pacific suggest that the initial diversification of crown
1153 odontocetes must have occurred during the latest Eocene to earliest Oligocene (Boersma and
1154 Pyenson, 2016). This highlights the importance of the fossil record of the North Pacific towards
1155 further understanding the early history and radiation of odontocetes.

1156 At present, there are no published accounts of simocetids from the western North Pacific,
1157 although these are expected to be present based on the occurrence of closely-related marine
1158 tetrapods in Oligocene deposits on both sides of the basin (e.g., plotopterids, desmostylians,
1159 aetiocetids; Olson, 1980; Domning et al., 1986; Ray et al., 1994; Olson and Hasegawa, 1996;
1160 Inuzuka, 2000; Barnes and Goedert, 2001; Sakurai et al., 2008; Ohashi and Hasegawa, 2020;
1161 Mayr and Goedert, 2016, 2022; Mori and Miyata, 2021; Hernández-Cisneros and Vélez-Juarbe,
1162 2021), which makes this apparent absence an interesting question. However, some records from
1163 Japan bear close resemblance to simocetids and should be analyzed further. These include a
1164 mandible with two cheek teeth (KMNH VP 000011) and an isolated tooth (KMNH VP 000012)
1165 referred by Okazaki (1988) to *Squalodon* sp. from the Oligocene Waita Formation of the Ashiya
1166 Group. The general morphology of the mandible (KMNH VP 000011) resembles *Olympicetus*
1167 *thalassodon* and other basal odontocetes with multi-cusped cheek teeth, such as *Prosqualodon*
1168 *davidis* Flynn, 1947, and *Waipatia maerewhenua*, where the dorsal surface of the condyle is at
1169 about the same level as the horizontal ramus and the ventral border is relatively straight (Flynn,
1170 1947; Fordyce, 1994). Furthermore, the two cheek teeth preserved with KMNH VP 000011 are
1171 much more like those of *Olympicetus*, with the more anterior tooth (B3 in Okazaki, 1988) having
1172 only a small accessory denticle along the base of the mesial edge, while three larger ones
1173 distally, that increase in size apically, greatly resembling the premolars of *O. thalassodon* (Figs.
1174 11A, C, 12G). Meanwhile, the second tooth (B7 in Okazaki, 1988) resembles the m3 of
1175 *Olympicetus thalassodon*, by being smaller than the more anterior teeth, and having three
1176 accessory denticles along the distal edge that diminish in size towards the base of the crown,
1177 lacking accessory denticles along the mesial carina, and little to no ornamentation on the buccal
1178 side. The isolated tooth (KMNH VP 000012) resembles cheek tooth ‘pp4’ of *Olympicetus avitus*,
1179 as they are relatively low and long, with multiple accessory denticles along the mesial and distal
1180 edges, as well as having lingual and buccal cingula (Okazaki, 1988; Vélez-Juarbe, 2017). One
1181 distinguishing character is that the accessory denticles of *Olympicetus* spp. and the Waita Fm.
1182 odontocetes are closer in size to the main cusp than those of other basal odontocetes with multi-
1183 cusped cheek teeth. For example, lower cheek teeth of *Squalodon calvertensis*, *Prosqualodon*
1184 *davidis*, *P. australis* Lydekker, 1894, *Phoberodon arctirostris* Cabrera, 1926, and *Waipatia* spp.
1185 do have accessory denticles along their distal edges, but are obviously much smaller than the
1186 main cusp (Kellogg, 1923; Flynn, 1947; Fordyce, 1994; Tanaka and Fordyce, 2015; Gaetan et
1187 al., 2019; Viglino et al., 2019). The combination of these morphological features suggest that the
1188 specimens described by Okazaki (1988), could be considered as aff. *Olympicetus* sp., although
1189 this needs to be confirmed by direct observation of the specimens. Other cetaceans from the
1190 Ashiya Group include a toothed mysticete from the Waita Fm., originally assigned to
1191 *Metasqualodon symmetricus*, but now considered to represent an aetiocetid, and the eomysticetid
1192 *Yamatocetus caniliculatus* from the Jinnobaru Fm. (Okazaki, 1987, 2012; Fitzgerald, 2010).
1193 Similarly, other potential records of simocetids are found in the late Oligocene El Cien
1194 Formation of Baja California Sur. Hernández-Cisneros et al. (2017) briefly discussed two skulls
1195 from the El Cien Fm., comparing one with *Simocetus rayi* and the other with an undescribed

1196 skull (USNM 205491) from the Alsea Fm., and may represent other undescribed simocetids.
1197 These odontocetes from El Cien Fm. are currently under study (A. E. Hernández-Cisneros, pers.
1198 comm.), and other described taxa from this formation include kekenodontids, aetiocetids,
1199 eomysticetids and other stem mysticetes (Hernández-Cisneros and Tsai, 2016; Hernández-
1200 Cisneros et al., 2017; Solis-Añorve et al., 2019; Hernández-Cisneros, 2022; Hernández-Cisneros
1201 and Nava-Sánchez, 2022). These records from the Jinnobaru Fm., and El Cien Fm., resemble the
1202 odontocete assemblage of the Pysht Fm., which includes simocetids, aetiocetids and other early
1203 mysticetes, and is therefore likely that simocetids are would be present in these units as well
1204 (Barnes et al., 1995; Peredo and Uhen, 2016; Vélez-Juarbe, 2017; Shipps et al., 2019; Hernández
1205 Cisneros and Vélez-Juarbe, 2021; this work).

1206

1207 Dentition and Feeding in Simocetids

1208 As in most other groups of stem odontocetes (e.g. xenorophids, agorophiids), simocetids have
1209 heterodont dentition, but do seem to have a more conservative tooth count, closer to that of
1210 basilosaurids such as *Cynthiacetus peruvianus* (Martínez-Cáceres and Muizon, 2011), which
1211 consists of three incisors, one canine, four premolars, two upper and three lower molars, a
1212 pattern that is also observed in early mysticetes like *Janjucetus hunderi* Fitzgerald, 2006, and
1213 *Mystacodon selenensis* (Fitzgerald, 2010; Lambert et al., 2017). While the tooth count of some
1214 simocetids is hard to interpret (e.g. *Olympicetus avitus*; Vélez-Juarbe, 2017), others such as
1215 *Simocetus rayi* and *Olympicetus thalassodon* offer more definite clues with regards to their
1216 dentition. In the case of *Simocetus rayi*, its tooth count seems to be secondarily reduced from the
1217 plesiomorphic condition through the loss of the upper incisors, while the lower ones are retained
1218 (Fordyce, 2002). Although mostly missing, the teeth of *S. rayi* were widely separated and
1219 comparatively small (when compared to those of *Olympicetus*). In contrast, the teeth of
1220 *Olympicetus thalassodon* are closely spaced and based on the preserved teeth and alveoli, its
1221 dental formula is tentatively interpreted as ?I3, C, P4, M2/?i3, c, p4, m3. If these interpretations
1222 are correct, then the dentition of simocetids is the most plesiomorphic amongst odontocetes,
1223 paralleling that of basal mysticetes. This would contrast with xenorophids which seem to have
1224 polydont dentition; for example, *Xenorophus sloanii* and *Echovenator sandersi*; both have
1225 significantly higher count of postcanine teeth (Sanders and Geisler, 2015; Churchill et al., 2016).
1226 Nevertheless, the dentition of many xenorophids is still unknown, including key taxa, such as
1227 *Archaeodelphis patrius*, which may offer additional insight into early odontocete dental
1228 evolution.

1229 Although simocetids seem to share similar conservative tooth counts and generalized features of
1230 their teeth, there are some interesting differences between some of the species. One conspicuous
1231 difference between the dentition of *Olympicetus avitus* and *O. thalassodon* is the presence of a
1232 “carnassial”-like tooth in the former (tooth ‘mo3’ in Vélez-Juarbe, 2017:fig.70,Bb). This tooth is
1233 distinguished from all other postcanine teeth by having a ridge with accessory denticles that
1234 descends lingually from the apex, while its root is expanded lingually, giving the impression of
1235 the presence of three roots (mesial, distal and lingual), rather than two (mesial and distal) as in

1236 the other postcanine teeth. Meanwhile, a **third, lingual root** seems to be present in the P4 of
1237 *Simocetus rayi* (Fordyce, 2002), as well as in an unnamed *Simocetus*-like taxon from the Lincoln
1238 Creek Fm. (Barnes et al., 2001), and could be a character that is shared among some simocetids,
1239 although better preserved specimens are needed to corroborate this. Interestingly, tooth B7
1240 (*sensu* Sanders and Geisler, 2015) of *Xenorophus sloani* seems to present a more inconspicuous
1241 version of the “carnassial” tooth of simocetids, this tooth occupies a **similar** position of that of P4
1242 of *Simocetus rayi*, and **is likely a** character that should be explore further as more specimens
1243 become available.

1244 Some of the morphological characters observed in described simocetids, such as the arched
1245 palate, short and broad rostrum, smaller and widely-spaced teeth, as in *Simocetus rayi*, **are**
1246 interpreted as features of a bottom suction feeder (Fordyce, 2002; Werth, 2006; Johnston and
1247 Berta, 2011). Some of these features, such as the arched palate are also present in *Olympicetus*,
1248 however, *O. thalassodon*, has closely spaced, larger teeth, as well as a relatively gracile, unfused
1249 hyoid apparatus (Figs. 11-13A-C; Johnston and Berta, 2011; Viglino et al., 2021), which suggest
1250 that this taxon was instead a raptorial or combined feeder. Taking this into account, it is likely
1251 that simocetids employed different methods of prey acquisition, likely akin to the amount of
1252 variation observed in other contemporaneous groups, such as xenorophiids, which include taxa
1253 with long narrow rostra (e.g. *Cotylocara macei*; Geisler et al., 2014) that can be interpreted as
1254 raptorial feeders, as well as **brevirostrine** suction feeding taxa (i.e. *Inermorostrum xenops*;
1255 Boessenecker et al., 2017). Thus it seems that **multiple** methods of prey acquisition evolved
1256 iteratively across different groups of odontocetes soon after their initial radiation.

1257

1258 **Conclusions**

1259 Three new specimens of odontocetes from the middle Oligocene Pysht Formation were described
1260 herein further increasing our understanding of **richness** and diversity of early odontocetes,
1261 specially for the North Pacific region. Inclusion of this new material in a phylogenetic analysis
1262 showed that Simocetidae is a much more inclusive clade, **that**, besides *Simocetus rayi*, **it** now
1263 includes *Olympicetus avitus*, *O. thalassodon* sp. nov., *Olympicetus* sp. 1, and a large unnamed
1264 taxon. Of these, *Olympicetus thalassodon* is **the** one of the most completely known simocetids,
1265 offering new information on the **morphology** of early odontocetes, while the inclusion of
1266 CCNHM 1000 within this clade suggest that simocetids **may represent a clade of non-**
1267 **echolocating odontocetes**. This shows that some morphological features that have been
1268 correlated with the capacity to echolocate, such as an enlarged attachment area for the
1269 maxillonasolabialis muscle, and presence of a premaxillary sac fossae (Fordyce, 2002; Geisler et
1270 al., 2014), **appeared** before the acquisition of ultrasonic hearing. Furthermore, the dentition of
1271 simocetids, as interpreted here, seems to be the most plesiomorphic amongst odontocetes, while
1272 other craniodental features within members of this clade suggests various forms of prey
1273 acquisition, including raptorial or combined in *Olympicetus* spp., and suction feeding in
1274 *Simocetus* (as suggested by Fordyce, 2002). Meanwhile, body size estimates for simocetids show
1275 that small to moderately large taxa are present in the group, **with** the largest taxon represented by

1276 LACM 124104 with an estimated body length of 3 meters, ~~which places it as the largest known~~
1277 ~~simocetid, and~~ amongst the largest Oligocene odontocetes, only surpassed in bizygomatic width
1278 (and therefore estimated body length) by the xenorophids *Mirocetus riabinini* and *Ankylorhiza*
1279 *tiedemani* (Boessenecker et al., 2020; Sander et al., 2021). Finally, the new specimens described
1280 here add to a growing list of Oligocene marine tetrapods from the North Pacific, further
1281 facilitating faunistic comparisons across other contemporaneous and younger assemblages, thus
1282 improving our understanding of the evolution of marine faunas in the region.
1283

1284 Acknowledgements

1285 I wish to extend my gratitude to E. M. G. Fitzgerald (MV), N. D. Pyenson (USNM), R. E.
1286 Fordyce (UO) and M. Viglino (CONICET-CENPAT) for discussions about early odontocete
1287 morphology. To E. M. G. Fitzgerald (MV), N. D. Pyenson (USNM) and D. J. Bohaska (USNM)
1288 for access to collections under their care. Also, to James L. Goedert and the late Gail H. Goedert,
1289 for collecting and donating the specimens described in this work to the Natural History Museum
1290 of Los Angeles County.
1291

1292 References

- 1293 Aguirre-Fernández, G., and R. E. Fordyce. 2014. *Papahu taitapu*, gen. et sp. Nov., an early
1294 Miocene stem odontocete (Cetacea) from New Zealand. *Journal of Vertebrate Paleontology*
1295 34:195–210.
1296
- 1297 Albright III, L. B., A. E. Sanders, and J. H. Geisler. 2018. An unexpectedly derived odontocete
1298 from the Ashley Formatio (upper Rupelian) of South Carolina, U.S.A. *Journal of Vertebrate*
1299 *Paleontology* 38(4):e1482555.
1300
- 1301 Allen, G. M. 1921. A new fossil cetacean. *Bulletin of the Museum of Comparative Zoology at*
1302 *Harvard College* 65:1–14.
1303
- 1304 Allen, J. A. 1887. Note on squalodont remains from Charleston, S.C. *Bulletin of the American*
1305 *Museum of Natural History* 12:35–39.
1306
- 1307 Andrews, C. W. 1906. A descriptive catalogue of the Tertiary Vertebrata of Fayum, Egypt.
1308 *British Museum of Natural History, London* 324 pp.
1309
- 1310 Barnes, L. G. 1984. Fossil odontocetes (Mammalia: Cetacea) from the Almejas Formation, Isla
1311 Cedros, Mexico. *PaleoBios* 42:1–46.
1312
- 1313 Barnes, L. G. 1998. The sequence of fossil marine mammal assemblages in Mexico. *Avances en*
1314 *Investigación, Paleontología de Vertebrados, Publicación Especial* 1:26–79.
1315

- 1316 Barnes, L. G. 2008. Miocene and Pliocene Albireonidae (Cetacea, Odontoceti), rare and unusual
1317 fossil dolphins from the eastern North Pacific Ocean. Natural History Museum of Los Angeles
1318 County Science Series 41:99–152.
1319
- 1320 Barnes, L. G., and J. L. Goedert. 2001. Stratigraphy and paleoecology of Oligocene and Miocene
1321 desmostylian occurrences in Western Washington State, U.S.A. Bulletin of Ashoro Museum of
1322 Paleontology 2:7–22.
1323
- 1324 Barnes, L. G., J. L. Goedert, H. Furusawa. 2001. The earliest known echolocating toothed whales
1325 (Mammalia; Odontoceti): preliminary observations of fossils from Washington State. Mesa
1326 Southwestern Museum Bulletin 8:92–100.
1327
- 1328 Barnes, L. G., M. Kimura, H. Furusawa, and H. Sawamura. 1995. Classification and distribution
1329 of Oligocene Aetiocetidae (Mammalia; Cetacea; Mysticeti) from western North America and
1330 Japan. Island Arc 3:392–431.
1331
- 1332 Beatty, B. L. 2006. Specimens of *Cornwallius sookensis* (Desmostyilia, Mammalia) from
1333 Unalaska Island, Alaska. Journal of Vertebrate Paleontology 26:785–787.
1334
- 1335 Beatty, B. L., and T. Cockburn. 2015. New insights on the most primitive desmostylian from a
1336 partial skeleton of *Behemotops* (Desmostyilia, Mammalia) from Vancouver Island, British
1337 Columbia. Journal of Vertebrate Paleontology e979939.
1338
- 1339 Berta, A. 1991. New *Enaliarctos** (Pinnipedimorpha) from the Oligocene and Miocene of
1340 Oregon and the role of “enaliarctids” in pinniped phylogeny. Smithsonian contributions to
1341 Paleobiology 69:1–33.
1342
- 1343 Blainville, H. de. 1838. Sur les cachalots. Annales Francaises et Étrangères D’anatomie et de
1344 Phsiologie. 2:335–337.
1345
- 1346 Boersma, A. T., and N. D. Pyenson. 2016. *Arktocara yakataga*, a new fossil odontocete
1347 (Mammalia, Cetacea) from the Oligocene of Alaska and the antiquity of Platanistoidea. PeerJ
1348 4:e2321. DOI 10.7717/peerj.2321
1349
- 1350 Boessenecker, R. W., D. Fraser, M. Churchill, and J. H. Geisler. 2017. A toothless dwarf dolphin
1351 (Odontoceti: Xenorophidae) points to explosive feeding diversification of modern whales
1352 (Neoceti). Proceedings of the Royal Society B 284:20170531.
1353

- 1354 Boessenecker, R. W., M. Churchill, E. A. Buchholtz, B. L. Beatty, and J. H. Geisler. 2020.
1355 Convergent evolution of swimming adaptations in modern whales revealed by a large
1356 macrophagous dolphin from the Oligocene of South Carolina. *Current Biology* 30:3267–3273.
1357
- 1358 Brisson, M. J. 1762. *Regnum Animale in Classes IX Distributum, Sive Synopsis Methodica*
1359 *Sistens Generalem Animalium Distributionem in Classes IX, et Duarum Primarum Classium,*
1360 *Quadrupedum Scilicet & Cetaceorum, Particulare Divisionem in Ordines, Sectiones, Genera, et*
1361 *Species.* T. Haak, Paris, 296 pp.
1362
- 1363 Cabrera, A. 1926. Cetáceos fósiles del Museo de La Plata. *Revista Museo de La Plata* 29:363–
1364 411.
1365
- 1366 Churchill, M., M. Martinez-Caceres, C. de Muizon, J. Mneckowski, and J. H. Geisler. 2016. The
1367 origin of high-frequency hearing in whales. *Current Biology* 26:1–6.
1368
- 1369 Cohen, K. M., S. C. Finney, P. L. Gibbard, and J. X. Fan. 2013 (updated). The ICS international
1370 chronostratographic chart. *Episodes* 36:199–204.
1371
- 1372 Domning, D. P., C. E. Ray, and M. C. McKenna. 1986. Two new Oligocene desmostylians and a
1373 discussion of tethytherian systematics. *Smithsonian Contributions to Paleobiology* 59:1–56.
1374
- 1375 Dickson, M. R. 1964. The skull and other remains of *Prosqualodon marplei*, a new species of
1376 fossil whale. *New Zealand Journal of Geology and Geophysics* 7:626–635.
1377
- 1378 Dubrovo, I. A., and A. E. Sanders. 2000. A new species of *Patriocetus* (Mammalia, Cetacea)
1379 from the late Oligocene of Kazakhstan. *Journal of Vertebrate Paleontology* 20:577–590.
1380
- 1381 Dyke, G. J., X. Wang, and M. B. Habib. 2011. Fossil pterid seabirds from the Eo-Oligocene
1382 of the Olympic Peninsula (Washington State, USA): descriptions and functional morphology.
1383 *PLoS ONE* 6(10):e25672.
1384
- 1385 Emlong, D. R. 1966. A new archaic cetacean from the Oligocene of Northwest Oregon. *Bulletin*
1386 *of the Oregon University Museum of Natural History* 3:1–51.
1387
- 1388 Fitzgerald, E. M. G. 2006. A bizarre new toothed mysticete (Cetacea) from Australia and the
1389 early evolution of baleen whales. *Proceedings of the Royal Society B* 273:2955–2963.
1390
- 1391 Fitzgerald, E. M. G. 2010. The morphology and systematics of *Mammalodon colliveri* (Cetacea:
1392 Mysticeti), a toothed mysticete from the Oligocene of Australia. *Zoological Journal of the*
1393 *Linnean Society* 158:367–476.

- 1394
1395 Flower, W. H. 1867. Description of the skeleton of *Inia geoffensis* and the skull of *Pontoporia*
1396 *blainvillii*, with remarks on the systematic position on these animals in the order Cetacea.
1397 Transactions of the Zoological Society of London 6:87–116.
1398
1399 Flynn, T. T. 1947. Description of *Prosqualodon davidi* Flynn, a fossil cetacean from Tasmania.
1400 Transactions of the Zoological Society of London 26:153–197.
1401
1402 Fordyce, R. E. 1994. *Waipatia maerewhenua*, a new genus and species (Waipatiidae, new
1403 family), an archaic late Oligocene dolphin (Cetacea: Odontoceti: Platanistoidea) from New
1404 Zealand. Proceedings of the San Diego Society of Natural History 29:147–176.
1405
1406 Fordyce, R. E. 2002. *Simocetus rayi* (Odontoceti: Simocetidae, New Family): a bizarre new
1407 archaic Oligocene dolphin from the Eastern Pacific. Smithsonian Contributions to Paleobiology
1408 93:185–222.
1409
1410 Gaetan, C. M., M. R. Buono, and L. C. Gaetano. 2019. *Prosqualodon australis* (Cetacea:
1411 Odontoceti) from the early Miocene of Patagonia, Argentina: redescription and phylogenetic
1412 analysis. Ameghiniana 56:1–27.
1413
1414 Geisler, J. H., M. W. Colbert, and J. L. Carew. 2014. A new fossil species supports an early
1415 origin for toothed whale echolocation. Nature 508:383–386.
1416
1417 Goedert, J. L., R. L. Squires, and L. G. Barnes. 1995. Paleocology of whalefall habitats from
1418 deep-water Oligocene Rocks, Olympic Peninsula, Washington State. Paleogeography,
1419 Palaeoclimatology, Paleoecology 118: 151–158.
1420
1421 Hernández Cisneros, A. E. 2022. A new aetiocetid (Cetacea, Mysticeti, Aetiocetidae) from the
1422 late Oligocene of Mexico. Journal of Systematic Palaeontology 20:2100725.
1423
1424 Hernández Cisneros, A. E., and E. H. Nava-Sánchez. 2022. Oligocene dawn baleen whales in
1425 Mexico (Cetacea, Eomysticetidae) and paleobiogeographic notes. Paleontología Mexicana 11:1–
1426 12.
1427
1428 Hernández Cisneros, A. E., and C.-H. Tsai. 2016. A possible enigmatic kekenodontid (Cetacea,
1429 Kekenodontidae) from the Oligocene of Mexico. Paleontología Mexicana 5:147–155.
1430
1431 Hernández Cisneros, A. E., and J. Vélez-Juarbe. 2021. Paleobiogeography of the North Pacific
1432 toothed mysticetes (Cetacea, Aetiocetidae): a key to Oligocene cetacean distributional patterns.
1433 Palaeontology 64:51–61.

- 1434
1435 Hernández Cisneros, A. E., G. González Barba, and R. E. Fordyce. 2017. Oligocene cetaceans
1436 from Baja California Sur, Mexico. *Boletín de la Sociedad Geológica Mexicana* 69:149–173.
1437
- 1438 Hirota, K., and L. G. Barnes. 1995. A new species of middle Miocene sperm whale of the genus
1439 *Scaldicetus* (Cetacea; Physeteridae) from Shiga-mura, Japan. *Island Arc* 3:453–472.
1440
- 1441 Hunt, R. M., Jr., and L. G. Barnes. 1994. Basicranial evidence for ursid affinity of the oldest
1442 pinnipeds. *Proceedings of the San Diego Society of Natural History* 29:57–67.
1443
- 1444 Ichishima, H., S. Kawabe, and H. Sawamura. 2021. The so-called foramen singulare in cetacean
1445 periotics is actually the superior vestibular area. *Anatomical Record* 304:1792–1799.
1446
- 1447 Inuzuka, N. 2000. Primitive late Oligocene desmostylians from Japan and phylogeny of the
1448 Desmostylia. *Bulletin of the Ashoro Museum of Paleontology* 1:91–123.
1449
- 1450 Johnston, C., and A. Berta. 2011. Comparative anatomy and evolutionary history of suction
1451 feeding in cetaceans. *Marine Mammal Science* 27:493–513.
1452
- 1453 Kellogg, R. 1923. Description of an apparently new toothed cetacean from South Carolina.
1454 *Smithsonian Contributions to Knowledge* 76(7):1–7.
1455
- 1456 Kiel, S., W.-A. Kahl, and J. L. Goedert. 2013. Traces of the bone-eating annelid *Osedax* in
1457 Oligocene whale teeth and fish bones. *Paläontologische Zeitschrift* 87:161–167.
1458
- 1459 Kimura, T., and Y. Hasegawa. 2019. A new species of *Kentriodon* (Cetacea, Odontoceti,
1460 Kentriodontidae) from the Miocene of Japan. *Journal of Vertebrate Paleontology* 39:e1566739.
1461
- 1462 Lambert, O., M. Martínez-Cáceres, G. Bianucci, C. Di Celma, R. Salas-Gismondi, E. Steurbaut,
1463 M. Urbina, and C. de Muizon. 2017. Earliest mysticete from the late Eocene of Peru sheds new
1464 light on the origin of baleen whales. *Current Biology* 27:1535–1541.
1465
- 1466 Lydekker, R. 1894. Cetacean skull from Patagonia. *Anales del Museo de La Plata* 2:1–13.
1467
- 1468 Martínez-Cáceres, M., and C. de Muizon. 2011. A new basilosaurid (Cetacea, Pelagiceti) from
1469 the late Eocene to early Oligocene Otuma Formation of Peru. *Comptes Rendus Palevol* 10:517–
1470 526.
1471

- 1472 Martínez-Cáceres, M., O. Lambert, and C. de Muizon. 2017. The anatomy and phylogenetic
1473 affinities of *Cynthiacetus peruvianus*, a large durodontine basilosaurid (Cetacea, Mammalia)
1474 from the late Eocene of Peru. *Geodiversitas* 39:7–163.
1475
- 1476 Marx, F. G., C.-H. Tsai, and R. E. Fordyce. 2015. A new early Oligocene toothed ‘baleen’ whale
1477 (Mysticeti: Aetiocetidae) from western North America: one of the oldest and the smallest. *Royal*
1478 *Society Open Science* 2:150476.
1479
- 1480 Marx, F. G., O. Lambert, and M. D. Uhen. 2016a. *Cetacean Paleobiology*. John Wiley & Sons,
1481 Hoboken, 319 pp.
1482
- 1483 Marx, F. G., D. P. Hocking, T. Park, T. Ziegler, A. R. Evans, and E. M. G. Fitzgerald. 2016b.
1484 Suction feeding preceded filtering in baleen whale evolution. *Memoirs of Museum Victoria*
1485 75:71–82.
1486
- 1487 Mayr, G., and J. L. Goedert. 2016. New late Eocene and Oligocene remains of the flightless,
1488 penguin-like plotopterids (Aves, Plotopteridae) from western Washington State, U.S.A. *Journal*
1489 *of Vertebrate Paleontology* 36:e1163573.
1490
- 1491 Mayr, G., and J. L. Goedert. 2022. New late Eocene and Oligocene plotopterid fossils from
1492 Washington State (USA), with a revision of “*Tonsala*” *buchanani* (Aves, Plotopteridae). *Journal*
1493 *of Paleontology* 96:224–236.
1494
- 1495 McGowen, M. R., G. Tsagkogeorga, A. Álvarez-Carretero, M. dos Reis, M. Struebig, R.
1496 Deaville, P. D. Jepson, S. Jarman, A. Polanowski, P. A. Morin, and S. J. Rossiter. 2020.
1497 Phylogenomic resolution of the cetacean tree of life using target sequence capture. *Systematic*
1498 *Biology* 69:479–501.
1499
- 1500 Mchedlidze, G. A. 1970. Nekotorye Obschchie Chery Istorii Kitoobraznykh. Chast’ I. Akademia
1501 Nauk Gruzinskoi S.S.R., Institut Paleobiologii. Metsniereba, Tbilisi, 112 p.
1502
- 1503 Mead, J. G., and R. E. Fordyce. 2009. The therian skull: a lexicon with emphasis on the
1504 odontocetes. *Smithsonian Contributions to Zoology* 627:1–248.
1505
- 1506 Montagu, G. 1821. Description of a species of *Delphinus*, which appears to be new. *Memoirs of*
1507 *the Wernerian Natural History Society* 3:75–82.
1508
- 1509 Moreno, F. 1892. Ligeros apuntes sobre dos géneros de cetáceos fósiles de la República
1510 Argentina. *Museo La Plata, Revista* 3:393–400.
1511

- 1512 Mori, H., and K. Miyata. 2021. Early Plotopteridae specimens (Aves) from the Itanoura and
1513 Kakinoura Formations (latest Eocene to early Oligocene), Saikai, Nagasaki Prefecture, western
1514 Japan. *Paleontological Research* 25:145–159.
1515
- 1516 Muizon, C. de. 1987. The affinities of *Notocetus vanbenedeni*, an early Miocene platanistoid
1517 (Cetacea, Mammalia) from Patagonia, southern Argentina. *American Museum Novitates*
1518 2904:1–27.
1519
- 1520 Muizon, C. de, G. Bianucci, M. Martínez-Cáceres, and O. Lambert. 2019. *Mystacodon*
1521 *selenenesis*, the earliest known toothed mysticete (Cetacea, Mammalia) from the late Eocene of
1522 Peru: anatomy, phylogeny, and feeding adaptations. *Geodiversitas* 41:401–499.
1523
- 1524 Müller, J. 1849. Über die fossilen Reste der Zeuglodonten von Nordamerika mit Rücksicht auf
1525 die europäischen Reste aus dieser Familie. G. Reimer, Berlin, 38 pp.
1526
- 1527 Ohaski, T., and Y. Hasegawa. 2020. New species of Plotopteridae (Aves) from the Oligocene
1528 Ashiya Group of Northern Kyushu, Japan. *Paleontological Research* 24:285–297.
1529
- 1530 Okazaki, Y. 1987. Additional material of *Metasqualodon symmetricus* (Cetacea: Mammalia)
1531 from the Oligocene Ashiya Group, Japan. *Bulletin of the Kitakyushu Museum of Natural History*
1532 7:133–138.
1533
- 1534 Okazaki, Y. 1988. Oligocene squalodont (Cetacea: Mammalia) from the Ashiya Group, Japan.
1535 *Bulletin of the Kitakyushu Museum of Natural History* 8:75–80.
1536
- 1537 Okazaki, Y. 2012. A new mysticete from the upper Oligocene Ashiya Group, Kyushu, Japan and
1538 its significance to mysticete evolution. *Bulletin of the Kitakyushu Museum of Natural History*
1539 and Human History, Series A 10:129–152.
1540
- 1541 Olson, S. L. 1980. A new genus of penguin-like peleciform bird from the Oligocene of
1542 Washington (Pelecaniformes: Plotopteridae). *Contributions in Science* 330:51–57.
1543
- 1544 Olson, S. L., and Y. Hasegawa. 1996. A new genus and two new species of gigantic
1545 Plotopteridae from Japan (Aves: Plotopteridae). *Journal of Vertebrate Paleontology* 16:742–751.
1546
- 1547 Peredo, C. M., and M. D. Uhen. 2016. A new basal Chaemysticete (Mammalia: Cetacea) from
1548 the late Oligocene Pysht Formation of Washington, USA. *Papers in Palaeontology* 2:533–554.
1549

- 1550 Peredo, C. M., and N. D. Pyenson. 2018. *Salishicetus meadi*, a new aetiocetid from the late
1551 Oligocene of Washington State and implications for feeding transitions in early mysticete
1552 evolution. *Royal Society Open Science* 5:172336.
1553
- 1554 Peredo, C. M., N. D. Pyenson, C. D. Marshall, and M. D. Uhen. 2018. Tooth loss precedes the
1555 origin of baleen in whales. *Current Biology* 28:3992–4000.
1556
- 1557 Poust, A. W., and R. W. Boessenecker. 2018. Expanding the geographic and geochronologic
1558 range of early pinnipeds: new specimens of *Enaliarctos* from Northern California and Oregon.
1559 *Acta Palaeontologica Polonica* 63:25–40.
1560
- 1561 Pritchard, G. B. 1939. On the discovery of a fossil whale in the older Tertiaries of Torquay,
1562 Victoria. *Victorian Naturalist* 55:151–159.
1563
- 1564 Prothero, D. R., A. Streig, and C. Burns. 2001. Magnetic stratigraphy and tectonic rotation of the
1565 upper Oligocene Pysht Formation, Clallam County, Washington. *Pacific Section, SEPM, Special*
1566 *Publication* 91:224–233.
1567
- 1568 Pyenson, N. D., and S. N. Sponberg. 2011. Reconstructing body size in extinct crown Cetacea
1569 (Neoceti) using allometry, phylogenetic methods and tests from the fossil record. *Journal of*
1570 *Mammalian Evolution* 18:269–288.
1571
- 1572 Racicot, R. A., R. W. Boessenecker, S. A. F. Darroch, and J. H. Geisler. 2019. Evidence for
1573 convergent evolution of ultrasonic hearing in toothed whales (Cetacea: Odontoceti). *Biology*
1574 *Letters* 15:20190083.
1575
- 1576 Ray, C. E., D. P. Domning, and M. C. McKenna. 1994. A new specimen of *Behemotops proteus*
1577 (Order Desmostylia) from the marine Oligocene of Washington. *Proceedings of the San Diego*
1578 *Society of Natural History* 29:205–222.
1579
- 1580 Russel, L. S. 1968. A new cetacean from the Oligocene Sooke Formation of Vancouver Island,
1581 British Columbia. *Canadian Journal of Earth Sciences* 5:929–933.
1582
- 1583 Reidenberg, J. S., and J. T. Laitman. 1994. Anatomy of the hyoid apparatus in Odontoceti
1584 (toothed whales): specializations of their skeleton and musculature compared with those of
1585 terrestrial mammals. *Anatomical Record* 240:598–624.
1586
- 1587 Sakurai, K., M. Kimura, and T. Katoh. 2008. A new penguin-like bird (Pelecaniformes:
1588 Plotopteridae) from the late Oligocene Tokoro Formation, northeastern Hokkaido, Japan.
1589 *Oryctos* 7:83–94.

- 1590
1591 Sander, P. M., E. M. Griebeler, N. Klein, J. Vélez-Juarbe, T. Wintrich, L. J. Revell, and L.
1592 Schmitz. 2021. Early giant reveals faster evolution of large body size in ichthyosaurs than in
1593 cetaceans. *Science* 374:eabf5787.
1594
1595 Sanders, A. E., and J. H. Geisler. 2015. A new basal odontocete from the upper Rupelian of
1596 South Carolina, U.S.A., with contributions to the systematics of *Xenorophus* and
1597 *Mirocetus*(Mammalia, Cetacea). *Journal of Vertebrate Paleontology* 35:e890107.
1598
1599 Shippis, B. K., C. M. Peredo, and N. D. Pyenson. 2019. *Borealodon osedax*, a new stem
1600 mysticete (Mammalia, Cetacea) from the Oligocene of Washington State and its implications for
1601 fossil whale-fall communities. *Royal Society Open Science* 6:182168.
1602
1603 Solis-Añorve, A., G. Gozález-Barba, and R. Hernández-Rivera. 2019. Description of a new
1604 toothed mysticete from the late Oligocene of San Juan de La Costa, B.C.S., México. *Journal of*
1605 *South American Earth Sciences* 89:337–346.
1606
1607 Swofford, D. L. 2003. PAUP*. Phylogenetic Analysis Using Parsimony (*and Other Methods),
1608 Version 4.0 B10. Sunderland, MA, Sinauer Associates.
1609
1610 Tanaka, Y., and R. E. Fordyce. 2014. Fossil dolphin *Otekaikea marplei* (latest Oligocene, New
1611 Zealand) expands the morphological and taxonomic diversity of Oligocene cetaceans. *PLoS*
1612 *ONE* 9(9):e107972.
1613
1614 Tanaka, Y., and R. E. Fordyce. 2015. A new Oligo-Miocene dolphin from New Zealand:
1615 *Otekaikea huata* expands diversity of the early Platanistoidea. *Paleontologia Electronica*
1616 18.2.23A:1–71.
1617
1618 Uhen, M. D. 2004. Form, function, and anatomy of *Durodon atrox* (Mammalia, Cetacea): an
1619 archaeocete from the middle to late Eocene of Egypt. *University of Michigan Papers on*
1620 *Paleontology* 34:1–222.
1621
1622 Uhen, M. D. 2008. A new *Xenorophus*-like odontocete cetacean from the Oligocene of North
1623 Carolina and a discussion of the basal odontocete radiation. *Journal of Systematic Palaeontology*
1624 6:433–452.
1625
1626 Vélez-Juarbe, J. 2015. Simocetid diversity in the Oligocene of the Eastern Pacific region. *Journal*
1627 *of Vertebrate Paleontology, Program and Abstracts* 2015:230.
1628

- 1629 Vélez-Juarbe, J. 2017. A new stem odontocete from the late Oligocene Pysht Formation in
1630 Washington State, U.S.A. *Journal of Vertebrate Paleontology* 37(5):e1366916.
1631
- 1632 Viglino, M., C. M. Gaetán, J. I. Cuitiño, and M. R. Buono. 2021. First toothless platanistoid from
1633 the early Miocene of Patagonia: the golden age of diversification of the Odontoceti. *Journal of*
1634 *Mammalian Evolution* 28:337–358.
1635
- 1636 Viglino, M., M. R. Buono, R. E. Fordyce, J. I. Cuitiño, and E. M. G. Fitzgerald. 2019. Anatomy
1637 and phylogeny of the large shark-toothed dolphin *Phoberodon arctirostris* Cabrera, 1926
1638 (Cetacea: Odontoceti) from the early Miocene of Patagonia (Argentina). *Zoological Journal of*
1639 *the Linnean Society* 185:511–542.
1640
- 1641 Viglino, M., M. R. Buono, Y. Tanaka, J. I. Cuitiño, and R. E. Fordyce. 2022. Unravelling the
1642 identity of the platanistoid *Notocetus vanbenedeni* Moreno, 1892 (Cetacea, Odontoceti) from the
1643 early Miocene of Patagonia (Argentina). *Journal of Systematic Palaeontology* 20:2082890.
1644
- 1645 Werth, A. J. 2006. Mandibular and dental variation and the evolution of suction feeding in
1646 odontoceti. *Journal of Mammalogy* 87:579–588.
1647
- 1648 Whitmore, F. C., Jr., and A. E. Sanders. 1977. Review of the Oligocene Cetacea. *Systematic*
1649 *Zoology* 25:304–320.

Figure 1

Dorsal view of skull of Simocetidae gen. et sp. A (LACM 124104).

Unlabeled (A) and labeled (B) skull in dorsal view. Diagonal lines denote broken surfaces, gray shaded areas are obscured by sediment. Abbreviations: as, alisphenoid; cp, coronoid process; eo, exoccipital; f, frontal; oc, occipital condyle; oi, optic infundibulum; pa, parietal; pp, paroccipital process; pt, pterygoid; smf, sternomastoid fossa; so, supraoccipital; sq, squamosal; zps, zygomatic process of squamosal.

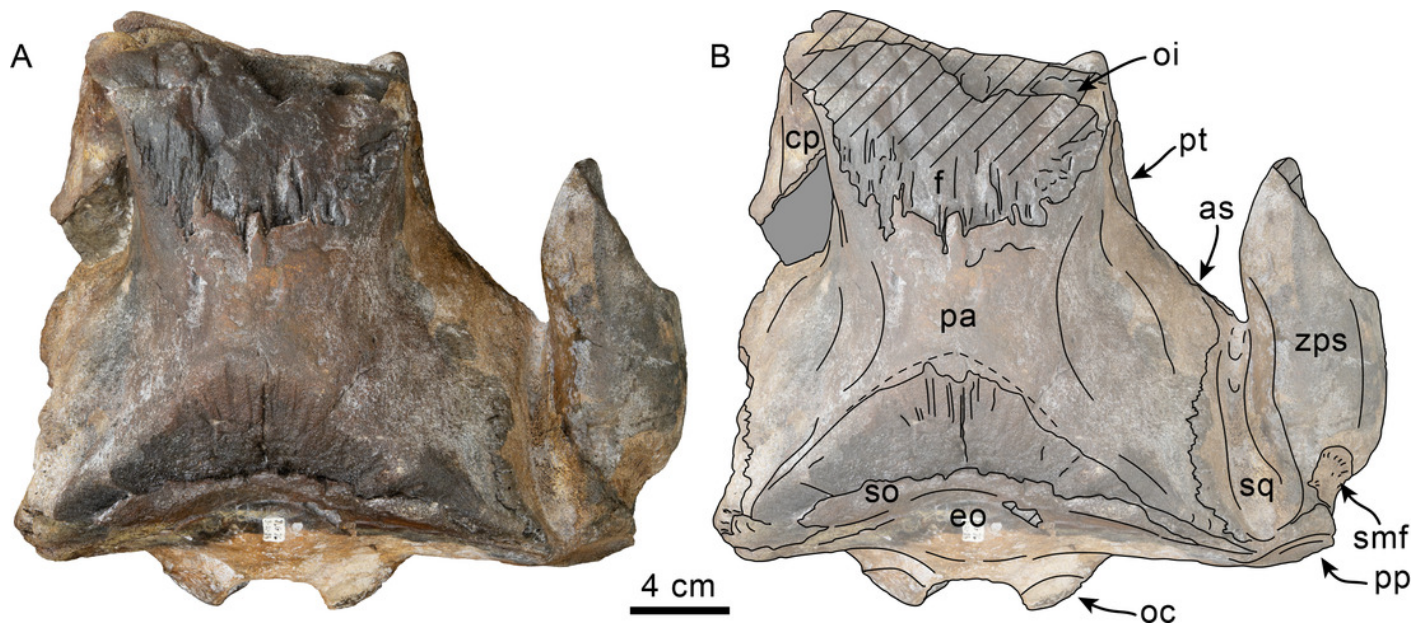


Figure 2

Posterior and ventral views of skull of Simocetidae gen. et sp. A (LACM 124104).

Unlabeled (A) and labeled (B) skull in posterior view; unlabeled (C) and labeled (D) skull in ventral view. Diagonal lines denote broken surfaces, gray shaded areas are obscured by sediment. Abbreviations: as, alisphenoid; bo, basioccipital; bo, basioccipital crest; cp, coronoid process; eo, exoccipital; fm, foramen magnum; fs, foramen spinosum; g, glenoid; hf, hypoglossal foramen; jn, jugular notch; oc, occipital condyle; pa, parietal; pe, periotic; ppg, postglenoid process; ph, pterygoid hamulus; pl, palatine; pll, pterygoid lateral lamina; pml, pterygoid medial lamina; pp, paroccipital process; psf, pterygoid sinus fossa; pt, pterygoid; scf, supracondylar fossa; smf, sternomastoid fossa; so, supraoccipital; sq, squamosal; tr, tympanosquamosal recess; V3, groove and path of mandibular branch of trigeminal nerve; vo, vomer; zps, zygomatic process of squamosal.

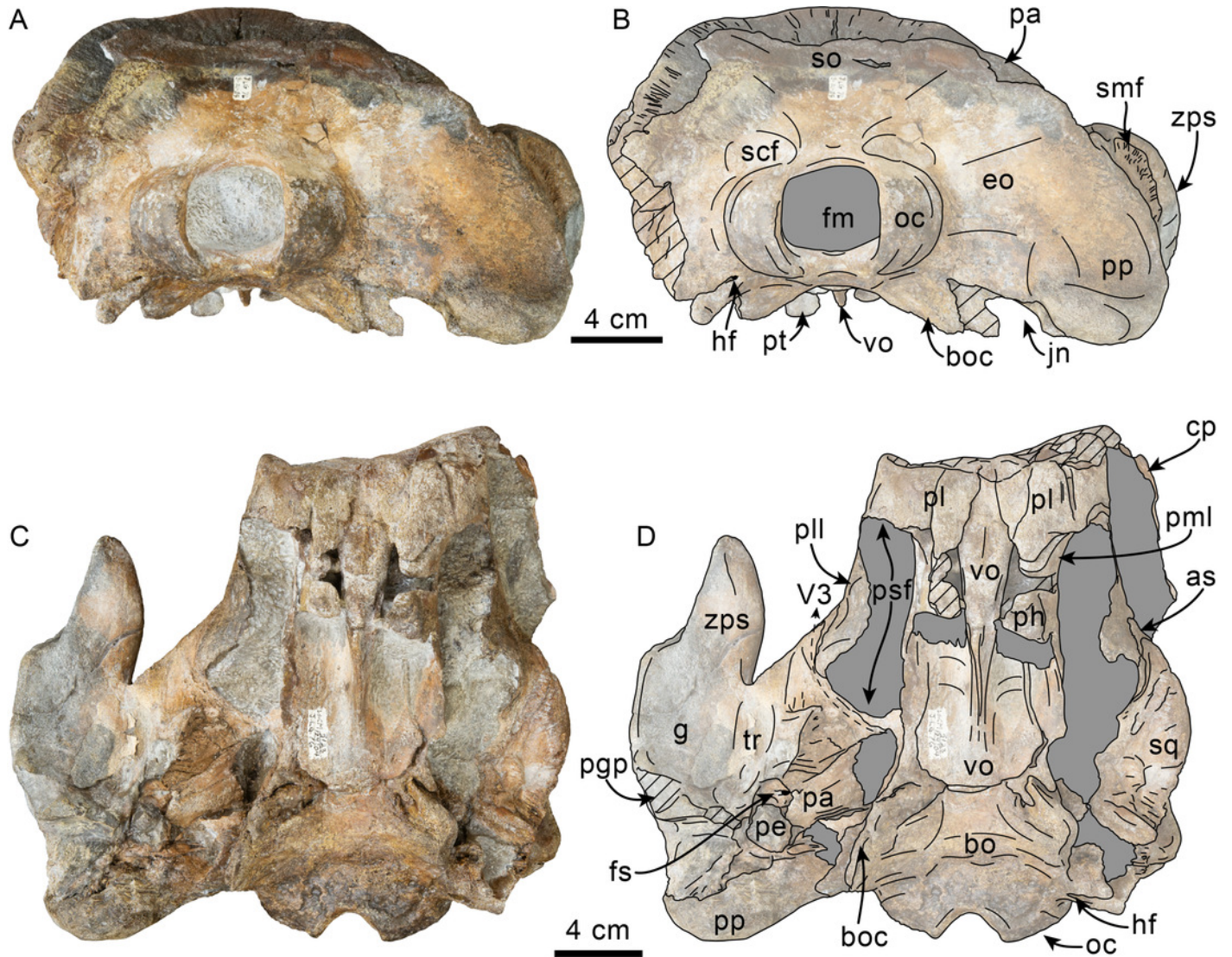
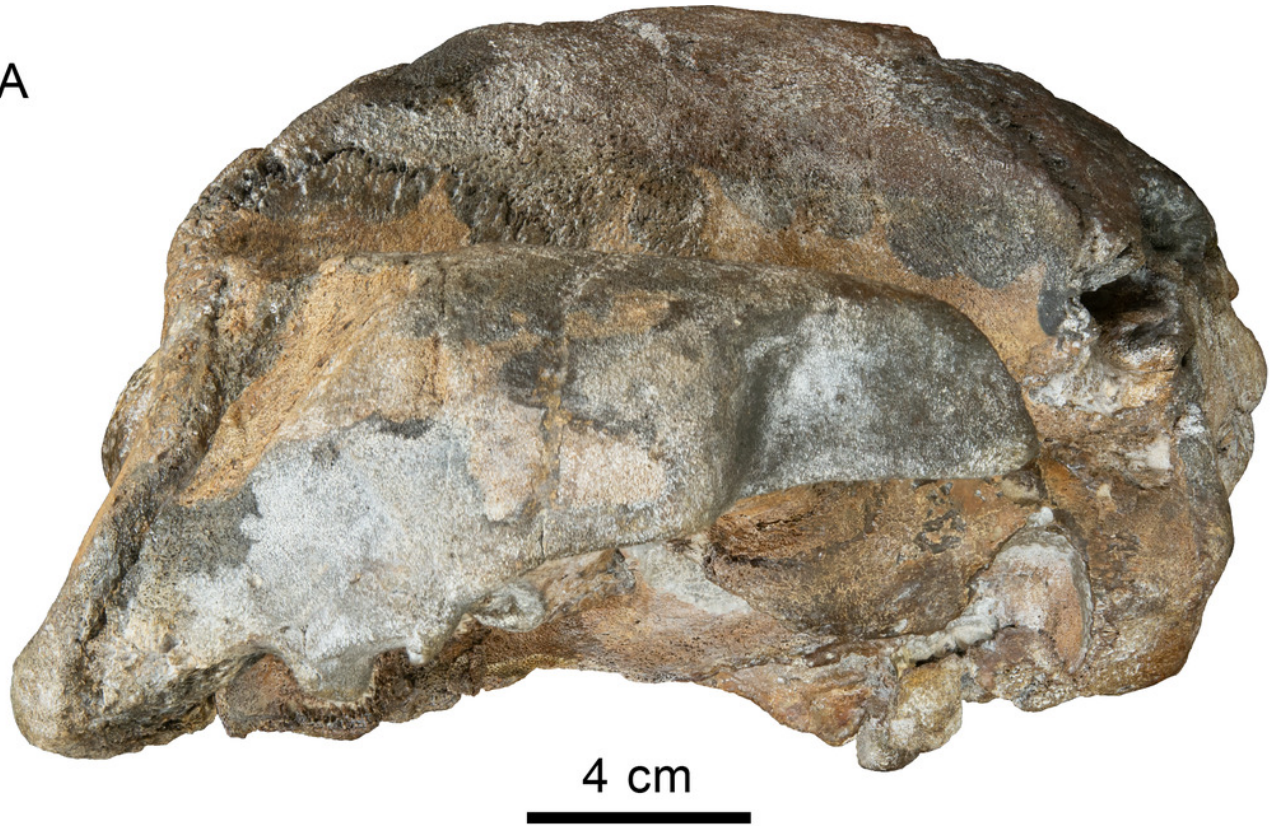


Figure 3

Lateral view of skull of Simocetidae gen. et sp. A (LACM 124104).

Unlabeled (A) and labeled (B) skull in right lateral view. Diagonal lines denote broken surfaces, gray shaded areas are obscured by sediment. Abbreviations: as, alisphenoid; boc, basioccipital crest; eo, exoccipital; f, frontal; fp, falciform process; oc, occipital condyle; oi, optic infundibulum; pa, parietal; ph, pterygoid hamulus; pl, palatine; pll, pterygoid lateral lamina; pml, pterygoid medial lamina; pp, paroccipital process; psf, pterygoid sinus fossa; smf, sternomastoid fossa; sq, squamosal; vo, vomer; zps, zygomatic process of squamosal.

A



B

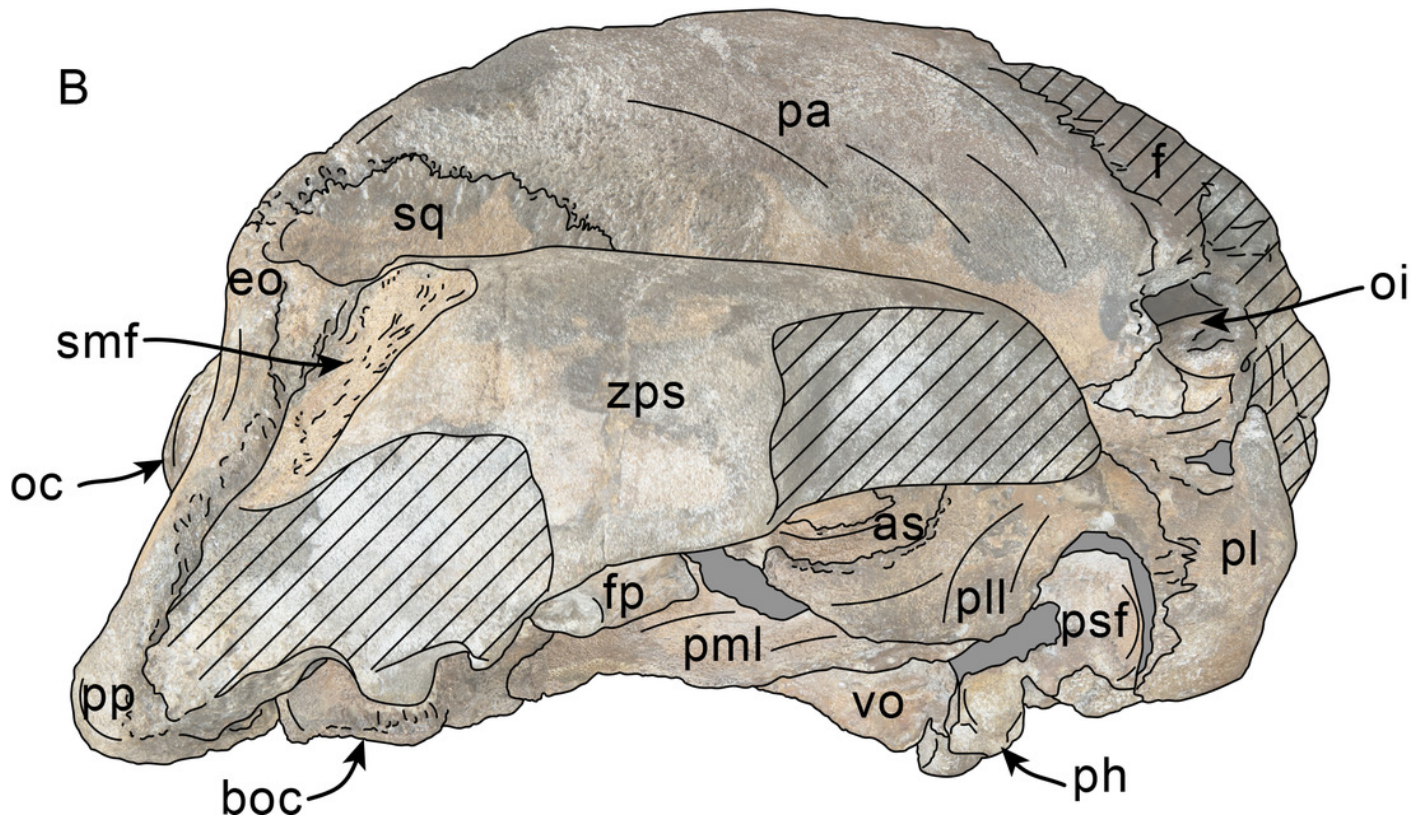
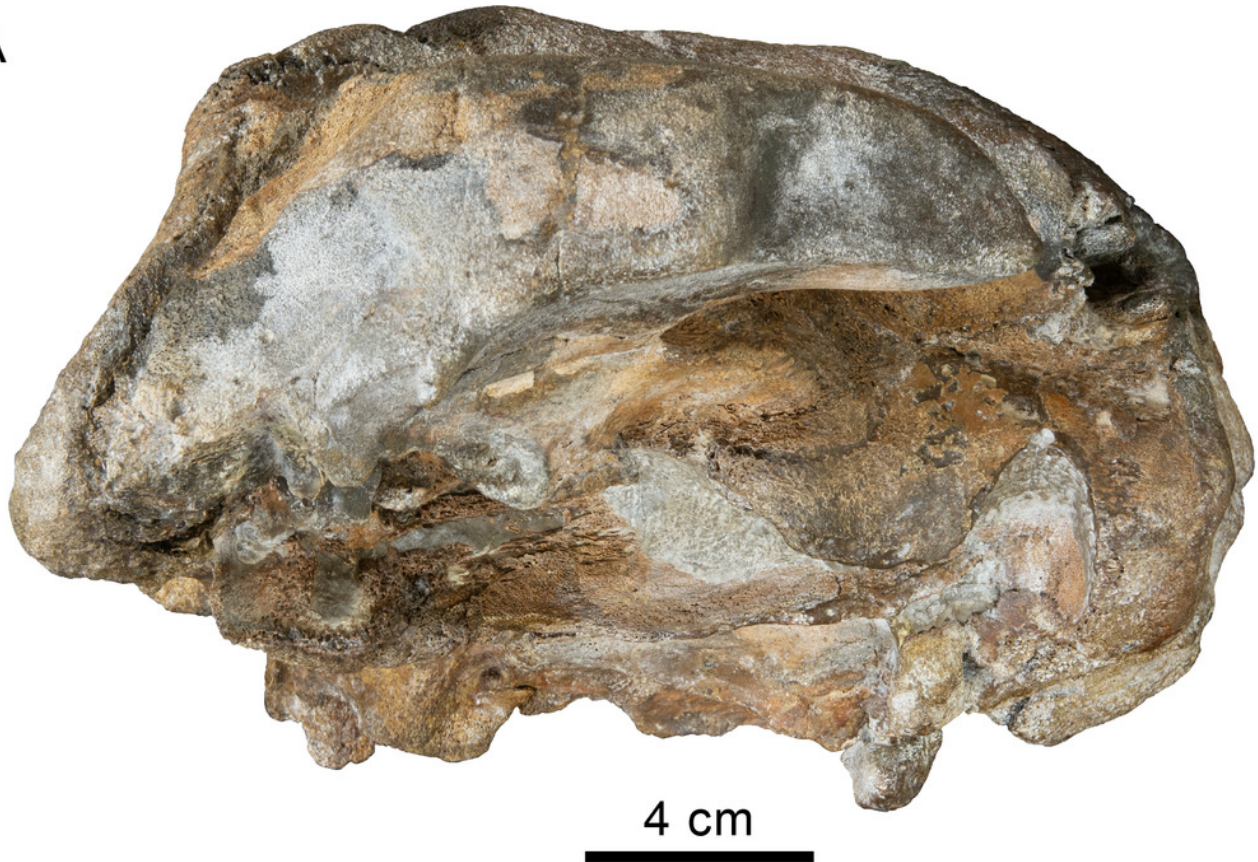


Figure 4

Ventrolateral view of skull of Simocetidae gen. et sp. A (LACM 124104).

Unlabeled (A) and labeled (B) skull in right ventrolateral view. Diagonal lines denote broken surfaces, gray shaded areas are obscured by sediment. Abbreviations: as, alisphenoid; boc, basioccipital crest; f, frontal; fp, falciform process; g, glenoid; oi, optic infundibulum; pa, parietal; pe, periotic; pgg, postglenoid process; ph, pterygoid hamulus; pl, palatine; pll, pterygoid lateral lamina; pml, pterygoid medial lamina; pp, paroccipital process; psf, pterygoid sinus fossa; smf, sternomastoid fossa; sq, squamosal; tr, tympanosquamosal recess; vo, vomer; zps, zygomatic process of squamosal.

A



B

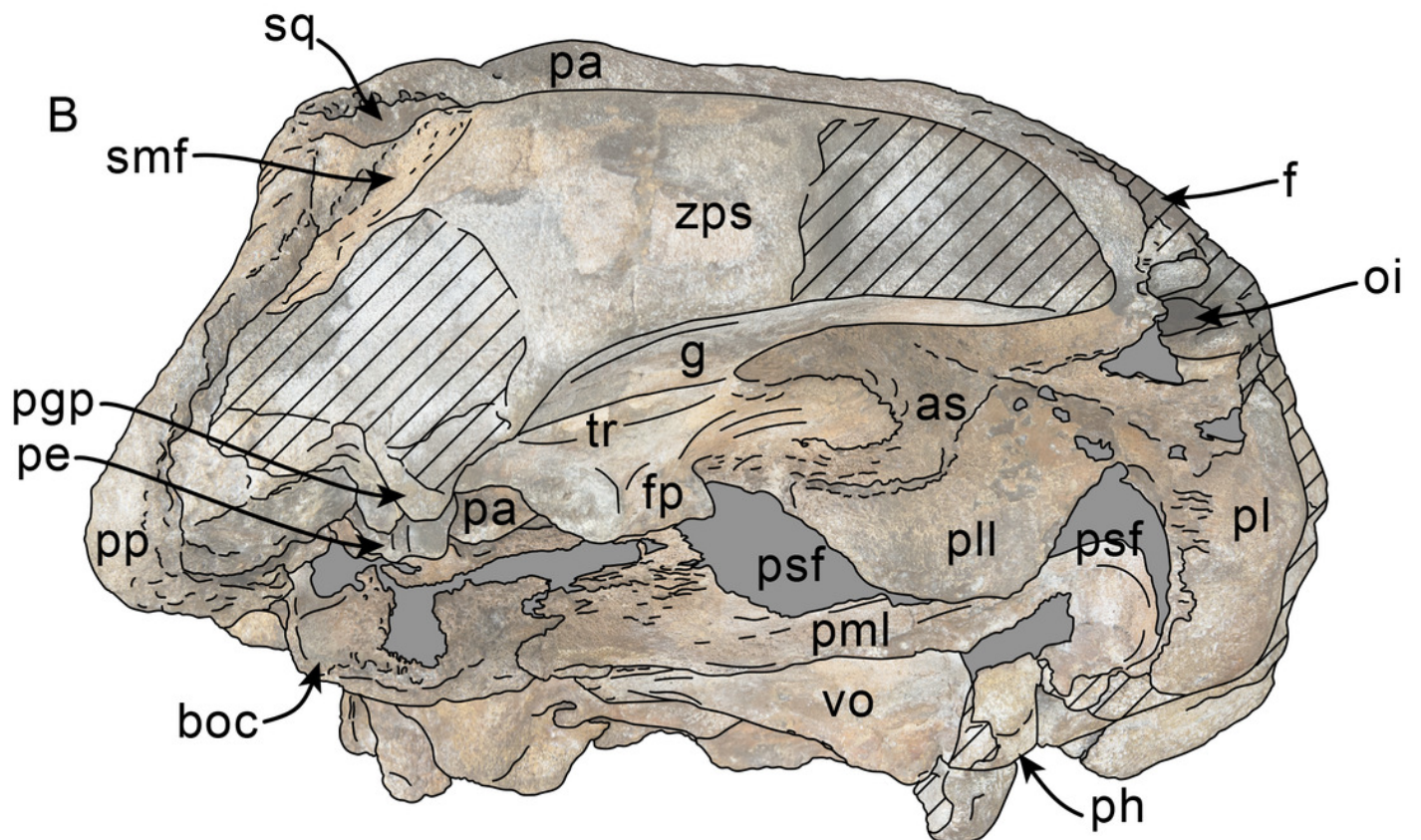


Figure 5

Tooth and vertebrae of Simocetidae gen. et sp. A (LACM 124104).

Upper postcanine tooth in buccal (A), lingual (B) and occlusal (C) views. Atlas (D, E), axis (F, G) and third cervical (H, I) vertebrae in anterior (D, F, H) and posterior (E, G, I) views.

Abbreviations: aa, anterior articular facet; ad, accessory denticles; c, centrum; lc, lingual cingulum; fop, facet for odontoid process; md, main denticle; op, odontoid process; przp, prezygapophysis; tf, transverse foramen; tp, transverse process; va, ventral arch.

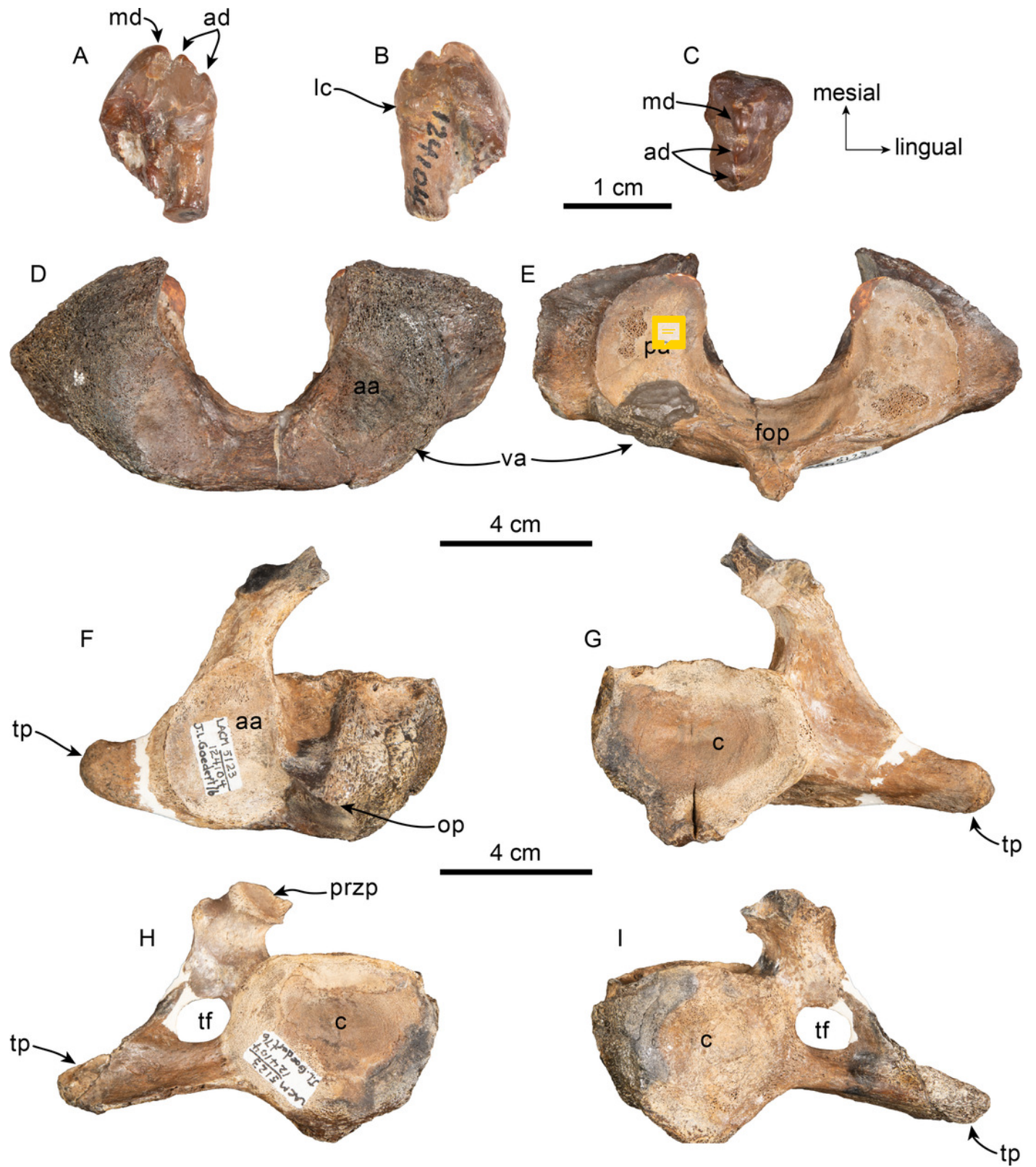


Figure 6

Dorsal view of skull of *Olympicetus thalassodon* sp. nov. (LACM 158720).

Unlabeled (A) and labeled (B) skull in dorsal view. Diagonal lines denote broken surfaces, gray shaded areas are obscured by sediment. Abbreviations: anterior dorsal infraorbital foramina; aon, antorbital notch; ascending process of maxilla; appx, ascending process of premaxilla; as, alisphenoid; eo, exoccipital; f, frontal; la, lacrimal; n, nasal; oc, occipital condyle; P2, second upper premolar; pa, parietal; pf, premaxillary foramen; pls, posterolateral sulcus; pms, posteromedial sulcus; pmx, premaxilla; pop, postorbital process; pp, paroccipital process; psf, premaxillary sac fossa; so, supraoccipital; sop, supraorbital process; sq, squamosal; vo, vomer; zps, zygomatic process of squamosal.

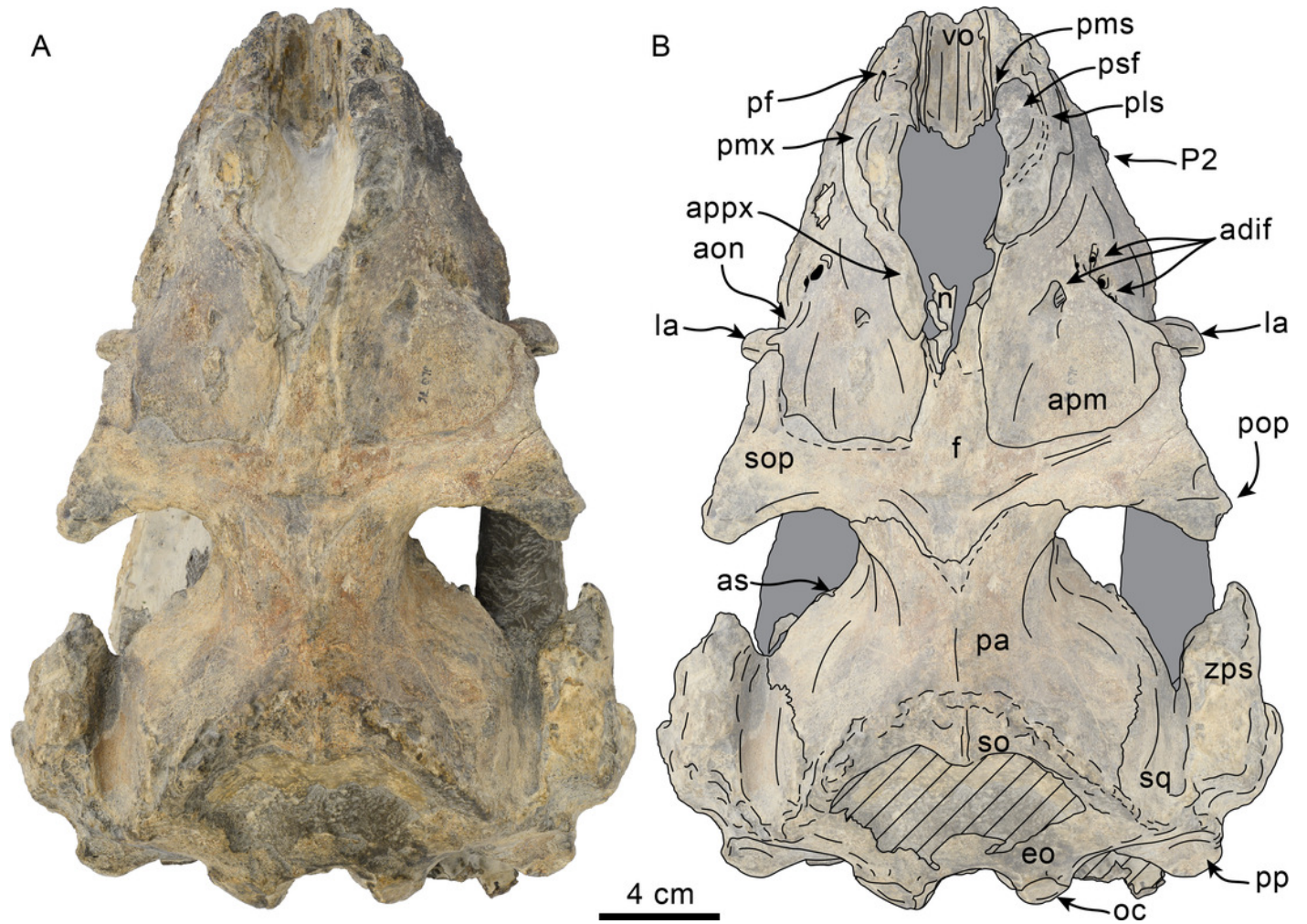


Figure 7

Posterior and ventral views of skull of *Olympicetus thalassodon* sp. nov. (LACM 158720).

Unlabeled (A) and labeled (B) skull in ventral view; (C) unlabeled and labeled skull in right lateral view. Diagonal lines denote broken surfaces, gray shaded areas are obscured by sediment. Abbreviations: at, atlas; bo, basioccipital; boc, basioccipital crest; eam, external auditory meatus; ef, ethmoid foramen; la, lacrimal; m1, first lower molar; ma, mandible; mx, maxilla; p3-4, third and fourth lower premolars; pc, palatal crest; pc?, postcanine teeth of unknown placement; pf, palatine foramen; pgg, postglenoid process; ph, pterygoid hamulus; pl, palatine; pmx, premaxilla; pop, postorbital process; pp, paroccipital process; ppt, posterior process of tympanic; psf, pterygoid sinus fossa; pt, pterygoid; sth, stylohyal; trh, thyrohyal; ty, tympanic; vo, vomer; zps, zygomatic process of squamosal.

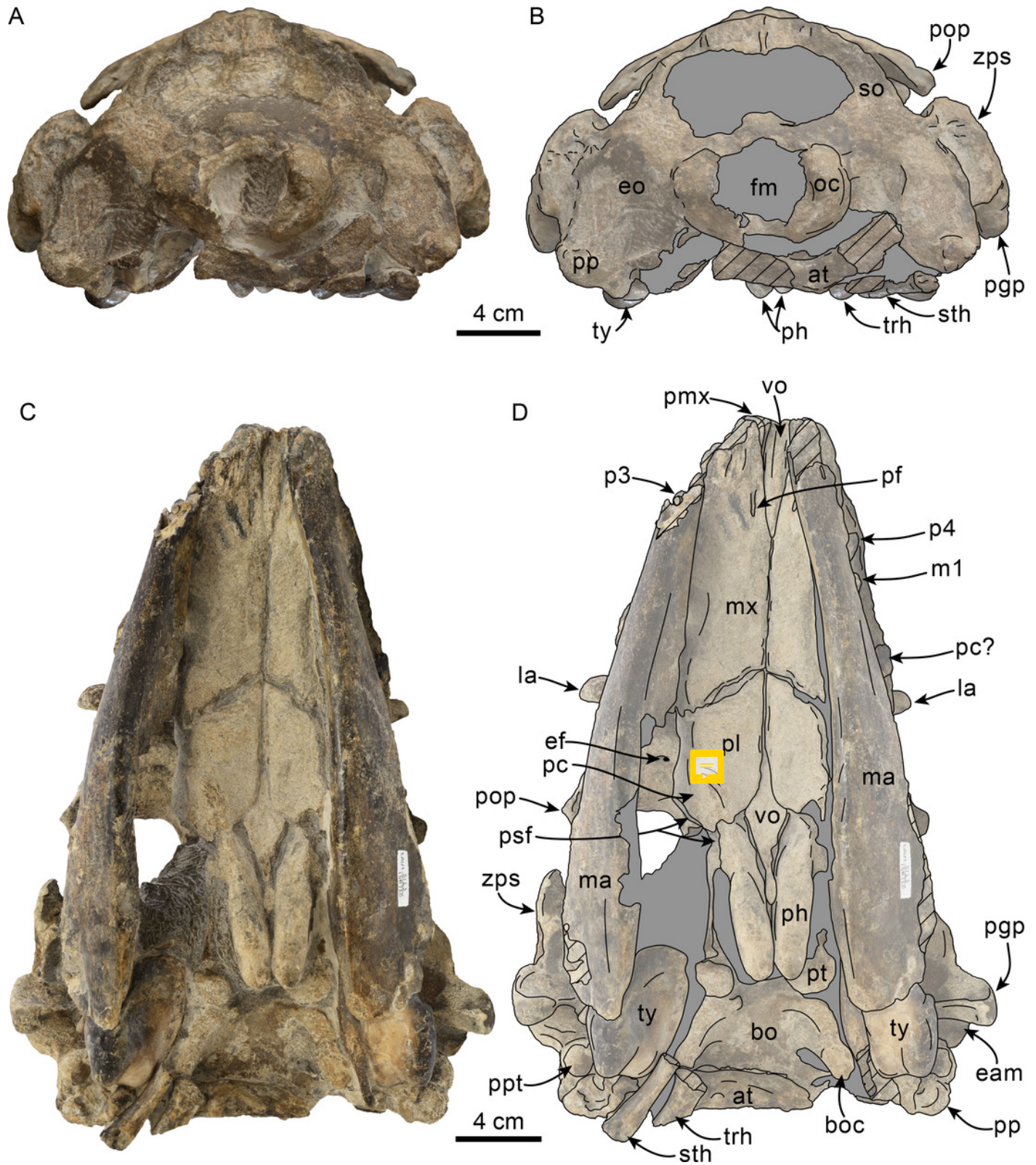


Figure 8

Lateral view of skull of *Olympicetus thalassodon* sp. nov. (LACM 158720).

Unlabeled (A) and labeled (B) skull in right lateral view. Diagonal lines denote broken surfaces, gray shaded areas are obscured by sediment. Abbreviations: a.C, alveolus for upper canine; a.P1, alveoli for upper premolar ~~one~~; adif, anterior dorsal infraorbital foramina; apm, ascending process of maxilla; eam, external auditory meatus; f, frontal; j, jugal; la, lacrimal; m1-3, lower molars ~~one, two and three~~; ma, mandible; mc, mandibular condyle; mip, maxillary infraorbital process; mf, mental foramina; mx, maxilla; n, nasal; nc, nuchal crest; oc, occipital condyle; p3, lower third premolar; P4, upper fourth premolar; pa, parietal; pgg, postglenoid process; pl, palatine; pls, posterolateral sulcus; pop, postorbital process; pp, paroccipital process; psf, pterygoid sinus fossa; ptp, posttympanic process; spf, sphenopalatine foramen; sq, squamosal; sth, stylohyoid; ~~tym~~ tympanic; viof, ventral infraorbital foramen; zc, zygomatic cleft; zps, zygomatic process of squamosal.

A



4 cm



B

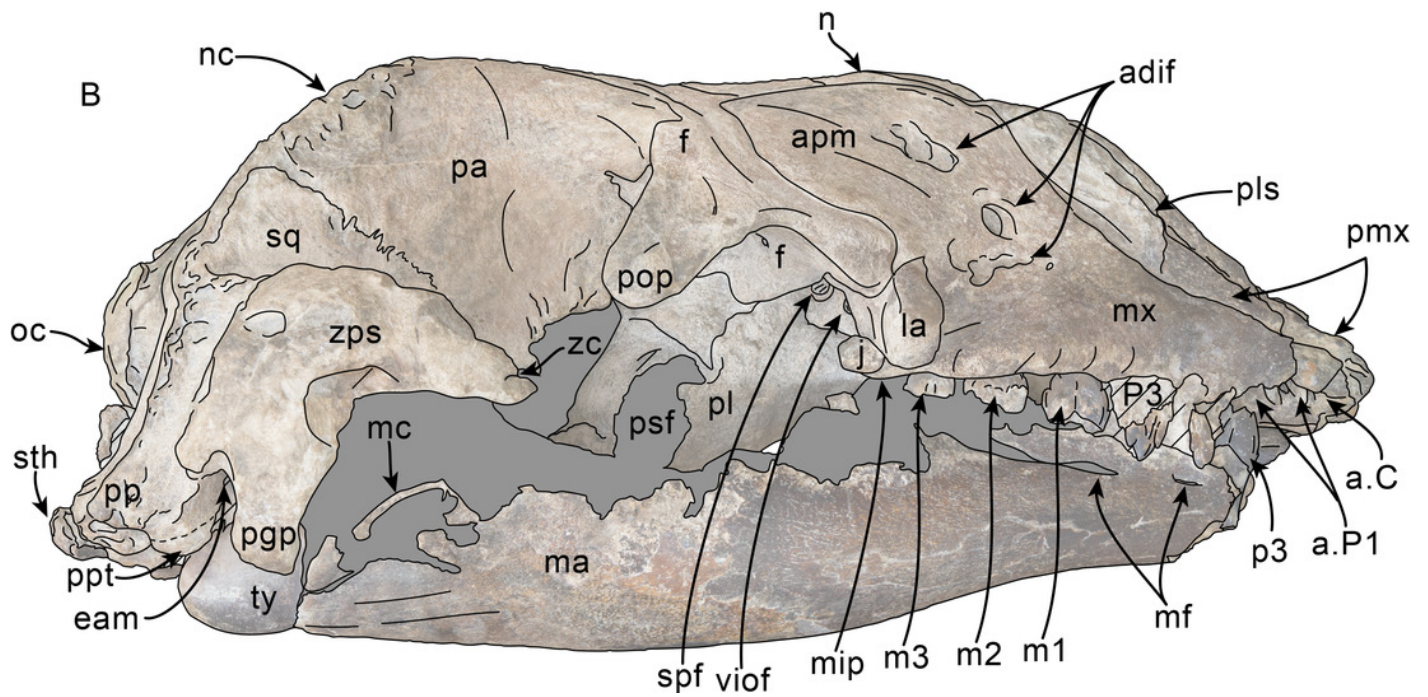


Figure 9

Orbital region of skull of *Olympicetus thalassodon* sp. nov. (LACM 158720).

Unlabeled (A) and labeled (B) orbital region in right lateral view. Diagonal lines denote broken surfaces, gray shaded areas are obscured by sediment. Abbreviations: adif, anterior dorsal infraorbital foramina; ef, ethmoid foramen; f, frontal; ffdv, foramina for frontal diploic vein; j, jugal; la, lacrimal; m1-3, first through third lower molars; ma, mandible; mip, maxillary infraorbital plate; mx, maxilla; of, optic foramen; P4, fourth upper premolar; pa, parietal; pl, palatine; pls, posterolateral sulcus; pmx, premaxilla; pop, postorbital process; psf, pterygoid sinus fossa; spf, sphenopalatine foramen; viof, ventral infraorbital foramen; zps, zygomatic process of squamosal.

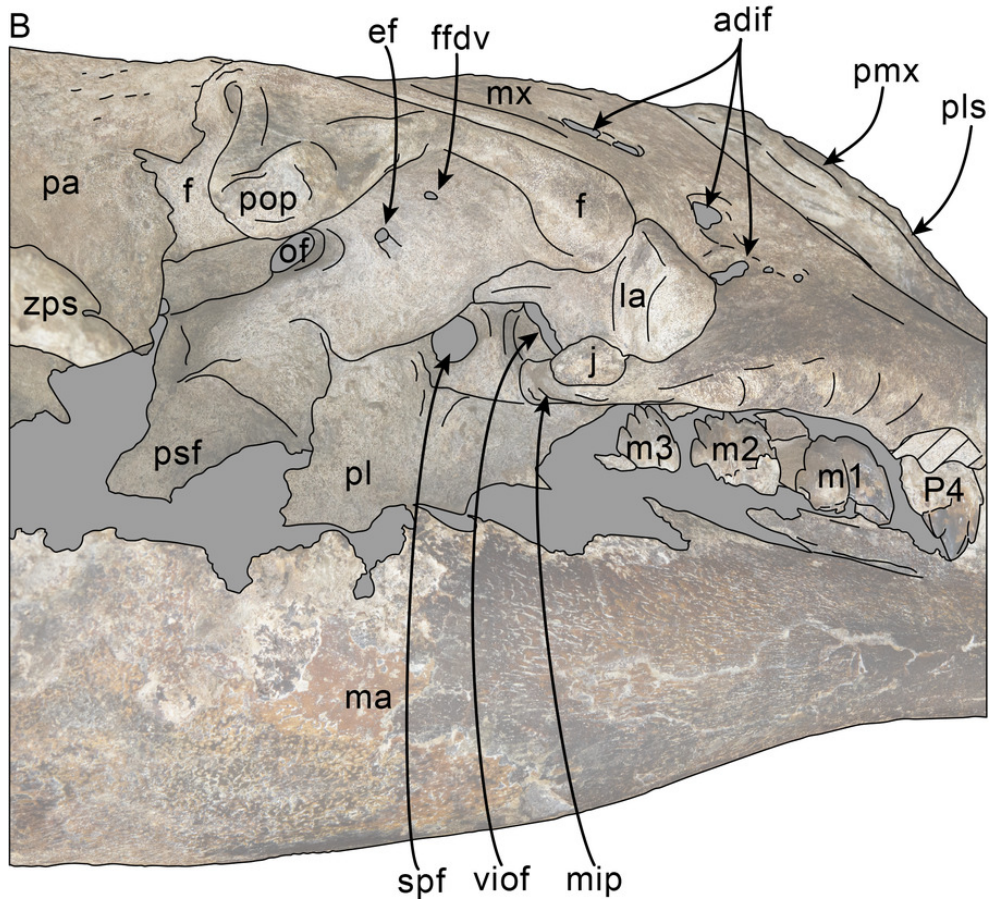


Figure 10

Tympanic bullae of *Olympicetus thalassodon* sp. nov. (LACM 158720).

Articulated left tympanic bulla in ventral (A) and lateral (B) views; articulated right tympanic bulla in anterolateral (C) view. The bullae have been highlighted to differentiate them from the surrounding bones which obscure some parts. Abbreviations: cp, conical process; fp, falciform process; ipp, inner posterior prominence; lf, lateral furrow; ma, mandible; mr, malleolar ridge; opp, outer posterior prominence; pe, periotic; pgg, postglenoid process; pp, posterior process; sp, sigmoid process; sth, stylohyal.

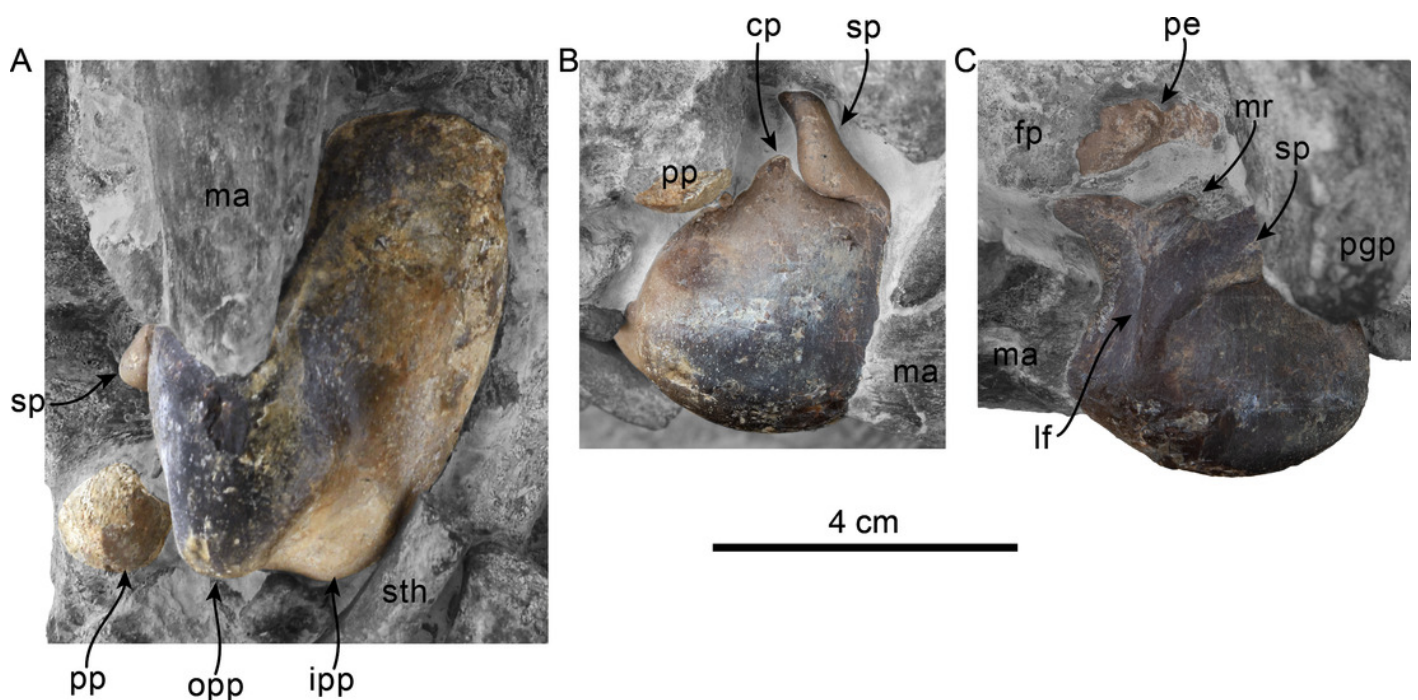


Figure 11

Upper and lower right dentition of *Olympicetus thalassodon* sp. nov. (LACM 158720).

Upper and lower right postcanine teeth in buccal (A-B) views; lower right postcanine teeth (p3-m3) in lingual (C) view; upper right P4-M2 in buccal (D-F) and lingual (G-I) views.

Abbreviations: a.P1, alveoli for first upper premolar; M1-2, first and second upper molars; m1-3, first through third lower molars; P2-4, second through fourth upper premolars; p3-4, third and fourth lower premolars.

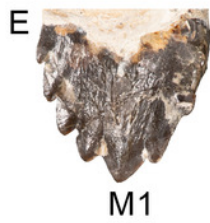
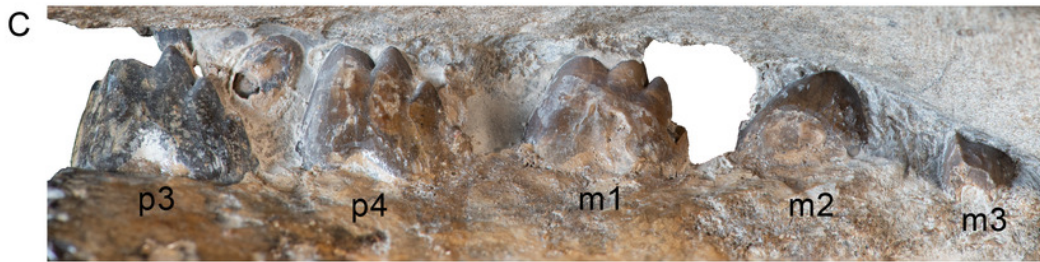
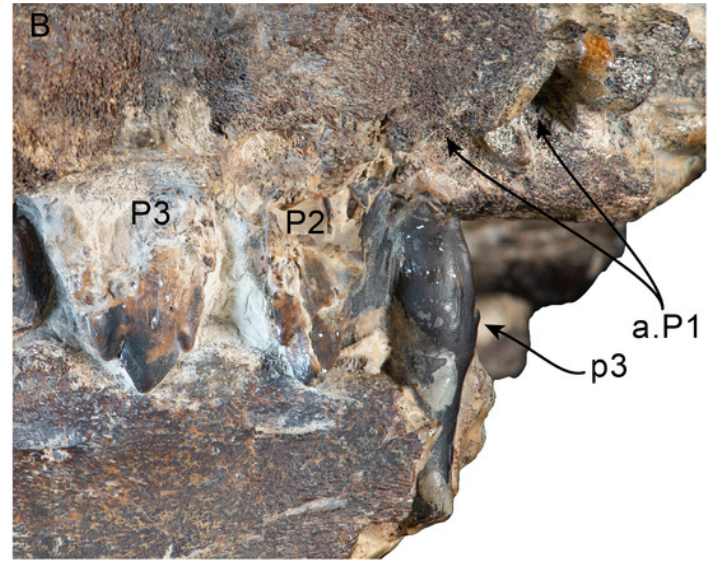
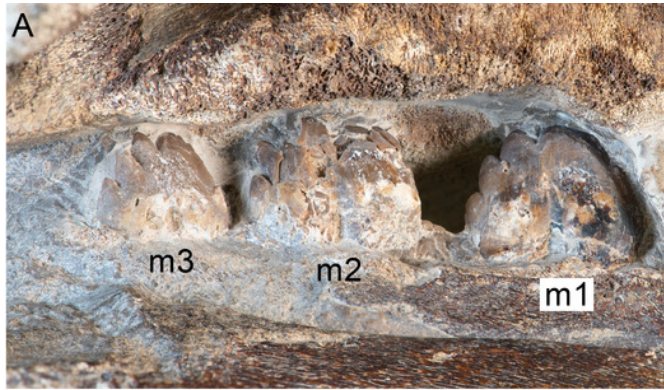


Figure 12

Upper and lower left dentition of *Olympicetus thalassodon* sp. nov. (LACM 158720).

Upper left P4-M2 in buccal (A-C) and lingual (D-F) views; lower left postcanine teeth (p4-m2) in buccal (G) view; canine or incisor in buccal (H) and mesial (I) views; postcanine tooth in lingual (J) view. Abbreviations: M1-2, first and second upper molars; m1-2, first and second lower molars; P4/p4, upper and lower fourth premolars.

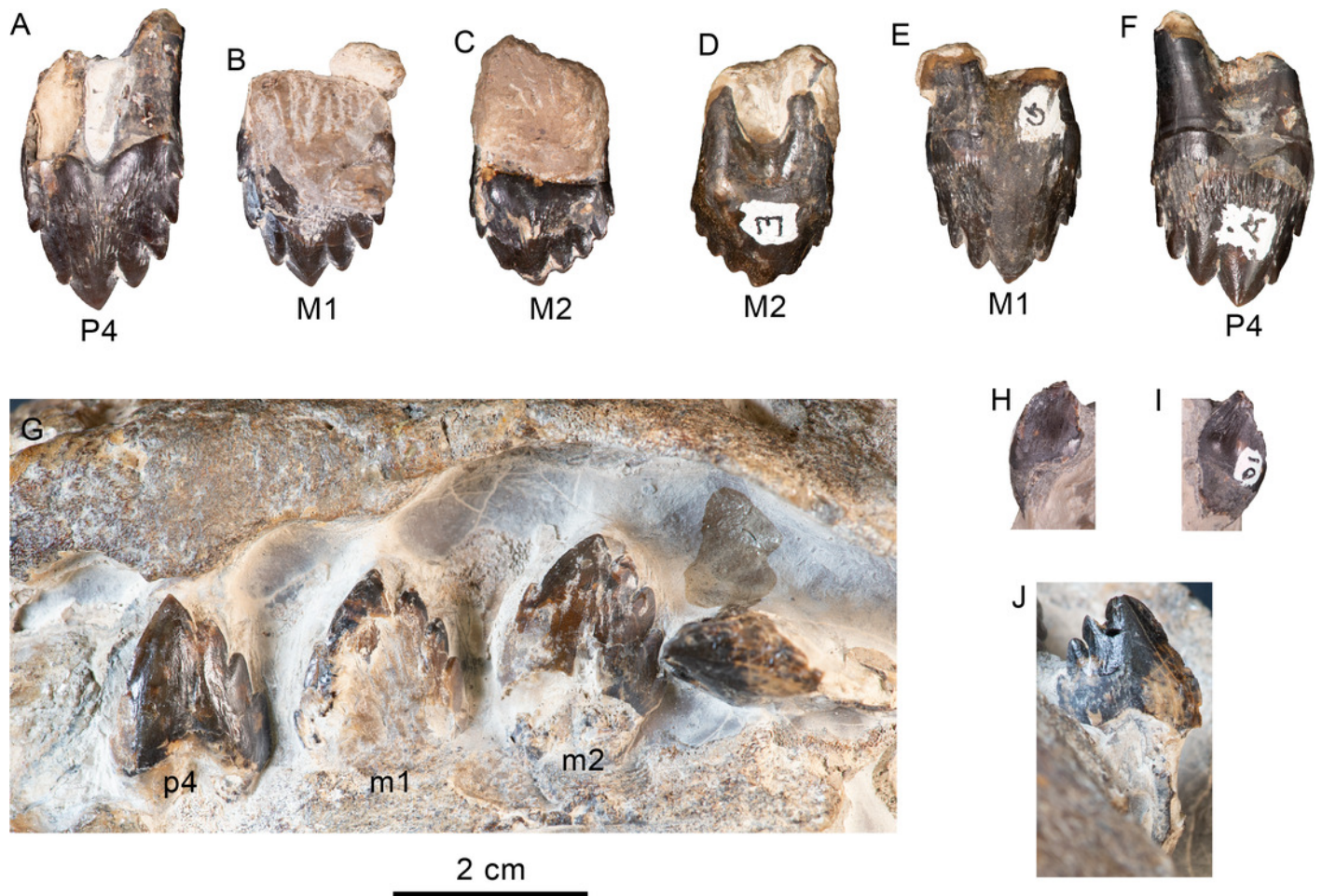


Figure 13

Hyoid elements of *Olympicetus thalassodon* sp. nov. (LACM 158720) and other odontocetes.

(A) Unlabeled and (B) labeled closeup of the right side of the basicranium of *Olympicetus thalassodon* in ventral view. Dorsal views of basihyal and thyrohyals of: (C) *Olympicetus thalassodon* (LACM 158720); (D) *Albireo whistleri* (UCMP 314589); (E) *Phocoenoides dalli* (LACM 43473); (F) *Kogia sima* (LACM 47142); and, (G), *Sagmatias obliquidens* (LACM 27077).

Abbreviations: at, atlas; boc, basioccipital crest; bsh, basihyal; eam, external auditory meatus; ma, mandible; mc, mandibular condyle; pgp, postglenoid process; pp, paroccipital process; ppt, posterior process of the tympanic; sth, stylohyal; trh, thyrohyal; ty, tympanic.

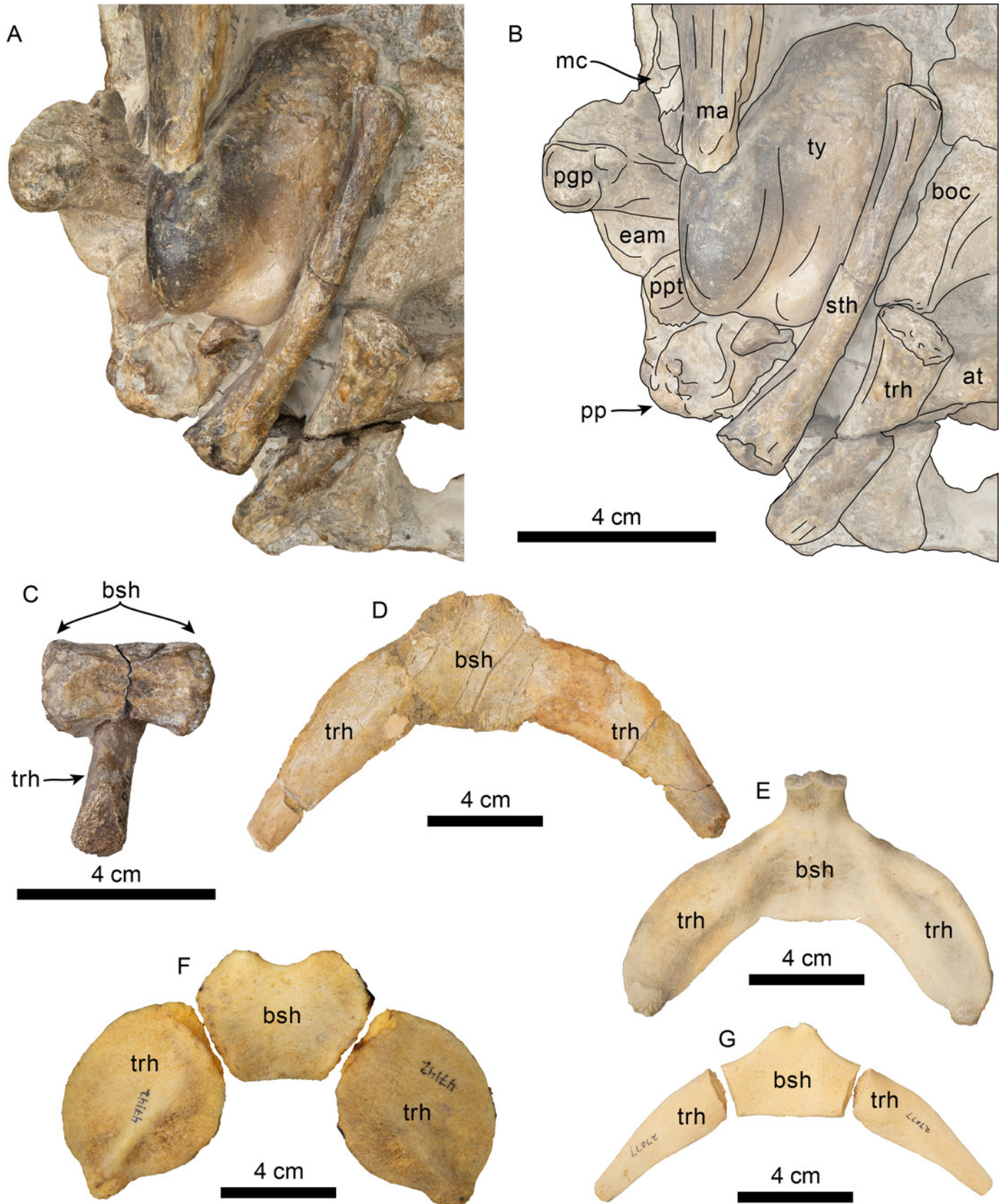


Figure 14

Cervical vertebrae of *Olympicetus thalassodon* sp. nov. (LACM 158720).

(A) atlas in posterior view; (B) axis in anterior view; (C) axis and third through seventh cervicals in right lateral view; (D) axis and third through seventh cervicals in dorsal view.

Abbreviations: aa, anterior articular surface; ax, axis; c3-7, third through seventh cervical vertebrae; da, dorsal arch; dp, dorsal process; fop, facet for odontoid process; op, odontoid process; pa, posterior articular surface; tp, transverse process; vp, ventral process.

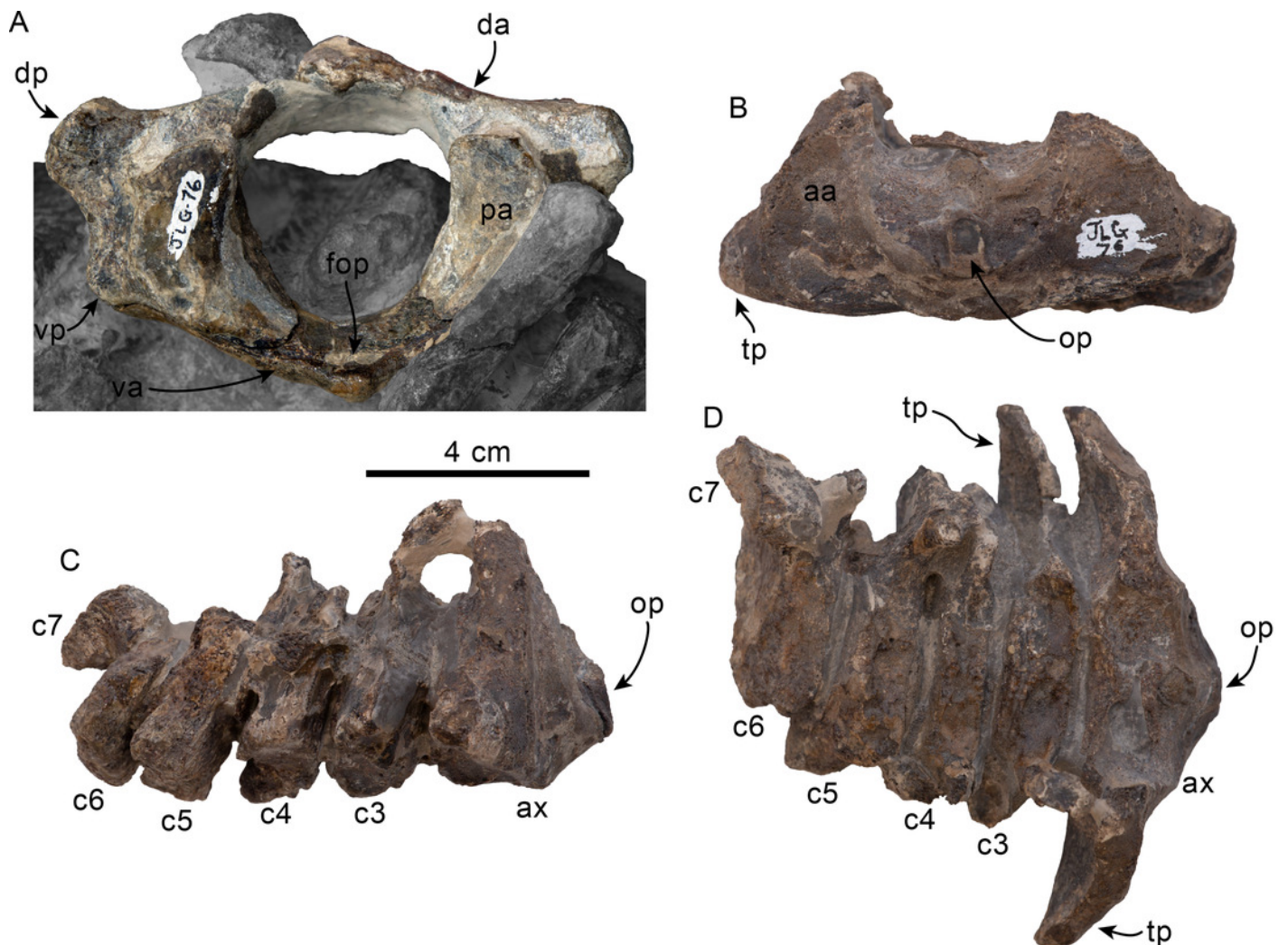


Figure 15

Dorsal view of skull of *Olympicetus* sp. 1 (LACM 124105).

Unlabeled (A) and labeled (B) skull in dorsal view. Diagonal lines denote broken surfaces, gray shaded areas are obscured by sediment. Abbreviations: adif, anterior dorsal infraorbital foramina; f, frontal; la, lacrimal; mx, maxilla; n, nasals; oc, occipital condyle; pa, parietal; pmx, premaxilla; pop, postorbital process; sop, supraorbital process of frontal; sq, squamosal; tc, temporal crest; vo, vomer; zps, zygomatic process of squamosal.

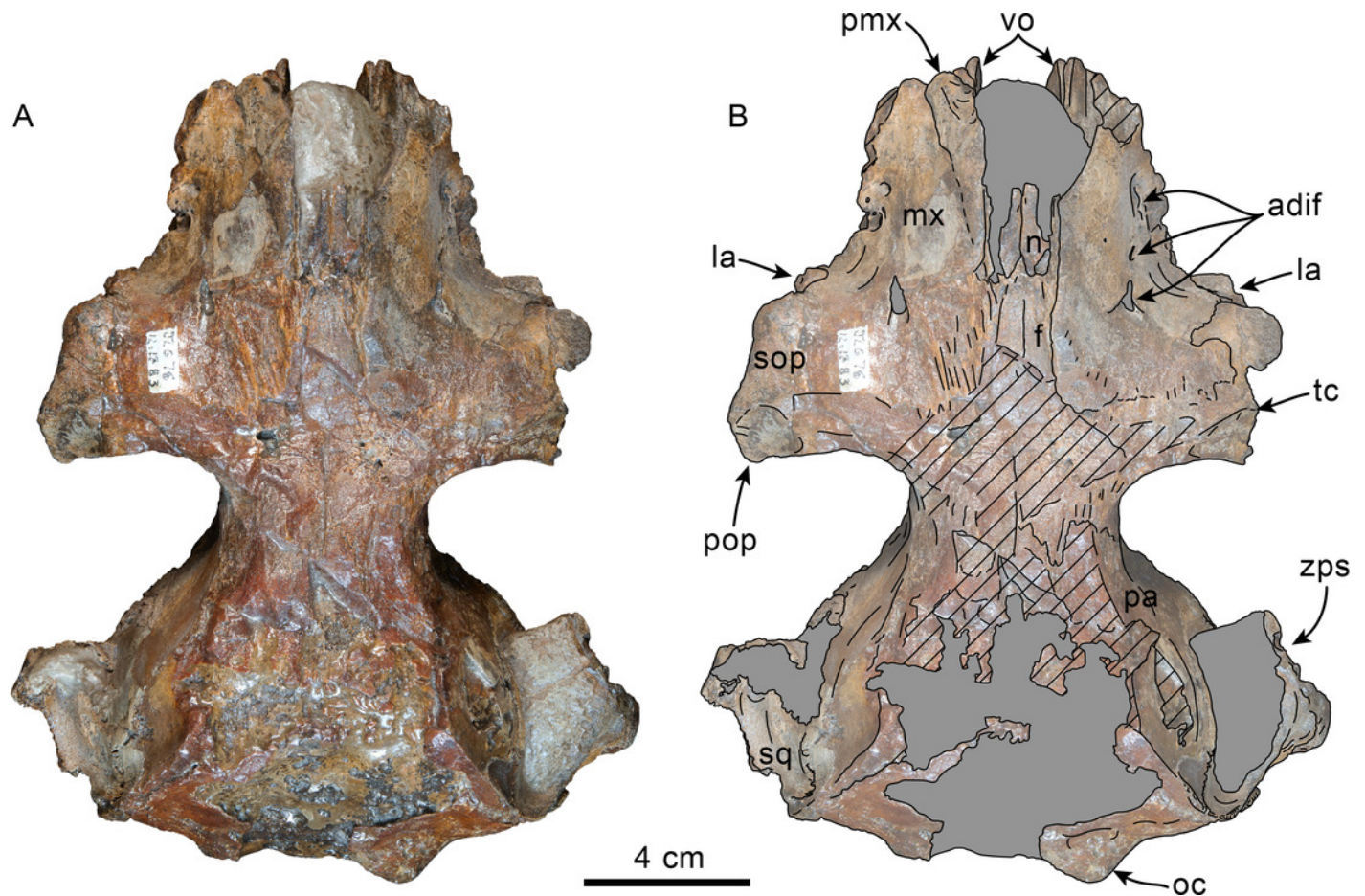


Figure 16

Ventral view of skull of *Olympicetus* sp. 1 (LACM 124105).

Unlabeled (A) and labeled (B) skull in ventral view. Diagonal lines denote broken surfaces, gray shaded areas are obscured by sediment. Abbreviations: a.ps, alveoli for postcanine teeth; as, alisphenoid; bo, basioccipital; boc, basioccipital crest; bs, basisphenoid; ef, ethmoid foramen; ffdv, foramina for frontal diploic veins; insphs, intersphenoidal synchondrosis; j, jugal; la, lacrimal; mx, maxilla; pa, parietal; pf, periotic fossa; pl, palatine; pmx, premaxilla, pop, postorbital process; psf, pterygoid sinus fossa; pt, pterygoid; vo, vomer; zps, zygomatic process of squamosal.

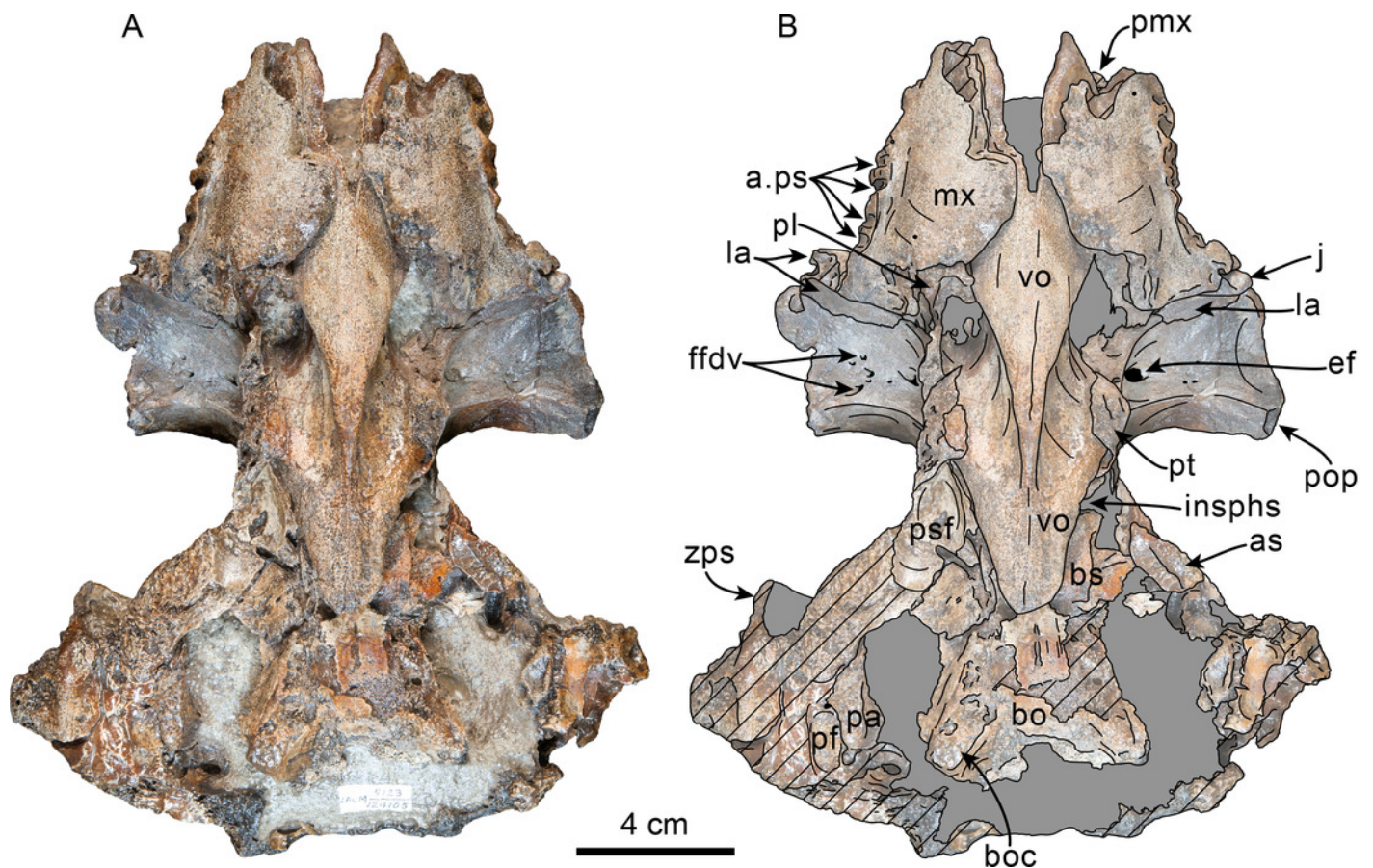


Figure 17

Ventrolateral view of skull of *Olympicetus* sp. 1 (LACM 124105).

Unlabeled (A) and labeled (B) skull in right ventrolateral view focusing on the features of the orbital region. Diagonal lines denote broken surfaces, gray shaded areas are obscured by sediment. Abbreviations: a.ps, alveoli for postcanine teeth; adif, anterior dorsal infraorbital foramina; as, alisphenoid; boc, basioccipital crest; ef, ethmoid foramen; ffdv, foramina for frontal diploic veins; f, frontal; j, jugal; la, lacrimal; mx, maxilla; oa, path for ophthalmic artery; oi, optic infundibulum; pa, parietal; pl, palatine; psf, pterygoid sinus fossa; pt, pterygoid; spf, sphenopalatine foramen; viof, ventral infraorbital foramen; V2, path for maxillary nerve; vo, vomer; zps, zygomatic process of squamosal.

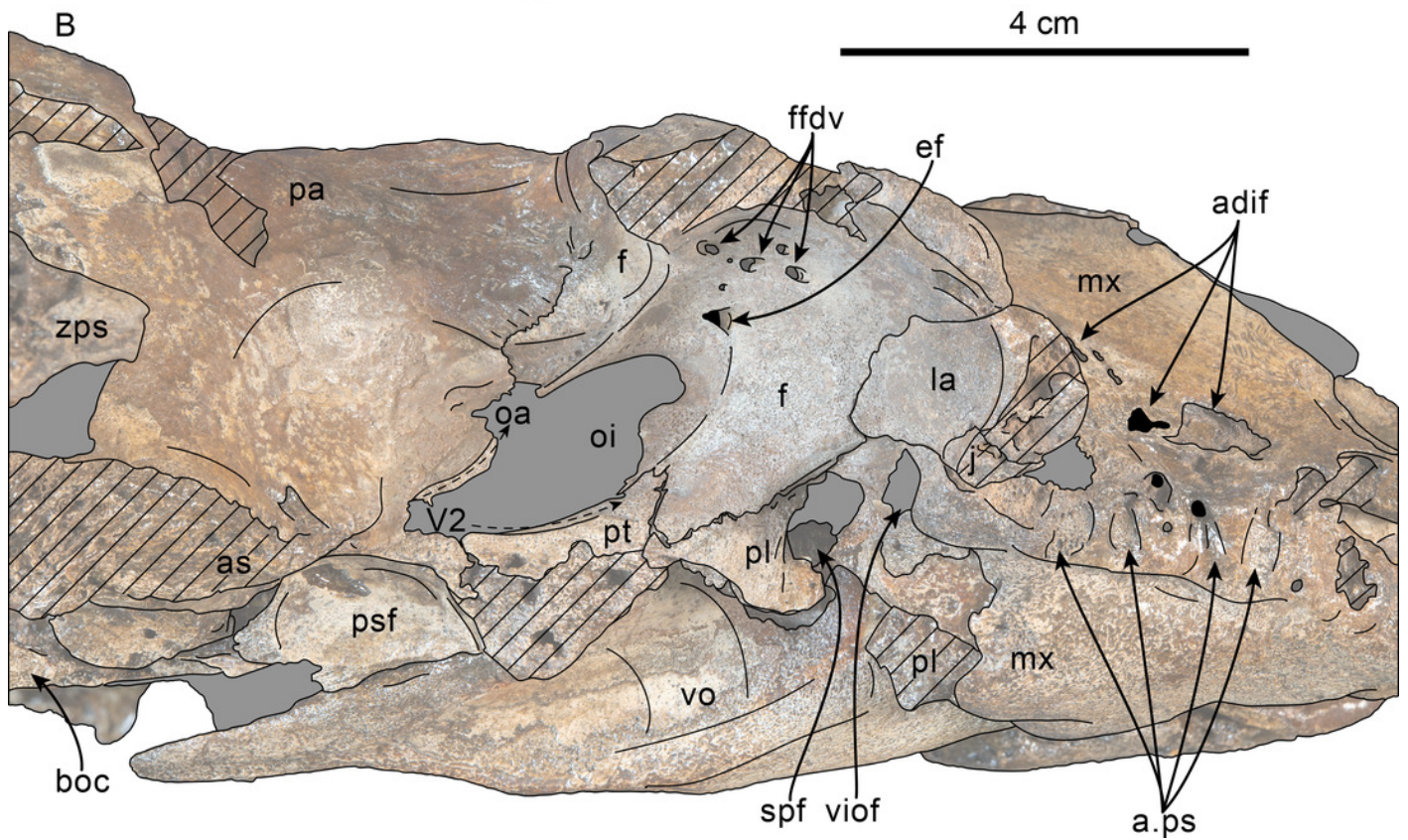


Figure 18

Malleus and tympanic bulla of *Olympicetus* sp. 1 (LACM 124105).

Left malleus and tympanic bullae in medial (A), lateral (B), anterior (C), posterior (D), and dorsal (E) views. Abbreviations: ac, anterodorsal crest; ap, anterior process; cp, conical process; ef, elliptical foramen; fi, facet for incus; hm, head of malleus; in, involucrum; ipp, inner posterior prominence; ippe, inner posterior pedicle; lf, lateral furrow; mn, manubrium; mp, muscular process; mr, malleolar ridge; ol, outer lip; opp, outer posterior prominence; sc, sigmoid cleft; sct, sulcus for chorda tympani; sp, sigmoid process; tc, tympanic cavity; tr, transverse ridge.

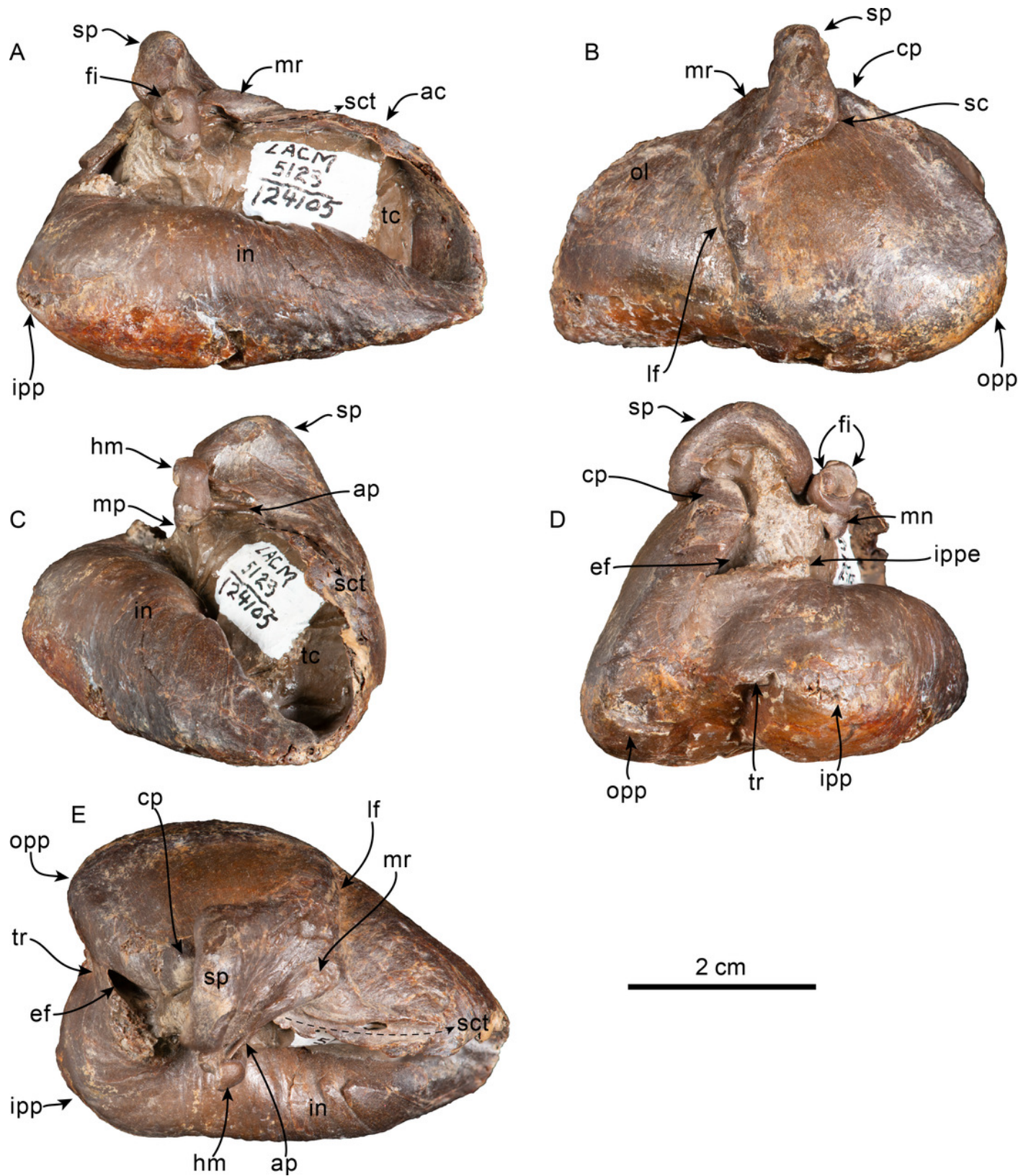


Figure 19

Periotic and teeth of *Olympicetus* sp. 1 (LACM 124105).

Unlabeled and labeled right periotic in dorsal (A-B), medial (C-D), ventral (E-F), and lateral (G-H) views. Postcanine teeth in buccal (I-J) and lingual (K-L) views. Abbreviations: abf, anterior bullar facet; acm, area cribosa media; aepb, anteroexternal+parabullary sulcus; ap, anterior process; ctp, caudal tympanic process; ed, endolymphatic duct; eth, epitympanic hiatus; fc, facial canal; fgp, foramen for greater petrosal nerve; fo, foramen ovale; fr, foramen rotundum; iam, internal acoustic meatus; if, incudal fossa; pbf, posterior bullar facet; pc, pars cochlearis; pd, perilymphatic duct; lt, lateral tuberosity; mf, malleolar fossa; pp, posterior process; sct, spiral cribriform tract; sm, stapedial muscle fossa; smf, supramastoid fossa; sva, superior vestibular area; tt, tegmen tympani.

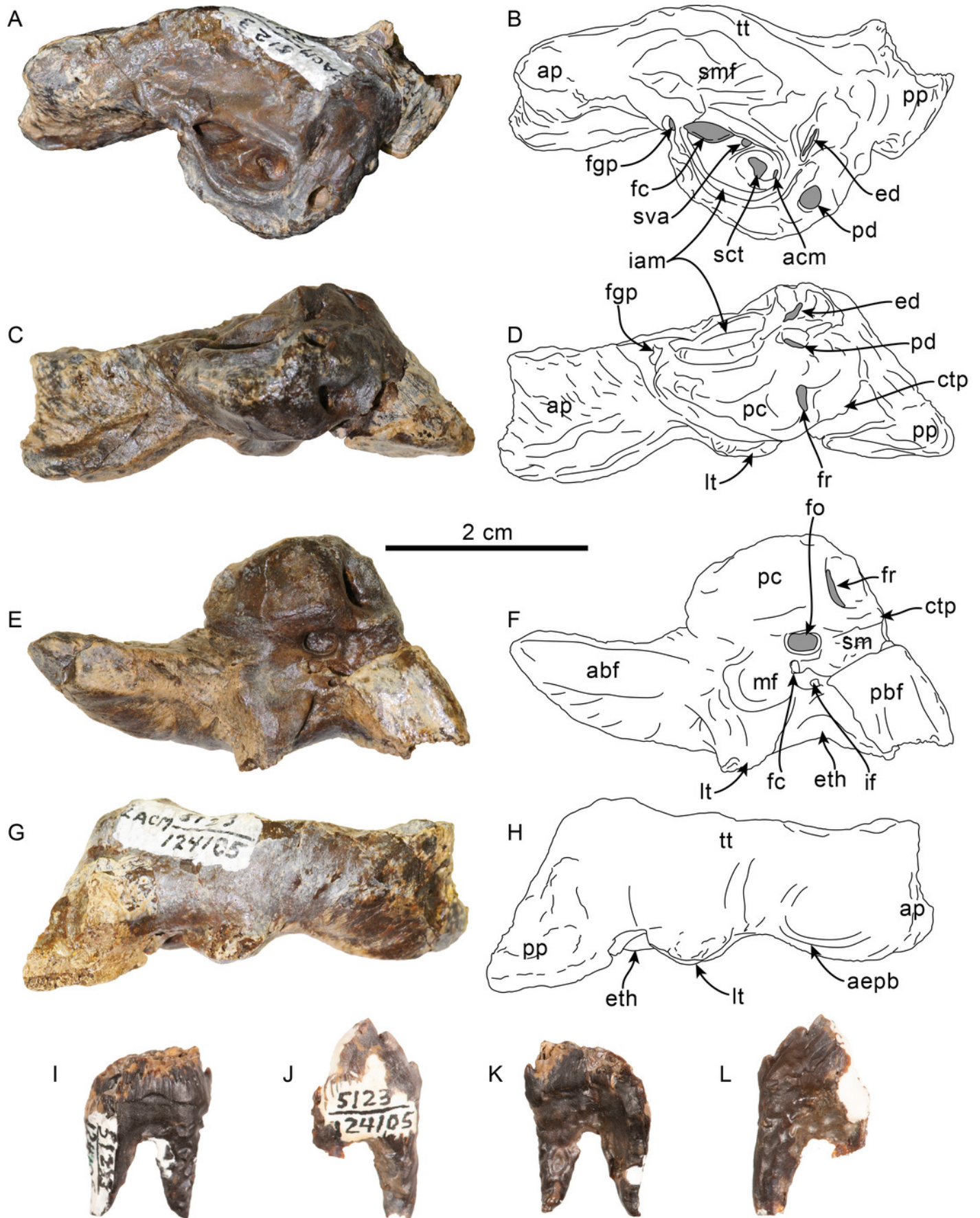


Figure 20

Time calibrated phylogeny of Cetacea.

Phylogenetic tree showing relationship between Simocetidae with other odontocetes; mysticetes and crown odontocete clades are pruned. Strict consensus tree based on 32 most parsimonious trees of length = 2567, with retention index (RI) = 0.519, and consistency index (CI) = 0.231. Arcs denote stem-based taxa, while closed circles denote node-based clades; the numbers at the nodes indicate decay indices/bootstrap values. Abbreviations: Aq., Aquitanian; Bar., Bartonian; Burd., Burdigalian; Chatt., Chattian; Holo., Holocene; La., Langhian; M., Messinian; P, Piacenzian; P., Pliocene; Ple., Pleistocene; Priab., Priabonian; Rupel., Rupelian; S., Serravalian; Tort., Tortonian; Z, Zanclean. Time scale based on Cohen et al. (2013); skull outline for *Simocetus rayi* modified from Fordyce (2002).

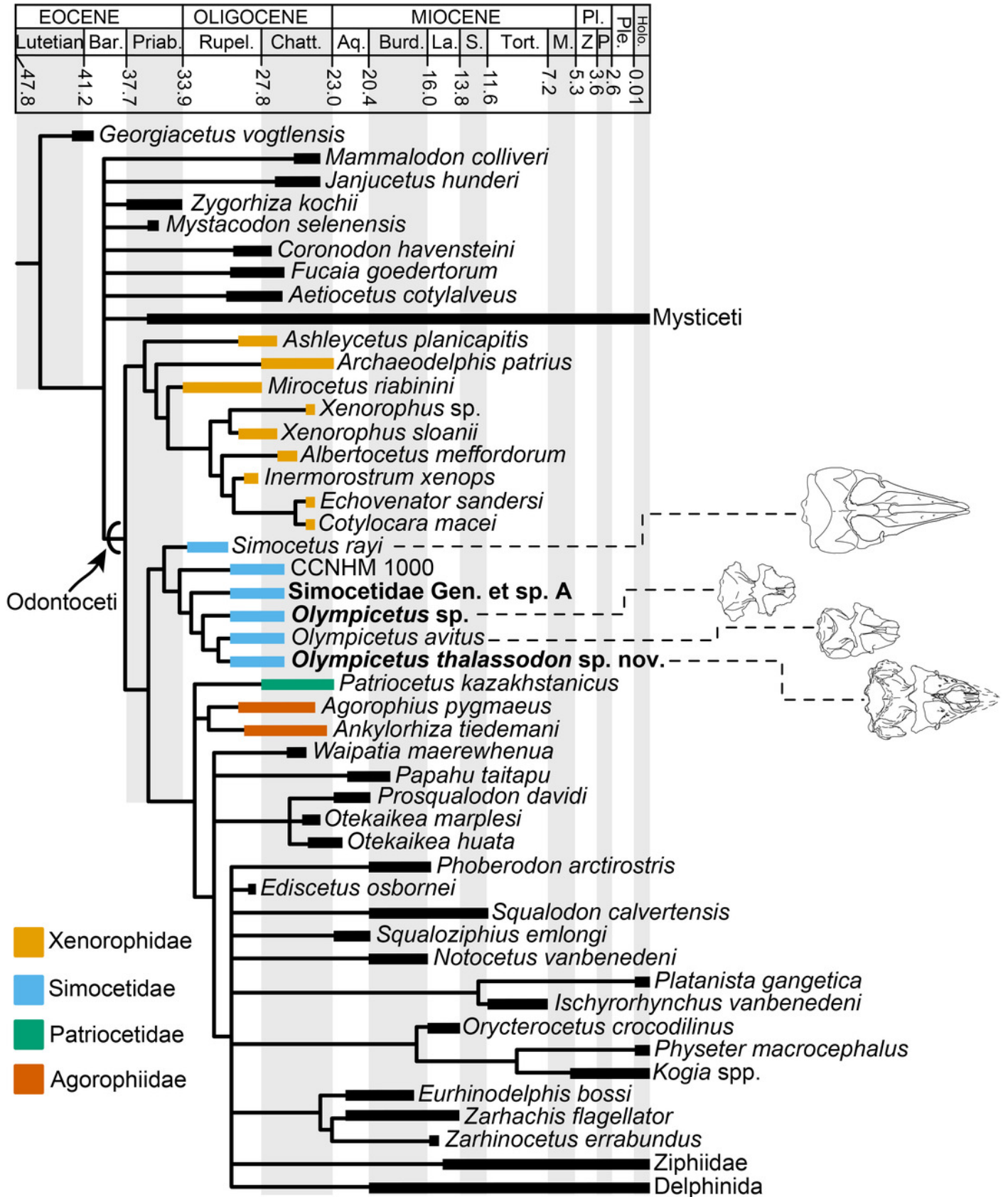


Table 1 (on next page)

Measurements of simocetid skulls and mandibles.

Measurements (in mm) of simocetid skulls and mandible, Simocetidae gen. et sp. A (LACM 124104), *Olympicetus thalassodon* gen. et sp. nov. (LACM 158720) and *Olympicetus* sp. 1 (LACM 124105). Modified after Perrin (1975).

TABLE 1. Measurements (in mm) of simocetid skulls and mandible, Simocetidae gen. et sp. A (LACM 124104), *Olympicetus thalassodon* gen. et sp. nov. (LACM 158720) and *Olympicetus* sp. 1 (LACM 124105). Modified after Perrin (1975).

	LACM	LACM	LACM
	124104	158720	124105
Width of rostrum at base	-	135	93+
Width of rostrum at 60 mm anterior to line across hindmost limits of antorbital notches	-	105	-
Greatest preorbital width (width across preorbital processes)	-	153	136
Greatest postorbital width	-	187	150e
Mid-orbital width	-	151	140e
Maximum width of external nares	-	33	-
Greatest width across zygomatic processes of squamosal	322e	220	186e
Greatest width of premaxillaries	-	83	-
Greatest parietal width within temporal fossae	154	135	100
Vertical external height of braincase from midline of basisphenoid to summit of supraoccipital, but not including external occipital crest	135	112	-
Greatest length of left posttemporal fossa, measured to external margin of raised suture	-	99	-
Greatest width of left posttemporal fossa at right angles to greatest length	-	51	-
Major diameter of left temporal fossa proper	-	111	-

1

TABLE 1. Continued.

Minor diameter of left temporal fossa proper	59	45	-
Distance from foremost end of junction between nasals to hindmost point of margin of supraoccipital crest	-	143e	-
Length of orbit – from apex of preorbital process of frontal to apex of postorbital process	-	55	40+
Length of antorbital process of lacrimal	-	18	12
Greatest length of left pterygoid	132	79	-
Maximum width across occipital condyles	92	78	-
Height of foramen magnum	33	35	-
Width of foramen magnum	39	32	-
Cranial length – antorbital notch to condyles	-	211	165+
Greatest length of left mandibular ramus (as preserved)	-	251+	-
Greatest length of right mandibular ramus (as preserved)	-	244+	-
Maximum height at mandibular condyle	-	54	-

Abbreviations: e, estimate; + = measurement on incomplete element.

2

Table 2 (on next page)

Measurements of simocetid cervical vertebrae.

Measurements (in mm) of cervical vertebrae of Simocetidae gen. et sp. A (LACM 124104) and *Olympicetus thalassodon* sp. nov. (LACM 158720).

TABLE 2. Measurements (in mm) of cervical vertebrae of Simocetidae gen. et sp. A (LACM 124104) and *Olympicetus thalassodon* sp. nov. (LACM 158720).

	LACM 124105	LACM 158720
Atlas		
Maximum height	-	70
Maximum length	32	27
Width across anterior articular facets	80+	-
Width across posterior articular facets	94	74
Maximum width (across transverse processes)	-	108
Mid-dorsal length	-	24
Mid-ventral length (including odontoid process)	37	22
Neural canal height	-	44
Neural canal width	45	38
Axis		
Maximum height of centrum	46	33
Maximum width of centrum	47	-
Maximum length of centrum	44	30
Width across anterior articular facets	92e	77
Maximum width (across transverse processes)	144e	97
Width of neural canal	46	33
Cervical 3		
Height of centrum	49	34

Width of centrum	53	34
Length of centrum	20	12
Maximum width (across transverse processes)	164e	96e
Width of neural canal	38e	-
<hr/>		
Cervical 4		
Height of centrum	-	34
Width of centrum	-	35
Length of centrum	-	12
<hr/>		
Cervical 5		
Height of centrum	-	31
Width of centrum	-	32
Length of centrum	-	12
<hr/>		
Cervical 6		
Height of centrum	-	27+
Length of centrum	-	10+
<hr/>		
Abbreviations: e = estimate; + = measurement on incomplete element.		

Table 3(on next page)

Measurements of simocetid tympanic bullae.

Measurements (in mm) of tympanic bullae of *Olympicetus thalassodon* sp. nov. (LACM 158720), *Olympicetus avitus* (LACM 126010), and *Olympicetus* sp. A (LACM 124105) (modified from Kasuya, 1973, and Geisler et al., 2014).

TABLE 3. Measurements (in mm) of tympanic bullae of *Olympicetus thalassodon* sp. nov. (LACM 158720), *Olympicetus avitus* (LACM 126010), and *Olympicetus* sp. A (LACM 124105) (modified from Kasuya, 1973, and Geisler et al., 2014).

	LACM 158720	LACM 126010	LACM 124105
Maximum length (without posterior process)	65	50	49
Maximum length (including posterior process)	74	54	-
Distance from anterior tip to inner posterior prominence	61	50	48
Maximum width at level of the sigmoid process	40	35	34
Height at sigmoid process	46	37	36
Maximum width of sigmoid process	-	15	15
Maximum length of posterior process	16+	18	-

Abbreviations: +, measurement on incomplete or obscured element.

1

Table 4(on next page)

Measurements of simocetid teeth.

Measurements (in mm) of left (l) and right (r) teeth of *Olympicetus thalassodon* sp. nov. (LACM 158720).

TABLE 4. Measurements (in mm) of left (l) and right (r) teeth of *Olympicetus thalassodon* sp. nov. (LACM 158720).

Designation	Length	Width	Height
?Canine	7.4	7.2	7.7
P2 (r)	-	-	15.6
P3 (r)	15.7	-	17.5
P4 (r)	16.5	9.7	17.5
P4 (l)	17.9	9.3	18.3
M1 (r)	16.4	9.4	17.9
M1 (l)	16.5	9.4	16.7
M2 (r)	14.1	8.1	11.9
M2 (l)	14.6	8.4	11.7
p3 (r)	17.1	7.4	14.4+
p4 (r)	15.2	-	13.6+
p4 (l)	16.7	-	18.6
m1 (r)	17.8	6.4	13.9+
m1 (l)	17.6	-	18.3
m2 (r)	16.5	-	13.5+
m2 (l)	17.4	-	17.3
m3 (r)	13.4	-	11.6
Molariform indet.	15.4	9.0	13.5

Abbreviations: +, measurement on incomplete element.

Table 5 (on next page)

Measurements of simocetid hyoid elements.

Measurements (in mm) of hyoid elements of *Olympicetus thalassodon* sp. nov. (LACM 158720) (modified after Johnston and Berta, 2011).

TABLE 5. Measurements (in mm) of hyoid elements of *Olympicetus thalassodon* sp. nov. (LACM 158720) (modified after Johnston and Berta, 2011).

Stylohyal (right)	
Maximum length	85
Maximum width of distal articular surface	11
Anteroposterior thickness at mid length	10
Transverse width at mid length	6
Maximum width of proximal articular surface	16
Anteroposterior thickness of proximal articular surface	8
Basihyal	
Maximum length along the midline	14
Maximum depth along the midline	10
Maximum transverse width	33
Length of articular surface	20
Height of articular surface	14
Thyrohyal (right)	
Maximum length	59
Maximum width of distal articular surface	11
Maximum height of distal articular surface	16
Dorsoventral thickness at mid length	7
Transverse width at mid length	11
Maximum width of proximal articular surface	18
Maximum height of proximal articular surface	13

Table 6 (on next page)

Measurement of simocetid periotic.

Measurements (in mm) of periotic of *Olympicetus* sp. 1 (LACM 124105) (modified from Kasuya, 1973, and Racicot et al., 2019).

TABLE 6. Measurements (in mm) of periotic of *Olympicetus* sp. 1 (LACM 124105) (modified from Kasuya, 1973, and Racicot et al., 2019).

Maximum length	43
Proximal dorsoventral thickness of anterior process	12
Length of anterior process	16
Transverse width of anterior process at mid-length	9
Dorsoventral height of anterior process at mid-length	13
Maximum width of periotic	22
Least distance between fundus of internal auditory meatus and aperture for endolymphatic foramen	2
Least distance between fundus of internal auditory meatus and aperture for perilymphatic foramen	3
Least distance between fenestra rotunda and endolymphatic foramen	7
Least distance between fenestra rotunda and perilymphatic foramen	3
Length of articular surface of posterior process	11
Width of articular surface of posterior process	8
Transverse width of cochlear portion	10
Anteroposterior length of cochlear portion	15